u

Cape Peninsula
University of Technology

A COMPARATIVE STUDY OF THE EFFICIENCY OF ION EXCHANGE AND EXTRACTION CHROMATOGRAPHY FOR THE SEPARATION OF MILLIGRAM AMOUNTS OF SCANDIUM FROM GRAM AMOUNTS OF CALCIUM

by

SHAHEEDA ADONIS

Thesis submitted in fulfilment of the requirements for the degree

Doctor of Philosophy in Chemistry

in the Faculty of Applied Science

at the Cape Peninsula University of Technology

Supervisor: Dr T Oosthuysen

Supervisor (external): Prof T N Van der Walt

Bellville

December 2022

DECLARATION

I, **Shaheeda Adonis, student number 197095895,** declare that the contents of this thesis represent my own unassisted work and that this thesis has not been submitted previously for academic examination towards any qualification. Furthermore, it represents my own opinions and not necessarily those of the Cape Peninsula University of Technology.

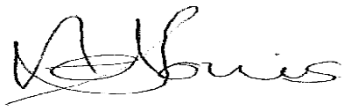

December 2022

Signed **Date**

ABSTRACT

The growing demand for scandium in various applications such as aerospace, special alloys, electronics and the nuclear industry, has lead to the need to finf more effiecient and cost-effective methods for its separation. The radioactive isotopes of scandium, in particular Scandium-44 and Scandium-47, have generated interest for use in radiopharmaceuticals, for both medical imaging and radiotherapy. It is commonly produced using a cyclotron in a calcium or sometimes a titanium based irradiation target. As the radiopharmaceutical use of scandium radionuclides commonly requires chelation, scandium needs to be separated from the target matrix. This is most often carried out either via extraction chromatography using a suitable solid phase or ion exchange chromatography.

The main focus of this study was to compare two methods, namely ion exchange chromatography and extraction chromatography, for the separation of milligram amounts of scandium from gram amounts of calcium.

For extraction chromatography (Solvent Impregnated Resins (SIR), unimpregnated XAD-4 resin (pure Amberlite XAD-4 resin) was used as a preliminary sorbent for the sorption of scandium and calcium from aqueous solutions. Owing to a low% sorption (about 70%) obtained, the extractant, Di-2-Ethylhexyl phosphoric acid (D2EHPA), was impregnated in the Amberlite XAD-4 resin for the sorption and separation of scandium and calcium from aqueous solutions. The Di-2-Ethylhexyl phosphoric acid - Amberlite XAD-4 impregnated resin (D2EHPA – XAD-4 impregnated resin) was prepared using the dry method of impregnation. The optimal conditions for the impregnation of the extractant (D2EHPA) were investigated using different volumes of the extractant (D2EHPA), ranging from 1 mL to 25 mL. The maximum value for the distribution coefficient was observed at a volume of 12mL of the extractant, which is approximately 11,500 g D2EHPA/g XAD-4.

X-Ray Diffraction (XRD), Fourier Transform Infrared Spectroscopy (FTIR), Brunauer-Emmett-Teller (BET), Scanning Electron Microscopy (SEM), and Transmission Electron Microscopes (TEM) techniques were used to characterize the physical properties of the unimpregnated and impregnated resins. Parameters such as sorbent dosage, pH, contact time, and initial metal ion concentration were investigated for the batch sorption studies of scandium and calcium using the D2EHPA – XAD-4 impregnated resin. The sorption studies were quantified using Inductively Coupled Plasma-Optical Emission Spectroscopy (ICP-OES). Experimental equilibrium data were subjected to four isotherm models (Langmuir, Freundlich, Temkin and Dubinin-Radushkevich). The kinetic reactions were assessed using pseudo-first order, pseudo-second order reactions, and the Weber Morris diffusion model.

The XRD spectra obtained for the unimpregnated and impregnated resin before adsorption, and impregnated resin after the adsorption showed no significant differences. The FTIR spectra showed minor changes in the P=O bond (1225 cm^{-1}) and the P-O-C stretching (1024 cm^{-1}) for the D2EHPA - XAD-4 impregnated resin compared to unimpregnated XAD-4, indicating the interaction between D2EHPA and the Amberlite XAD-4 resin. A decrease in surface area and an increase in pore size of the impregnated XAD-4 resin compared to the unimpregnated resin was observed, further supporting the impregnation of the extractant (D2EHPA) into the pores of the XAD-4 resin. The aggregated morphology of the unimpregnated resin appeared more agglomerated after impregnation with D2EHPA in both the SEM and TEM results, confirming the uptake of D2EHPA within the resin structure.

Batch adsorption studies demonstrated that the impregnated resin has a stronger affinity for scandium at a lower pH value (pH=2) compared to calcium (pH=4). The obtained sorption capacity for scandium, at a concentration of 2.0 mg/L, was in agreement with the maximum sorption capacity in the pH studies. The acquired sorption capacity for calcium (0.2428 mg/g) at a concentration of 10.0 mg/L was closely compared with the maximum sorption capacity in the pH studies. A scandium sorption efficiency of 100%, with a sorption capacity of 0.1 mg/g, was observed within the first 6 minutes. The maximum sorption efficiency (100%) for calcium was achieved within 15 minutes.

The Langmuir isotherm provided the best fit for the scandium sorption data, and the Dubinin-Radushkevich isotherm fitted the calcium sorption data best. The sorption energy calculated from the Dubinin-Radushkevich plot for both Sc and Ca metals could be the confirmation of a chemical mechanism process. The adsorption data for both Sc and Ca followed pseudo-second-order reaction kinetics, and theoretically, the second-order kinetics is customarily associated with chemisorption. Theoretical data had a good correlation with experimental data. The multi-linearity shown by the Weber-Morris diffusion model for both metals suggests both pore and film diffusion mechanisms are present and can thus control the sorption process.

For ion exchange chromatography, the sorption behaviour of scandium and calcium was assessed using Dowex 50W-X8 cation exchange resin in various HBr-methanol mixtures. Based on the experimental distribution coefficients and separation factors, a two-component separation of scandium and calcium was performed in a 2M HBr– 60% methanol mixture using a column method. The results showed that 100% of the scandium was absorbed by the resin and all of the calcium was eluted after 30 min (14 fractions) using 2M HBr-60% methanol mixture. Scandium was completely eluted after 14 min (7 fractions) using 5M HCl.

Published Articles (s)

One full research paper has been published from this study by Springer at the Monatshefte für Chemie/Chemical Monthly, an International Journal of Chemistry. The abstract of the published paper is screenshotted and presented below.

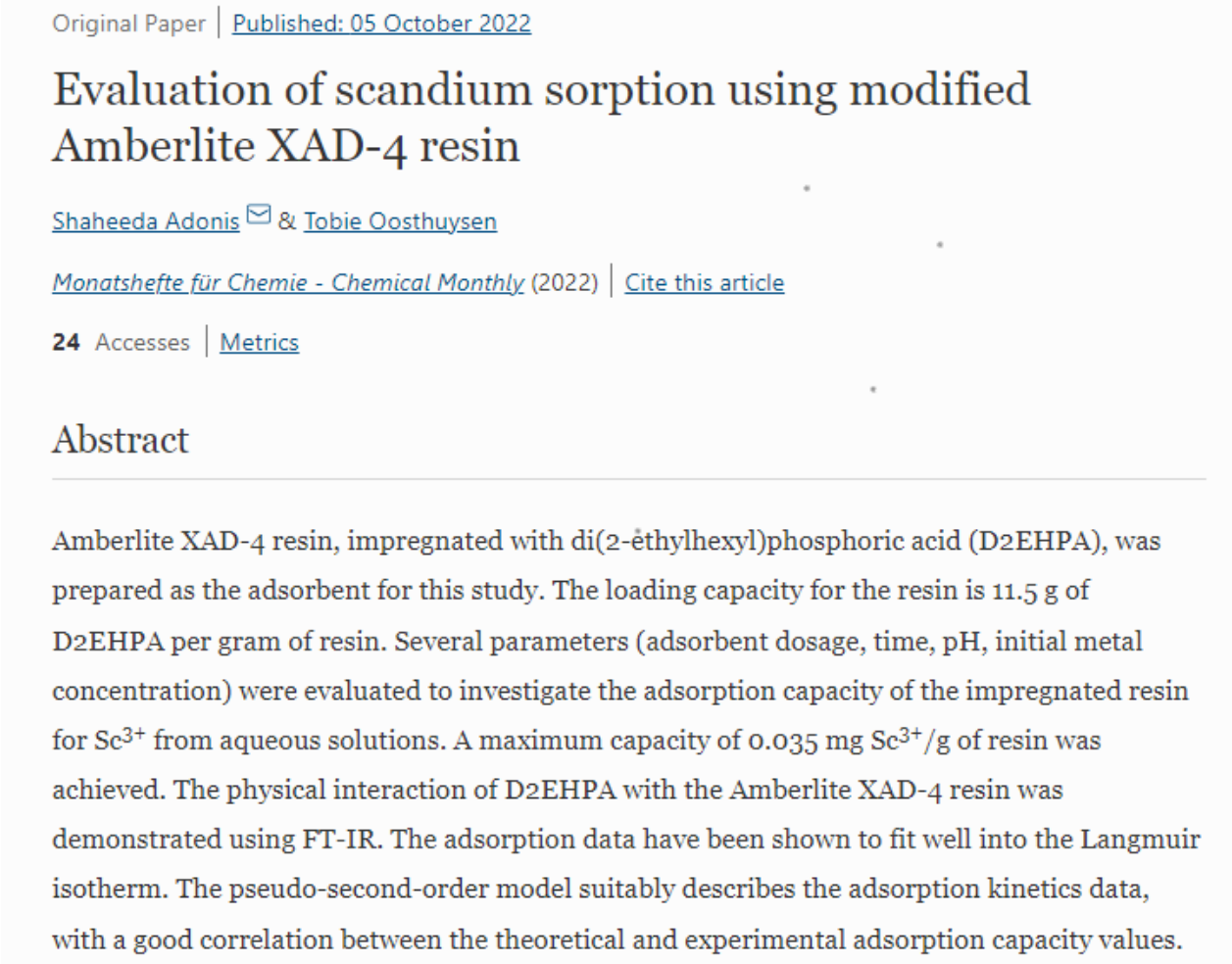

Original Paper | Published: 05 October 2022

Evaluation of scandium sorption using modified Amberlite XAD-4 resin

Shaheeda Adonis & Tobie Oosthuysen

Monatshefte für Chemie - Chemical Monthly (2022) | Cite this article

24 Accesses | Metrics

Abstract

Amberlite XAD-4 resin, impregnated with di(2-ethylhexyl)phosphoric acid (D2EHPA), was prepared as the adsorbent for this study. The loading capacity for the resin is 11.5 g of D2EHPA per gram of resin. Several parameters (adsorbent dosage, time, pH, initial metal concentration) were evaluated to investigate the adsorption capacity of the impregnated resin for Sc^{3+} from aqueous solutions. A maximum capacity of 0.035 mg Sc^{3+}/g of resin was achieved. The physical interaction of D2EHPA with the Amberlite XAD-4 resin was demonstrated using FT-IR. The adsorption data have been shown to fit well into the Langmuir isotherm. The pseudo-second-order model suitably describes the adsorption kinetics data, with a good correlation between the theoretical and experimental adsorption capacity values.

The paper can be cited as:

Adonis, S. & Oosthuysen, T. 2022. Evaluation of scandium sorption using modified Amberlite XAD-4 resin. *Monatshefte für Chemie-Chemical Monthly*, 1-12.

ACKNOWLEDGEMENTS

First and foremost, I want to express my gratitude to the Almighty for His abundant grace and mercy throughout this study

I would also like to express my sincere gratitude to:

- To my husband and children for their sacrifices, unconditional love, and always believing in me.
- My supervisor, Dr Tobie Oosthuysen, for your advice, patience and great assistance in guiding me through the completion of my thesis. Your comments pushed me to enhance my ideas and raise my standard of work.
- To my late co-supervisor, Professor Nico Van der Walt, for your guidance, motivation, and moral support during my PhD journey.
- Dr Dorcas Zide, thank you for your assistance and all the constructive critics. It is much appreciated.
- To my family, friends, and colleagues for all your encouragement and support.
- To the technical staff at CPUT, Bellville campus, Mrs Zandile Mthembu, and Mrs Gillian Fennessy-Yon, thank you for all your support.
- Cheryl Thomson, for her support and language and technical edit of this thesis.

DEDICATION

This dissertation is dedicated to my mother, Elizabeth Adams, and my husband and children. I cannot thank you enough for your unconditional love, support, and encouragement.

TABLE OF CONTENTS

LIST OF TABLES

LIST OF FIGURES

LIST OF APPENDICES

ABBREVIATIONS AND ACRONYMS

D2EHPA	Di-2-ethylhexyl phosphoric acid
SX	Solvent extraction
SIR	Solvent impregnated resins
K_d	Distribution coefficient
HBr	Hydrobromic acid
TBP	Tributyl phosphate
S-DVB	Styrene-divinylbenzene
HCl	Hydrochloric acid
PES	Polyethersulfone
NMP	N-methyl pyrolidone
PVA	Polyvinyl alcohol
ICP-OES	Inductively coupled plasma optical emission spectroscopy
PXRD	Powder X-Ray Diffraction
FTIR	Fourier Transform Infrared
BET	Brunauer-Emmett-Teller
SEM	Scanning electron microscope
TEM	Transmission Electron Microscopy

CHAPTER 1
INTRODUCTION AND BACKGROUND TO THE STUDY

1.1 Background

Lately, there has been adequate attention on scandium owing to its rising demand. Scandium is a pioneering material with applications in metallurgical, chemical, and electronic industries (Li et al*.,* 2018). The growing demand for scandium and its compounds in the chemical, optical, laser, and medical industries can be ascribed to their unique optical, mechanical, and electrical properties (Haque et al*.,* 2014; Xie et al*.,* 2014). Scandium is also applied in solid oxide fuel cells (Liu et al., 2010), organic chemistry catalysts (Kobayashi & Manabe, 2000), high-intensity discharge lamps, and as an alloying agent (Ahmad, 2003). According to Sharaf and co-workers, the price of scandium has risen from 2.54 US$/g in 2009 to 4.6 US$/g in 2016 (Sharaf et al*.,* 2018). The insufficiency of scandium is the empowering force for a magnified market price of scandium-based compounds such as scandium oxide and ingot metal (Ramasamy et al*.,* 2018). Scandium belongs to rare-earth elements, which denotes the insufficiency of concentrated deposits. It occurs in trace amounts (Sharaf et al*.,* 2018). As a result, scandium is recovered as a by-product from residues and tailing wastes, often containing much higher concentrations of Fe, Al, and other metals (Ramasamy et al*.,* 2018). Owing to the low abundance of scandium, the main route of its production is as a by-product during the processing of ores having a scandium content ranging between 20 ppm to 50 ppm (Wang et al*.,* 2011).

The separation and purification of scandium from aqueous solutions are customarily executed using precipitation, solvent extraction, and ion exchange chromatography. The downside of these methods includes but is not limited to the low scandium purity that yields from precipitation as a result of the co-precipitation of other metals present (Wang & Cheng, 2011). In addition, a large volume of organic reagents is required, sediment generation, and inefficiency for low concentrations (Van Nguyen et al*.,* 2016). Solvent extraction (SX) is a technique that is frequently used to separate and purify scandium from large amounts of impurities in leachates. Various scientists investigated the separation of scandium using many extractants such as di-2-Ethylhexyl phosphoric acid (Wang et al*.,* 2013), Cyanex series extractants (Nie et al*.,* 2018), tributyl phosphate (Zhang et al*.,* 2016), N-[N, N-di-(2-Ethylhexyl) aminocarbonyl methyl] glycine (Baba et al*.,* 2014) and betainium bis (trifluoromethylsulfonyl)imide [Hbet][Tf_2N] (Onghena and Binnemans 2015). Despite the advantages of solvent extraction, it also has a few drawbacks, such as loss of extractant, especially for the organophosphorus extractants (Van Nguyen et al*.,* 2013)

Ion-exchange chromatography displays high adsorption capacity and less complex operations, as well as lower maintenance costs than solvent extraction (Kumar & Jain 2013; Fadel et al*.,*

2016). Ion exchange chromatography has been shown to be advantageous in the separation of some problematic elements. Zirconium was separated from scandium by sorption with KRF-20t-60 cation exchanger successfully (Sokolova, 2001). The ampholite resins AFI-21 and AFI-22 were used to extract scandium and uranium from red mud (Smirnov & Molchanova, 1997; Zhou et al*.,* 2018). Separated Al, Fe(II) and (III), Ca, Zr and Ti from scandium chloride solutions using 732-type resin.

Extraction chromatography has progressively come to play a prominent role in the separation of scandium and many other metals for different applications. Extraction chromatography is a simple and effective method for the separation of a variety of metal ions. Extraction chromatographic materials are commonly known as extraction chromatographic resins or solvent-impregnated resins (SIR). Solvent-impregnated or chelating resins offer an alternative method for separating metal ions from each other. The use of solvent-impregnated resins dates back to the early 1970s. Solvent-impregnated resins (SIRs) involves incorporating the extractant (ligand) by physical impregnation into macroporous polymeric support (Warshawsky et al*.,* 1997). SIRs can selectively bind to specific metals owing to an organic functional group(s) impregnated into the support. SIRs have the combined advantage of ion exchange and solvent extraction (Bao et al*.,* 2016). SIRs have the benefits of having a wide selection of available extractants, simple and easy preparation and the ability of continuous operation. Regardless of SIRs being a good alternative to solvent extraction and ion exchange for the separation and purification of scandium, a review of published literature indicate the lack of research in this regard.

Organophosphorus extractants are preferred for the separation and purification of scandium. Several materials can be used as sorbents, such as inorganic materials such as silica gel, organic polymers such as polystyrene-divinylbenzene copolymers and polymethacrylate resins (Tranter, 2011). The most suitable sorbents for SIRs are macroporous polymeric resins. Their high specific area, high mechanical strength and low solvent swelling during the impregnation process make it possible to incorporate large amounts of extractant. The Amberlite XAD resins are the most commonly used macroporous polymeric resins. Taute et al. (2013) used the D2HEPA- Lewatit VP OC 1026 impregnated resin and Bao et al. (2016) used the PC-88A –XAD-7 impregnated resin for their separation studies of scandium. The elution of the adsorbed metal ions, however, posed to be a challenge. A recent study was done by Bao et al*.* (2018) using a Lewatit TP 272 solvent-impregnated resin and the Lewatit TP 260 and 209 chelating resins for the separation of Sc from Fe(II) and Al(III) reported selective adsorption of Sc over Fe(II) and Al(III).

1.2 Research problem

There has been an increased demand for scandium in the 21st century owing to its wide-

ranging applications such as aerospace, special alloys, electronics and the nuclear industry. However, the growing application of scandium in new technologies raised concerns about its accumulation in the environment following anthropogenic inputs (Pyrzyńska et al*.,* 2019). As a result, the recovery and separation of scandium have attracted a lot of attention (Yagmurlu et al*.,* 2018).

As the demand for new scandium sources exists, there is a need to develop an environmentally friendly and cost-effective method for the separation and purification of scandium. Several methods have been employed to separate and purify scandium for different applications (Pyrzyńska et al*.,* 2019). Solvent extraction is the most commonly used method (Wang & Cheng 2011). Yet, the drawbacks of solvent extraction persist, such as the uses amounts of solvent, which poses an environmental risk. Also, the loss of extractant, phase separation, and third phase formation, cannot always be easily overcome (Van Nguyen et al*.,* 2013).

The radioactive isotopes of scandium, in particular, have generated interest for use in radiopharmaceuticals, for both medical imaging and radiotherapy, already several decades ago, but this has not so far lead to clinical deployment of scandium radionuclides. Scandium-44 is a medically interesting positron and gamma emitting radionuclide. It is commonly produced using a cyclotron in a calcium or sometimes a titanium based irradiation target. As the radiopharmaceutical use of scandium radionuclides commonly requires chelation, scandium needs to be separated from the target matrix. This is most often carried out either via extraction chromatography using a suitable solid phase or ion exchange chromatography. Several methods have been used to evaluate the separation of scandium from differnet target materials.

In this study, ion exchange chromatography and extraction chromatography methods are evaluated for their efficiency in separating milligram amounts of scandium from gram amounts of calcium in an aqueous solution. Ion exchange chromatography has certain benefits over solvent extractions, such as high adsorption capacity, less complex operations and lower maintenance costs (Fadel et al*.,* 2016). Extraction chromatography, however, is an easy and effective method for separating a variety of metal ions. It serves as a bridge between solvent extraction and the conventional ion exchange processes. The simple preparation, the cost effectiveness and the ease of using this separation method in a hot cell make it a viable alternative to existing methods.

The ion exchange chromatographic methods for the separation of scandium from calcium, the HBr-methanol combination have not been investigated yet. Other methods used include HBr-acetone. Extraction chromatographic methods have been used for the separation of scandium from calcium for nuclear medical application. The use of Amberlite XAD 4 with DEHPA for this

particular application has not been investigated. This method could serves as a more cost effective alternative.

1.3 Aim of the study

This study aimed to evaluate the efficiency of ion exchange and extraction chromatography and find the optimal conditions for separating milligram amounts of scandium from gram amounts of calcium. To achieve this aim, the efficiency of extraction chromatography and ion exchange chromatography was first assessed and optimized individually through batch sorption studies. Then, column separation studies were conducted based on the achieved optimal conditions.

The specific objectives of this study for each chromatographic method were as follows:

1.3.1 Extraction chromatography

i. To prepare the Di-2-Ethylhexyl phosphoric acid - Amberlite XAD-4 solvent-impregnated resin (D2EHPA–XAD-4 impregnated resin) by impregnating the extractant, Di-2-Ethylhexyl phosphoric acid (D2EHPA) in an Amberlite XAD-4 resin using a dry method.
ii. To optimise the parameter (s) volumes of the extractant (D2EHPA) ranging from 1mL to 25 mL were used to impregnate the extractant, D2EHPA in an Amberlite XAD-4 resin.
iii. To characterize the D2EHPA–XAD-4 impregnated resin and unimpregnated XAD-4 resin using XRD, FTIR, BET, SEM and TEM.
iv. To establish optimal sorption parameters (pH, initial metal concentration, contact time, sorbent mass) for maximum scandium and calcium sorption.
v. To predict and assess the performance of the selected sorption isotherms (Langmuir, Freundlich, Temkin or Dubinin-Radushkevich models) and kinetics models (pseudo-first order, pseudo-second order reactions, and the Weber Morris) studies of scandium and calcium elements.
vi. Perform desorption studies using various eluants.

1.3.2 Ion exchange chromatography

i. To determine the distribution coefficients (Kd) for the scandium and calcium on cation exchange resin, Dowex 50W-X8, with different HBr-methanol mixtures.
ii. To use the optimal equilibrium distribution coefficients (Kd) conditions in (i) to perform column separation of scandium from calcium in an aqueous mixture solution

1.4 Delimitations

The separation methods chosen in this study were ion-exchange chromatography and extraction chromatography (SIRs). This study compared the efficiency of these two methods for the separation of scandium from calcium owing to the high demand of the scandium from the variety of industrial applications such as aerospace, special alloys, electronics and the nuclear industry. Ion exchange chromatography and extraction chromatography are chosen because they are easy and effective methods for separating a variety of metal ions (Fadel et al*.,* 2016).

Batch sorption studies and column studies were done for both methods. The mathematical models used to describe sorption equilibrium and kinetics in this study were the ones most commonly used in similar studies. Certain parameters (column length and flow rate) of the more efficient separation method were investigated and maximised to ensure the most efficient separation. The methods were only subjected to synthetic solution.

1.5 Significance of the research

In this study, the separation studies of scandium from calcium were performed using ion exchange resin and solvent impregnated resin (extraction method) methods which could serve as a more cost-effective alternative method contrary to the commonly used solvent extraction methods (Wang & Cheng 2011), that posed many drawbacks such as environmental risk caused by the use amounts of solvent, the loss of extractant, phase separation, and third phase formation that cannot always be easily overcome (Van Nguyen et al*.,* 2013).

Findings from this study may be used for the separation and purification of scandium isotopes for medical applications. A significant amount of published literature is available to develop a separation method applicable to the radiochemical separation of scandium (Bokhari et al*.,* 2010; Valdovinos et al*.,* 2015; Deilami-Nezhad et al*.,* 2016).

1.6 Thesis layout

This thesis consists of six chapters, which are outlined below:

Chapter 1- Introduction: This chapter provides an overview of the growing application of scandium as a pioneering material in many industries and the methods currently used for its separation and purification. This chapter also outlines the outcomes and specific objections of this study.

Chapter 2- Literature Review: An overview of rare earth elements, with a main focus on scandium, is provided in this chapter. An overview of various separation methods for scandium is provided, given the main objective of this study.

Chapter 3- Materials and methodology: Experimental methods and analytical techniques used for the characterisation of the impregnated resin in this study are discussed.

Chapter 4: Presents the sorption and separation studies of scandium from calcium using the extraction chromatography method. The preparation and characterisation of the impregnated resin are presented and discussed. The optimisation and the application of the impregnated resin are discussed, displaying the results obtained for the effects of pH, concentration, time, and sorbent mass on the sorption for scandium and calcium.

Chapter 5: Presents the sorption and separation studies of scandium from calcium using ion exchange chromatography.

Chapter 6: Conclusions and recommendation for future work. In this chapter, the two chromatographic separation methods are briefly compared in terms of their efficiency based on the experimental findings that are extensively discussed in Chapter 4 and Chapter 5.

CHAPTER 2
LITERATURE REVIEW

2.1 Introduction

This chapter provides an overview of rare earth elements, their occurrence, chemical and physical characteristics, environmental impact and health concerns. The focus is on scandium as a rare earth element and the separation of scandium from aqueous solution using different methods. The focus is on ion-exchange chromatography and extraction chromatography.

2.2 Rare earth elements

Hydrometallurgical techniques have been widely used for metal extraction from low-grade resources for the last two decades (Tavlarides et al*.,* 1987). The recovery and separation of metals from aqueous solutions in hydrometallurgy, environmental research, analytical chemistry, nuclear materials and the medical industry have become key research areas (Bao et al*.,* 2016). The recovery and separation of rare earth elements are becoming increasingly important owing to their unique chemical and physical properties and their broad field of applications that contribute to vital sectors (Das & Das, 2013). Rare earth elements are also beginning to play an essential role in transitioning to a green, low-carbon economy. With hybrid and electric cars, wind turbines and compact fluorescent lamps are increasingly becoming more popular, leading to an upsurge in the demand and cost of rare earth elements (Binnemans et al*.,* 2013). The use of rare earth elements has increased since the 1990s. A historical view of the application of rare earth elements is shown in Figure 2.1. The widespread use and importance of rare earth elements prompted increased rare earth ore deposits. The resultant escalating release of these elements into the environment has become a concern for human health and environmental impact (Migaszewski & Gałuszka, 2015).

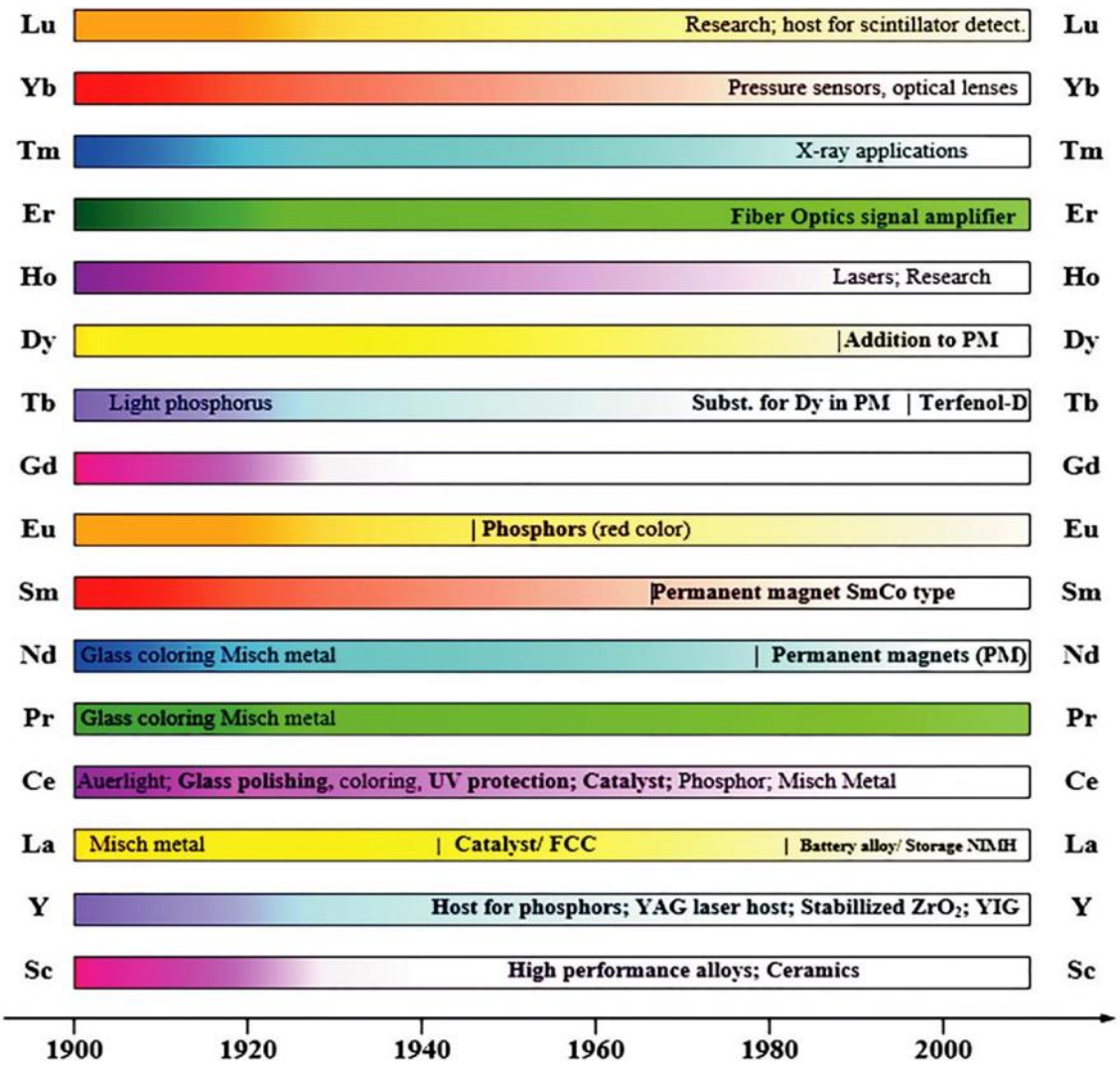

Figure 2.1: A historical view of the application of rare earth elements

2.3 Occurrence of rare earth elements

The rare earth elements are relatively abundant in the earth's crust and are thus not as rare as their name suggests. Rare earth elements are not naturally occurring metals. They occur in a wide range of mineral ores as primary or secondary deposits, including carbonates, oxides, phosphates and silicates. As much as rare earth occurs in many minerals, it is located in only a few geological environments (Balaram, 2019). The primary economic sources of rare earth minerals are bastnaesite, monazite, loparite and the lateritic ion-adsorption clays (Dostal, 2017). The primary deposits are generally associated with alkaline igneous rocks and are formed by metamorphic and hydrothermal. Secondary deposits result from erosion and weathering and are commonly associated with laterites and bauxites.

2.4 Chemical and physical characteristics of rare earth elements

The rare earth elements include the lanthanides, from lanthanum through to lutetium, including

ytterium and scandium, having similar chemical and physical properties. The rare earth elements exist in a trivalent state in nature, except for cerium (Ce^{3+}, Ce^{4+} and europium (Eu^{2+}, Eu^{3+}). The ionic radii of the rare earth decrease as the atomic number increases. Rare earth can be categorised into rare light earth and rare heavy earth, each having varying uses and demands. Lanthanum, cerium, praseodymium, neodymium and samarium are classified as light rare earth, and the heavy rare earth include europium, gadolinium, terbium, dysprosium, holmium, erbium, thulium, ytterbium, lutetium and yttrium (Emmanuel et al*.,* 2012). Owing to the unique magnetic, catalytic and phosphorescent properties of rare earth, they have become critically important to the technological world (Balaram, 2019).

2.5 Environmental impact and health concerns of rare earth exposure

Environmental contamination by various kinds of toxic inorganic, organic and organometallic species is becoming one of the major global concerns. The increased use of rare earth elements in modern industries to produce new materials and their many technological applications leads to the discarding of large amounts of electronic waste. This dumping aids in releasing these elements and other toxic elements into the soils and groundwater. Large quantities of rare earth elements are also released into agricultural soils through phosphate-based fertilisers (Balaram, 2019). Higher levels of rare earth are being released into the groundwater systems, and the atmosphere created new routes for bioaccumulation in plants, animals and human (Balaram, 2019). The current lack of understanding of the adverse effects of rare earth elements on human health and the environment highlights the need to understand the toxicological properties of rare earth elements, considering their extensive use in agriculture and medicine (Gwenzi et al*.,* 2018).

2.6 Scandium

Scandium is classified as a rare earth element. It has similar chemical properties as the rare earth element, having a low abundance in the Earth's crust and its stable 3+ oxidation state (Sc^{3+}) in aqueous solutions. Scandium has attracted much interest due to its numerous and vital applications in high-technology materials (Pęgier et al*.,* 2018). The growing use of scandium in various applications, such as catalysts, special alloys, nuclear materials, lasers, etc., resulted in a greater need to explore and produce scandium. The increased demand for scandium raises concerns about its accumulation in the environment due to anthropogenic inputs (Li et al*.,* 2013). In many ores, scandium occurs in trace amounts (Wang et al*.,* 2011). As a result of its low abundance, scandium is primarily produced as a by-product in the oxide form during the processing of various ores (Shaoquan & Suqing, 1996). To increase the supply of scandium, it became necessary to explore both the primary and secondary scandium-containing resources, particularly rare earth ore deposits and phosphoric ore (Jiyan et al*.,* 2013), bauxite ore (Liu et al*.,* 2009). With the recent increased demand for high-purity

scandium, scandium separation and purification processes received considerable attention.

2.6.1 Separation methods of scandium

Various techniques have been used to separate and purify scandium due to its growing demand in modern high-technology applications and its low abundance of natural minerals. The high level of purity of rare-earth required for its application in modern high-technological industries validates the need for effective separation techniques from an industrial and analytical point of view (Nash & Jensen, 2000). For recovering scandium from the various ores, leaching is often the most common acid medium method. Scandium is then separated and purified from the aqueous solution using different techniques such as chemical precipitation and solvent extraction (Wang et al*.,* 2013; Onghena & Binnemans 2015; Lu et al*.,* 2016; Van Nguyen et al*.,* 2016; Onghena et al*.,* 2017) adsorption and ion exchange (Ochsenkühn-Petropulu et al*.,* 1995; Avdibegović et al*.,* 2019). Leaching and precipitation methods are used to separate and recover scandium from low-grade scandium-bearing resources (Jha et al*.,* 2016). The purity of the products obtained from these methods is not very high.

Solvent extraction, ion-exchange chromatography and extraction chromatography (more recently) are the most widely used and applied techniques for separating scandium from various aqueous solutions. Despite solvent extraction being the most common technique used for separating and purifying scandium from aqueous solution, it had its disadvantages of high extractant loss and the use of large amounts of organic solvent (Abderrahim et al*.,* 2008). This study focused on ion-exchange chromatography and extraction chromatography as a method for scandium separation. A brief overview of solvent extraction will be done as well.

A number of methods have been developed and published for the efficient separation of microamount of scandium from excess amounts of calcium. Details of these are given in **Table 2-1.**

Table2.0-1:Summary of methods for separating scandium radionuclides from calcium targets

Methods	Solution of Sc elution	Vol. of Sc fraction	Yield of Sc recovery	Ref
Filtration	0.1M HCl	0.15	40%	Mamtimin et al. (2015)
Hydroxamate resin	0.1M HCl	1.0	63%	Domnanich et al. (2017)
Chelex 100	1M HCl	0.5	70%	Minegishi et al. (2016)
DGA + Dowex50Wx8	1M NaOAc	0.4	85%	Rane et al. (2015)
UTEVA	1M HCl	0.4	80%	Rotsch et al. (2018)

2.6.1.1 Solvent extraction

Solvent extraction is a much-publicised method and has been found to be one of the most widely used methods for separating and purification of scandium from aqueous solutions due to its high extraction capacity, high selectivity and high enrichment (Wang & Cheng, 2011; Baba et al*.,* 2014). The solvent extraction process involves the extraction of a metal ion from an aqueous phase into an organic phase that contains an extractant to create a neutral hydrophobic complex. Various scientists used different extractants to separate and purify scandium by solvent extraction. Cyanex 923 and Cyanex 925 extractants were used to study the extraction equilibria of Sc^{3+}, Zr^{4+}, Ti^{4+}, Th^{4+}, Fe^{3+} and Lu^{3+} from different acid media. The Cyanex 923 extractant demonstrated better scandium loading than Cyanex 925 (Li & Wang 1998). The extraction behaviour of selected rare earth elements (Sc, Y, Au and Gd) were investigated using bis(2,4,4 –trimethylpentyl)-mono thiophosphinic acid (Cyanex 302) in heptane. The results showed that the rare earth elements were extracted by a cation exchange mechanism (Wu et al*.,* 2004). The ionic liquid betainium bis(trifluoromethylsulfonyl)imide was used to evaluate the extraction of scandium from nitrate and chloride aqueous solution. The extractant was found to be suitable, with extraction efficiencies >95%, from solutions with pH ≥ 1.5 (Onghena & Binnemans, 2015). Three acidic organophosphorus extractants (Cyanex 272, Ionquest 801 and D2EHPA) were used to investigate scandium recovery from synthetic leach solutions. The D2EHPA extractant performed best among the three extractants. However, it showed poor phase separation and tributyl phosphate (TBP) as a phase modifier to overcome this problem. With a solution consisting of 0.05 M D2EHPA and 0.05 M TBP, 99% scandium was extracted (Wang et al*.,* 2013).

A review of published literature indicates that several organophosphorus extractants are being

used to separate scandium from aqueous solution. Scandium was successfully separated from other rare earth elements (Y^{3+}, La^{3+} and Yb^{3+}) using a Cyanex 925/ $[C_8mim][PF_6]$ extraction system. Infrared spectra of the extracting phase indicated a strong interaction between Sc^{3+} and Cyanex 925, which was evident that cation exchange was the extraction mechanism of scandium in this system (Sun et al*.,* 2007). The organophosphorus extractant, bis(2,4,4-trimethylpentyl) monothiophosphinic acid (Cyanex 302), was used to extract scandium from yttrium, gadolinium and lanthanum in a chloride medium. Scandium was completely stripped from Cyanex 302 with 5 M HNO_3 (Karve and Vaidya 2008). Di-(2-Ethylhexyl) phosphoric acid (D2EHPA), in particular, showed higher extraction efficiency than the other organophosphorus extractants for the separation of scandium.

Solvent extraction, however, has some shortcomings, such as:

- large-scale use of organic solvents, resulting in problems relating to waste disposal.
- time-consuming
- third phase formation
- loss of extractant during extraction.

2.6.1.2 Ion exchange chromatography

Ion exchange dates back to the 1940s, when it was explicitly designed to separate oppositely charged ions. This technique involves an insoluble stationary phase and a mobile phase. The ion exchange resins (stationary phase) are insoluble in most aqueous or organic solvents and consist of a cross-linked polymer matrix to which charged functional groups are attached by covalent bonding.

Ion exchange resins are naturally occurring inorganic materials or synthetically produced polymeric resins. The latter is most commonly used. Clay minerals and zeolites are characteristic representatives of inorganic ion exchange materials. They are crystalline hydrated aluminosilicates of alkali and alkaline earth cations with a three-dimensional structure (Mumpton, 1999). The first synthetic ion exchange resins were prepared more than a century ago. Synthetic organic resins are predominantly used today. The organic resins consist of a three-dimensional network matrix of macromolecular hydrocarbon chains consisting of a copolymer of styrene and divinylbenzene (S-DVB).

2.6.1.2.1 Synthesis of ion exchange resins

The synthesis of an organic resin is an intricate process. Suspension polymerisation is the classical method used for the preparation of organic resins. This process involves mixing monomers, which are then added to a vigorously agitated solution. The reaction mixture forms small droplets. The addition of a stabiliser, such as polyvinyl alcohol, magnesium silicate or gelatin, prevents the coagulation of these droplets. The reaction mixture is heated to a

stipulated temperature for polymerisation (80ºC–100ºC), upon which the tiny droplet polymerise to form the polymer beads. The basic structure of the polymer resin is provided by the styrene molecules, and the divinylbenzene (DVB) crosslinks the polymers to enable the durability and insolubility of the resin. The degree of crosslinking is vital to the resin to ensure the stability of the structure (Chanda, 2017). Functional groups are attached to the resins to give chemical functionality to the resin beads. The nature and number of functional groups and crosslinking determine the resin's chemical, thermal and mechanical stability (Zagorodni, 2006).

2.6.1.2.2 Classification of ion-exchange resins

Synthetic/organic ion exchange resins can be categorised into three main types: cation exchangers, anion exchangers, and selective chelating exchangers, depending on the chemical properties of the functional group. This study will be limited to the use of cation exchange resin.

Cation exchange resins have acidic functional groups that can exchange H^+ ions with surrounding solutions. A wide range of cation exchange resins with functional groups of different acid strengths is available, ranging from strong acid cationic exchange resins produced by the sulfonation of the styrene-DVB copolymer beads to weak-acid resins containing the carboxylic group. The production of strong acidic cationic exchange resins involves the introduction of the sulfonic group (SO_3^-) onto the polystyrene-DVB copolymer by reaction with sulphuric acid. Sulphuric acid is used to functionalise the copolymer beads. Strong acid cationic exchangers are favourable due to their constant exchange capacity over a wide pH range (Harland, 1994). Figure 2.2 illustrates the structure of a cation exchange resin.

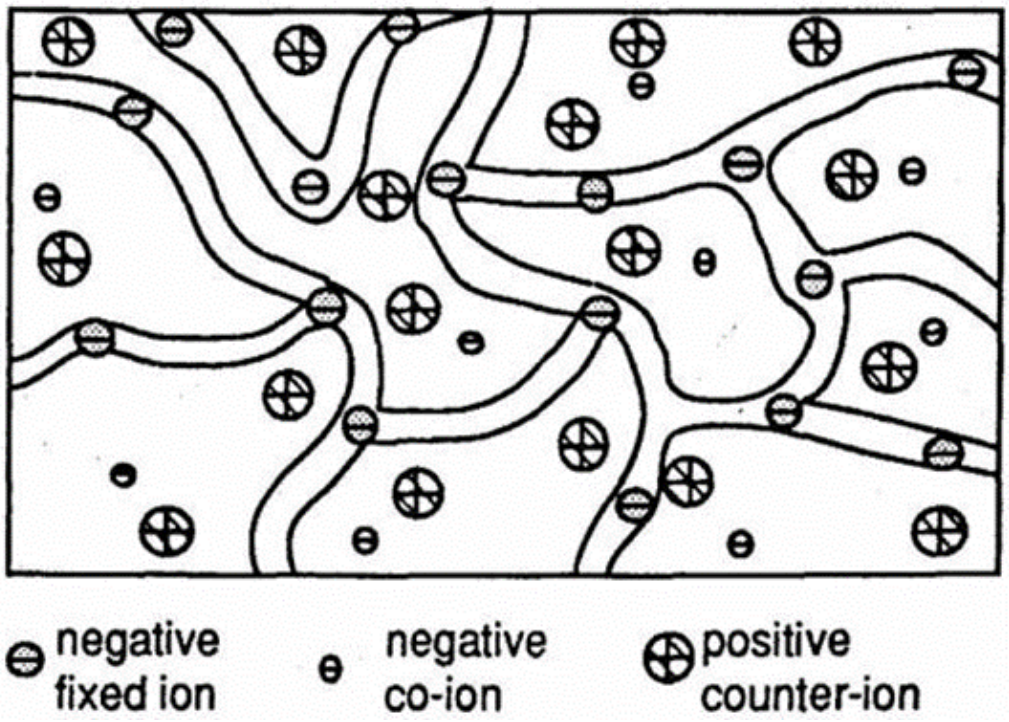

Figure 2.2: Structure of cation exchange resin

Source: Harland, 1994

The weak-acid cationic exchangers contain carboxylic acid functional groups and are prepared by the copolymerisation of an acid anhydride or an organic acid with a crosslinking agent. This is done by the combination of acrylic or methacrylic acid with divinylbenzene (Harland, 1994).

2.6.1.2.3 General properties of ion exchange resins

When preparing a synthetic resin, the main objective is to obtain a high-quality resin with high exchange rates, good chemical stability and mechanical strength, and high capacity. The general properties of synthetic resins will be briefly discussed below.

a) Particle Size

Particle size is vital in the resin's separation efficiency and ion exchange kinetics. The particle size of resin beads is obtainable in various sizes from 20-50 mesh, 50-100 mesh, 100-200 mesh, and 200-400 mesh. The required particle size depends on the application. The 50-100 mesh size resins are commonly used for batch experiments, whereas the 100-200 mesh size resins are used to investigate the distribution coefficients of metal cations for column separation studies. The larger mesh size resins are used for higher-resolution analytical separations.

b) Porosity

The porosity of a resin is defined as the ratio of the volume of voids to the total volume of the resin. The most commonly formed resins are macroporous sizes ranging from 5 -50%, which influences the resin's capacity and selectivity. The degree of resin crosslinking and the production process significantly influence the shape and size distribution of pores in the particles of ion exchange resins. The porosity of the resin beads contributes significantly to the overall surface area of the resin particles. In microporous resins, having diameters of less than 2 mm, the solute particles diffuse through the resin particle to interact with exchange sites, resulting in slow exchange kinetics. Macroporous resins, having larger diameters and surface areas, permit quicker and easier access to the exchange sites, thus resulting in faster exchange kinetics (Akelah, 2013).

c) Crosslinking and swelling

The crosslinking of a resin influences the mechanical strength, exchange capacity, and swelling in aqueous solutions. A decrease in the cross-linkage of a resin results in an increase in the permeability of the resin and allows the resin to accommodate larger ions. Low crosslinked resins (2%-4% S-DVB) will have a high degree of permeability and can accommodate larger ions and reach equilibrium more rapidly. Resins having high cross-linkage (8%-16% S-DVB) will have opposing properties than low crosslinked resins. The swelling of resins decreases with an increase in crosslinking. The exchange capacity of resins in the wet state decreases with decreasing crosslinking because of more noticeable swelling (Dorfner, 2011).

2.6.1.2.4 Ion exchange theory

The ion exchange mechanism involves the separation of ions according to their charge. When a sample is passed through a column whose packing consists of charged functional groups covalently bound to an insoluble support, the neutral ions or ions that have the same charge as the functional groups are eluted. The oppositely charged ions compete with the counterions for binding sites on the functional groups. Ions having a higher charge than the counterions are bound to the matrix and retained on the column. An eluent having a suitable pH and ionic strength will be selected to recover the bound sample.

2.6.1.2.5 Selectivity of ion exchange resins

Selectivity is the difference in affinity between individual ions. The selectivity of an ion exchange resin depends on the type and concentration of the reacting ions, the quality of the solvent and the nature of the exchange resin. When an ion exchange resin is brought into contact with an aqueous solution, an exchange reaction between the ions in the solution and the ion exchanger takes place according to the following reaction:

$$RsA + B+ \leftrightarrow RsB + A + \qquad \textit{Eq. 2-1}$$

where R_s is the resin matrix.

The reaction goes to equilibrium in a closed system because the ion exchange is a reversible process. The ions' equilibrium concentrations depend on the ion exchange affinity of the reacting ions to the ion exchanger and their initial concentrations. The affinity of various ions to the same resin was observed to increase with increasing ionic charge. However, for ions with the same charge, the affinities are inversely proportional to the radius of the hydrated ions (Korkisch, 2017). Primarily, the selectivity of an ion exchange resin depends on the following factors:

a) Selectivity of the resin increases with increasing content of the crosslinkage substance, e.g., divinylbenzene.
b) Ions with a smaller effective hydrated ionic radius are preferentially adsorbed.
c) If the ionogenic group of resin forms an ionic pair with the reacting ion, the selectivity of the resin to this type of ion is increased.
d) If substances in the solution form slightly dissociated compounds, then ions forming a more dissociated compound are preferentially adsorbed.
e) The selectivity of the resin decreases with increasing temperature.

Selectivity coefficients, distribution coefficients (K_d) and separation factors can be used to describe ion exchange equilibria (Korkisch, 2017).

2.6.1.2.6 Ion exchange equilibrium

a) Selectivity coefficients

The selectivity coefficient is defined as the ratio of the molar fractions of the exchanging ion pairs A and B in the resin and solution phases, respectively. The selectivity coefficient, $k_{,B,A}$, is expressed by the equation:

$$kB,A = \frac{[RsB]a\,[A]b}{[RsA]b\,[B]a} \qquad \textit{Eq. 2-2}$$

Where [ ] is the concentration (M) of the ion A or B, and a and b are the absolute charges of ions A and B, respectively. The selectivity coefficients are determined using the batch method and are used in connection with the determination of the distribution coefficients (Korkisch, 2017).

b) Separation factor

The separation factor, $\alpha\frac{B}{A}$, the ratio of the distribution coefficients of two different elements that were determined under specific experimental conditions is given by the ratio of the distribution coefficients of two different elements. The ratio determines the efficiency of the separation of

two elements via ion exchange. The separation factor can be expressed as shown in the following equation:

$$\alpha \frac{B}{A} = \frac{DB}{DA} \qquad \textit{Eq. 2-3}$$

A separation factor greater than 10 normally suggests efficient separation of ions A and B on a given resin (Korkisch, 2017).

c) Equilibrium distribution coefficients

The degree to which a metal ion is sorbed onto an ion exchange resin is determined by its distribution coefficient. The distribution coefficient, K_d, can be calculated by the following equation (Korkisch, 2017):

$$\frac{mass\ of\ element\ on\ resin(g)\ X\ volume\ of\ solution\ (mL)}{mass\ of\ element\ in\ solution\ (g)\ X\ mass\ of\ resin\ (g)} \qquad \textit{Eq. 2-4}$$

The distribution coefficient is most probably the most useful tool in ion-exchange chromatography. It helps to predict the behaviour of ions and, consequently, the elution order from a column (Smith-Jones et al*.,* 1986)). Distribution coefficients can be obtained by the batch method or the column method.

In the batch method, which is the method used in this study, the distribution coefficients were determined by adding a known amount of ion exchange resin to a known volume and composition solution. After equilibration, the resin was separated from the aqueous phase by filtration, and the metal ion in question was determined by analysing the filtrate (Korkisch, 2017).

2.6.1.2.7 Ion exchange process

The batch and column methods are the two methods used to bring the exchanger into contact with the ions in the solution. The batch method is more quantitative. The column method is the most suitable for separating two or more ion solutions. In this method, a solution containing the ions of interest is passed through the column and washed with small quantities of an eluting agent. The sorbed ionic species with different affinities for the ion exchanger will move at different rates through the column, separating the ionic species.

2.6.1.2.8 The ion exchange application in scandium separation

The separation of scandium from aqueous solutions using different types of ion exchange resins has been investigated by many researchers. The sulfonic cation exchange resins are ordinarily utilised to extract scandium from an aqueous solution (Peng et al*.,* 2018). Scandium was successfully adsorbed with the Dowex-50W-X8 resin, and desorption was achieved with

1.75M HCl (Akcil et al*.,* 2018). Scandium (Sc^{3+}) was separated from zirconium (Zr^{4+}), silicon (Si^{4+}) and titanium (Ti^{4+}) using a strong acidic styrene system cation exchange resin. The results showed that a pH of 2 and a contact time of three hours were optimal for scandium adsorption (LI et al*.,* 2016). A novel ion exchange resin containing amic glycol acid was synthesised to study the possible separation and recovery of scandium from an aqueous chloride solution. The resin effectively and selectively absorbed scandium at a solution pH of 1. The sorption kinetics was, however, very slow, and the optimal contact time was 24 hours. Scandium was successfully eluted from the resin using 2M HCl at 80^{o}C (Van Nguyen et al*.,* 2015). The sorption of scandium from simulated uranium leach liquors was studied using the following phosphorus-containing ion exchange resins, namely Purolite D 5041, Tulsion CH 93, Lewatit TP 260 and Purolite S 950. The Tulsion CH-93 resin displayed the highest ion exchange capacity and distribution coefficient for scandium. An elution solution containing 180 g/L Na_2SO_3 allowed for 94% of scandium to be eluted.

2.6.1.3 Extraction chromatography

Extraction chromatography proved to be an alternative method for the separation of metal ions to both solvent extraction and ion exchange chromatography. This separation technology was developed on the principles of ion exchange and solvent extraction. This technique is based on the modification of a solid support with an extractant that has selectivity towards metals. The extractants are generally in liquid form. Metal ions are essentially removed from the aqueous phase to active sites of the modified solid phase (Dave et al*.,* 2010).

Extraction chromatographic materials are also known as extraction chromatographic resins or solvent-impregnated resins (SIR). The concept of extraction chromatographic resins or solvent-impregnated resins (SIR) as a novel separation and recovery technique was proposed in the early 1970s (Cortina & Warshawsky, 2021). SIRs are characterized by having the following advantages over solvent extraction and ion exchange chromatography, namely:

- high efficiency and selectivity
- convenient preparation and ease of operation, which is a combination of the unique advantages of solvent extraction and ion exchange (Bao et al*.,* 2016)
- short analysis time
- small use of organic solvents
- high reusability of resin, without significant loss of metal extraction capacity

SIRs consists of three main parts: solid support, a stationary extractant phase and a mobile fluid phase. The three phases of solvent-impregnated resins (SIR) are illustrated in Figure 2.3.

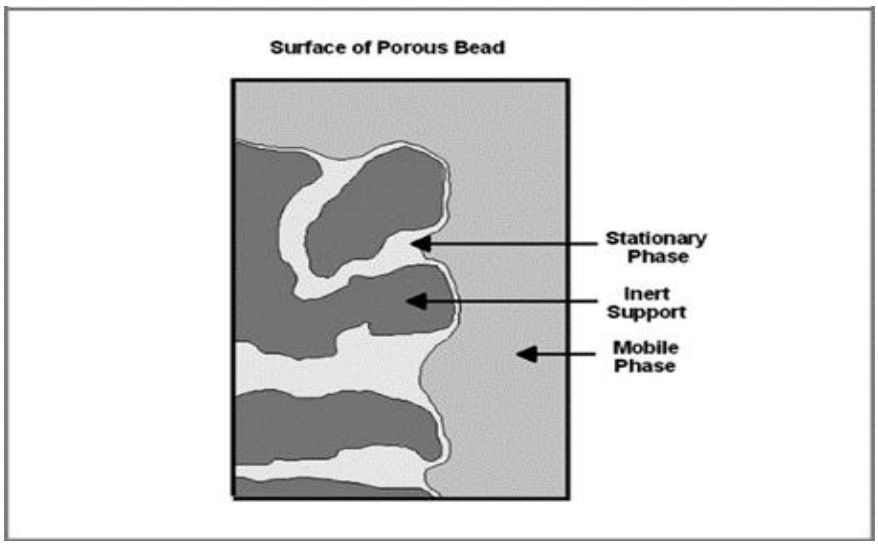

Figure 2.3: Extraction chromatography resin bead

Several materials can be used as a solid support, for example, an inorganic material such as silica gel, organic polymers such as polystyrene-divinylbenzene copolymers and polymethacrylate resins (Tranter, 2011). The most suitable solid support for SIRs is macroporous polymeric resins. Their high specific area, high mechanical strength and low solvent swelling during the impregnation process make it possible to incorporate large amounts of extractant. The Amberlite XAD resins are the most commonly used macroporous polymeric resins.

The stationary phase is usually an organic extractant. As in liquid-liquid extraction, the metals of interest are converted from the hydrated ionic form to a neutral organophilic metal complex within the stationary phase. The selected organic extractant should satisfy certain criteria such as high solubility in organic solvents, slight solubility in an aqueous medium, suitable kinetics and thermodynamics towards the metal ion, complexation abilities with the metal ion, acidic stability, non-volatile and inflammable (Momen et al*.,* 2019)

The performance of an extraction chromatographic material is characterised in terms of seven parameters: retention, selectivity, efficiency, capacity, stability (physical, chemical, and radiolytic), ease of reuse, and reproducibility.

2.6.1.3.1 Preparation of SIRs

The most commonly used methods for the preparation of SIRs are based on the physical adsorption of the extractant into the pores of the support material. Over the last 4 decades, literature reported preparation methods mainly involving the adsorption of the extractant into the pores of a polymer substrate (impregnation) or adding the extractant to a mixture of monomers during the bead polymerization process, i.e. the well-known Levextrel resins

(Yoshizuka et al*.,* 1990). (Warshawsky, 1981) and (Cortina & Warshawsky 1997) have done reviews of the methods for the efficient preparation of SIRs and have classified them as follows.

a) Dry method

This method is the most commonly used for the preparation of SIRs, where the extractant, diluted in an appropriate organic solvent, is placed in contact with the polymer for a certain period until maximum adsorption of the extractant within the lattice of the polymer occurs. The solvent is then removed via evaporation.

b) Wet method

In this method, the extractant is dissolved in an appropriate organic solvent and placed in contact with the polymer until all of the solvents are adsorbed by the polymer. The resultant resin beads are then placed in a metal ion solution and washed with distilled water after forming the metal-extractant complex. This is followed by eluting the metal using acid and rewashing the resin with distilled water. The resulting SIR is then ready for use. An alternative to this method is to first form the metal-extractant complex in the liquid phase and then impregnate directly as per the method above.

c) Modifier addition method

A selected modifier, typically more polar than the extractant to promote water penetration into the polymer, is added to the extractant solvent. The mixture is adsorbed into the polymer as per the dry and wet methods. The solvent is then removed by evaporation, resulting in a polymer-extractant-modifier resin. A standard modifier used is dibutylpolypropylene glycol.

d) Dynamic column method

After fully swelled by the solvent, the polymer is packed in a column. The extractant solution is passed through the column until the extractant concentration of the feed is similar to the outlet. The SIR is then rinsed with distilled water. This method of preparation has the advantages of short impregnation time and high efficiency.

2.6.1.3.2 Support materials for SIRs

Macroporous polymers are the most commonly used support substrates in the preparation of SIRs (Horwitz et al*.,* 2006). These macroporous polymeric resins have a rigid three-dimensional structure, which allows for minimum solvent swelling during impregnation and can absorb large amounts of extractant due to their high specific surface and large pores (Van Hecke & Goethals, 2006). It is commonly assumed that physical adsorption is the primary way to incorporate the extractant into the pores of the macroporous polymeric resins (Zagorodni, 2006). The physical properties of the support can significantly affect the adhesion strength of

the SIRs, which ultimately affects the adsorption performance of the SIRs. Thus, the preparation and adsorption characteristics of SIRs are closely linked to the support properties (Kumar et al*.,* 2011). As mentioned earlier, the Amberlite XAD resins are the most commonly used macroporous polymeric resins for SIR preparation. The resins in the Amberlite XAD series exhibit non-polar behaviour in solutions and are good at retaining organic extractants and ionic compounds (Iqbal & Datta 2022). Ion exchange resins can also be used as support substrates for SIRs. The basic anion-exchange resin, Lewatit MP 600, was impregnated with 8-hydroxyquinoline-5-sulfonic acid (HQS) using the wet method for cadmium chelation (Wang et al*.,* 2003).

2.6.1.3.3 Extractants in SIRs

Many organic substances can coordinate with metals in an aqueous medium to form metal complexes that are soluble in organic solvents. These organic substances are known as extractants (Rydberg, 2004). The efficiency of the SIRs in the purification and separation of metals largely depends on the extractant. Over the last few decades, numerous ionic liquid extractants such as organic extractants, amine groups, quinine groups and macrocyclic groups have been used in the preparation of SIRs (Ren et al*.,* 2011). The extractants widely adopted for use in SIRs are acidic organophosphorus compounds. This can be attributed to their chemical stabilities, extremely low aqueous solubilities, high distribution ratios and selectivities of metals.

Only the organo-phosphorus extractant, Di-2-Ethylhexyl phosphoric acid (D2EHPA), will be considered in this study.

a) Organo-phosphorus containing SIRs

The acidic organophosphorus extractants include the following: di-(2-Ethylhexyl) phosphoric acid (D2EHPA), di-(2-Ethylhexyl) dithiophosphoric acid, (2-ethylhexyl) phosphoric acid–mono-(2-Ethylhexyl) ester and bis-(2,4,4-trimethylpentyl) phosphinic acid. The acidic organophosphorus compounds mainly exist as dimers in non-polar or low-polar organic solvents. This is due to strong intermolecular hydrogen bonding. This intermolecular hydrogen bonding between the acids is broken by preferential hydrogen bonding with water in the aqueous phase. For the scope of this study, we will mainly consider di-(2-Ethylhexyl) phosphoric acid (D2EHPA).

Amberlite XAD-7, impregnated with D2EHPA by the dry impregnation method, was used to remove Cr^{3+} ions from water. The effects of different physio-chemical parameters such as pH, contact time and initial concentration of Cr were investigated. The XAD-7-D2EHPA SIR revealed that it had an adsorption capacity of 5 mg Cr^{3+}/g SIR, and an adsorption performance of about 90% was reached after 90 min (Davidescu et al*.,* 2011).

The extraction of Zn^{2+}, Cd^{2+} and Cu^{2+} in 0.1M $NaNO_3$ by SIR containing D2EHPA was investigated. Amberlite XAD-2 was used as polymeric support. The results from the study indicated that metal extraction is pH-dependent, with a general trend of higher extraction with an increase in pH. They also compared the extraction abilities of XAD-2-D2EHPA resin with solvent extraction using D2EHPA. It was concluded that the extraction ability of XAD-2-D2EHPA decreases as a function of pH in the order of $Zn^{2+} \rangle Cd^{2+} \rangle Cu^{2+}$ whereas, with solvent extraction, it decreases as a function pH in the order of $Zn^{2+} \rangle Cu^{2+} \rangle Cd^{2+}$. This observation indicates that the extraction reactions can be explained in terms of a competitive process between the polymeric network, the extractant molecules, the metal ions and the water molecules (Silva et al*.,* 2018).

The kinetic studies of the extractive behaviour of D2EHPA sorbed onto Amberlite XAD-7 on Cd were investigated by (Benamor et al*.,* 2008). The results showed that the polarity of the impregnation solvent had a positive effect on the impregnation rate of D2EHPA onto the Amberlite XAD-7 resin. The physio-chemical parameters considered in this study were at pH 2.5 to 4, initial Cd concentration of 10 ppm to 150 ppm, and D2EHPA content in the Amberlite XAD-7 was 0.84 -1.55 mmol D2EHPA/g SIR, using the batch method. The analysis of rate data for the metal extraction kinetics indicates that the process is controlled by the rate diffusion of the Cd ions through the liquid/liquid interface (aqueous solution/extractant) inside the pores of the resin.

A novel polymeric composite bead with D2EHPA was developed for the separation of rare earth metals from different aqueous media. These beads were prepared by dissolving polyethersulfone (PES) in N-methyl pyrolidone (NMP) in a desired w/v ratio. This prepared solution was added to D2EHPA at a fixed polymer-to-extractant ratio whilst stirring. This mixed solution was gradually dropped into deionised water through a nozzle with a syringe needle at an appropriate height. The droplets formed in the water bath slowly precipitated due to phase inversion of the relatively dense polymeric backbone, resulting in the formation of PES beads impregnating the extractant. For this study, three types of beads were used (a) PES beads without extractant, (b) PES with extractant and (c) PVA-doped PES beads with an extractant.

The results from this study proved that the PVA-doped PES beads with extractant were very efficient in recovering rare earth from aqueous media, even after 20 cycles with minimal loss of D2EHPA (Yadav et al*.,* 2013).

A study on the preparation and study of the retention and distribution of D2EHPA on Amberlite XAD-2 was done by (Silva et al*.,* 2018). The results concluded that the adsorption of D2EHPA molecules onto Amberlite XAD-2 can be explained in terms of the interactions of alkyl groups of D2EHPA with the vinyl and styrene groups of Amberlite XAD-2. This Amberlite XAD-2-D2EHPA resin was also found to be a good ion-specific resin for the metal ions since the

phosphoric group retains the mobility needed for the easy formation of metal complexes.

A study done on the kinetics of Cu^{2+} sorption from single aqueous sulfate solutions with D2EHPA impregnated Amberlite XAD-2 and XAD-4 macroporous resins had the following conclusions: the sorption process is controlled by particle diffusion using a modified shrinking-core mechanism. The difference between the distribution coefficient values obtained for the two SIR was insignificant (Batra et al*.,* 2022).

Batra, Awasti and co-workers studied the column separation of divalent Cu^{2+} and Zn^{2+} from binary sulphate solutions using impregnated resins with D2EHPA. As part of this study, the breakthrough curves for the column separation of Cu^{2+} and Zn^{2+} were measured by changing certain variables. The resins used were Amberlite XAD-2 and XAD-4. The SIRs were prepared by dissolving 3.5 - 5.0 g D2EHPA in 20 mL of *n*-hexane and mixing with 10 g of Amberlite XAD-2 and XAD-4 for 12 hours. The impregnated resin was filtered and oven-dried for 2 hours at 50 ^{o}C. The D2EHPA content was determined by potentiometric titration with a known amount of NaOH. It was observed that the concentration of D2EHPA had a negligible effect on the separation factor in the concentration range of 0.8 – 1.03 mol/kg. More effective separation of Zn^{2+} to Cu^{2+} was obtained with a lower flow rate, lower pH and higher concentration ratio of Zn^{2+} to Cu^{2+}. A larger separation factor was also obtained on the XAD2-D2EHPA than on the XAD 4-D2EHPA resin bed. Hence, the XAD-2 resin is a better sorbent for impregnation for metal separation, even though the XAD-4 resin has a larger specific surface area in the concentration range (Batra et al*.,* 2022).

A XAD8-DEHPA-impregnated resin loaded with Fe(III) ions was used to study the characteristics of arsenic adsorption on the laboratory scale using aqueous solutions and natural underground waters. The Fe(III) ions were loaded onto the impregnated resin due to the high affinity of arsenic towards iron. The studies were conducted by both batch experiments and the column method. The results from the study showed that the arsenate adsorption onto the Fe(III) loaded XAD8-DEHPA resin was mainly attributable to the adsorption of monovalent arsenate anions $H_2AsO_4^-$. The adsorption of monovalent arsenate could be attributed to the release of hydroxyl anions or neutral water molecules from the Fe(III) ions' coordination sphere loaded onto the XAD-8-DEHPA resin (Ciopec et al*.,* 2014)

Di-(2-Ethylhexyl) phosphoric acid (D2EHPA) fixed on the Amberlite XAD-1180 supported by extractant impregnated resin technique was used to investigate the effect of physical parameters on the kinetics of bismuth (II) extraction from nitrate medium by the newly SIR. The results showed that an optimal plateau value of the D2EHPA extractant loading was 6 g/g of dry resin. The maximum bismuth sorption was found to be 98,5%, which equates to 490.7 mg Bi/g of resin, an initial concentration of 250 ppm Bi(III) and a pH of 3.6. Numerous factors that can influence the extraction of bismuth(III) were considered, but only the initial bismuth

concentration and pH value can be considered as the key parameters that govern the efficiency of this process (Belkhouche & Didi, 2010).

The adsorption and recovery of rare earth elements from aqueous nitric acid using a solid-phase extraction resin were investigated. The resin was prepared by impregnating di-(2-Ethylhexyl)phosphoric acid into the macroporous silica-based polymeric (SiO_2-P) particles. The chemical stability of di(2-Ethylhexyl)phosphoric acid/SiO_2-P treated with nitric acid at different temperatures was also assessed and demonstrated that di(2-Ethylhexyl)phosphoric acid/SiO_2-P had substantial stability against nitric acid and high temperature. Di-(2-Ethylhexyl)phosphoric acid/SiO_2-P resin also proved to have a higher adsorption distribution coefficient for heavy rare earth elements than for light rare earth elements (Shu et al*.,* 2018).

An impregnation method where D2EHPA is loaded onto reverse-phase silica columns for the separation of lanthanides was developed by (Ramzan et al*.,* 2017). Optimal loading conditions for the impregnation were achieved by dissolving a suitable amount of D2EHPA in *n*-pentane, flushing the column twice with 5 mL of impregnation solution and finally heating the column for a short period to remove the solvent. They found that better separation between adjacent lanthanides was observed when the column was subjected to heat over a shorter period (15 min) and attributed it to the presence of *n*-pentane in the pores, which reduces the diffusion paths of the metal ions. A higher extractant loading was also observed at the low concentration of the extractant.

A solvent-impregnated resin containing TOPS 99, which is an equivalent of di-(2-Ethylhexyl) phosphoric acid (D2EHPA), was used to investigate the extraction of terbium from phosphoric acid solutions by Kumar and his co-researchers. Amberlite XAD-4 was used as sorbent. Their results concluded that the extraction was acid-dependent, and the metal extraction followed a cation exchange mechanism. The loading capacity was calculated to be 23.8 mg/g resin. Even after subjecting the resin to seven cycles of extraction and elution, no loss of performance was observed (Kumar et al*.,* 2011). Guo, Nishihama and co-workers investigated the selective recovery of value metals from spent Li-ion batteries using Solvent Impregnated Resins (Guo et al*.,* 2013).

A comparative study between XAD-7-D2EHPA impregnated resin, conventional solvent extraction using D2EHPA and an oil sorbent made of kapok fibre impregnated with D2EHPA (SIF) was done for the removal of Bi(III), Cd(II), Co(II), Cu(II), Fe(III), Ni(II), Pb(II), and Zn(II) from single-metal nitrate solutions (Huynh and Tanaka 2003). Amberlite XAD-7 impregnated with three different organophosphorus extractants, namely D2EHPA, ION-QUEST (phosphonic acid (2-Ethylhexyl)-mono-(2-Ethylhexyl) ester) and Cyanex 272 were used to evaluate the extraction of Pb(II) from nitrate solutions. The results indicated that Amberlite XAD-7 has a higher affinity for D2EHPA compared to ION-QUEST and Cyanex 272 (Draa et

al., 2004).

2.6.1.3.4 SIRs application in scandium separation

SIRs are mostly applied to the removal and separation of metal ion mixtures in environmental chemistry, analytical chemistry, hydrometallurgy, and radiochemical analysis. Its application has also been extended to the removal of organics from aqueous solutions. For the scope of this study, we will focus on the application of SIRs in the separation of scandium from aqueous solutions.

A novel binary Solvent Impregnated Resin was prepared using 2-Ethylhexyl phosphonic acid mono-2-Ethylhexyl ester (PC-88A), and neodecanoic acid (Versatic 10) impregnated onto XAD-7HP polymeric beads to investigate the separation and pre-concentration of scandium (Sharaf et al., 2018). The separation factor was high between scandium and the other metal ions. Scandium was quantitatively desorbed using 2M H_2SO_4. Good reusability was confirmed after repeated use five times (Sharaf et al., 2018). A macro-porous silica-polymer-based di-(2-Ethylhexyl) phosphate absorbent was used for adsorbing scandium from other rare earth elements in the solution. This novel adsorbent displayed good selectivity towards scandium over the other rare elements. The adsorption equilibrium was reached within 5 minutes, and the adsorption isotherm data fit well with the Langmuir isotherm model (Zhang et al., 2019). The adsorption of scandium onto two chelating resins and one solvent-impregnated resin, TP 272 impregnated with Cyanex 272, was investigated. Of the three resins, the solvent-impregnated resin reached equilibrium almost three times faster compared to the other two chelating resins. The kinetic models show that the rate of scandium adsorption on all three resins is controlled by intraparticle diffusion (Bao et al., 2018).

The separation of scandium and yttrium was investigated with SIRs, using HP2MG as support, containing varying amounts of Cyanex 272 as an extractant and 1-octanol as the modifier. The modifier was added to enhance the stripping efficiency of the metals. Scandium was effectively adsorbed with all the SIRs, with low adsorption of yttrium. Scandium was successfully eluted using 5 M HCl (Moon et al., 2020). Amberlite XAD-7 impregnated with 2-Ethylhexyl hydrogen 2-ethylhexylphosphonate (PC-88A) was applied to selectively recover scandium from wolframite and tin slag. This impregnated resin had the following advantages for the recovery of scandium: it had a high distribution ratio for scandium, allowing for the quantitative recovery of scandium from a solution having high acidity, and the separation factors against the other metals were sufficient for the separation of scandium from common metals (Wang et al., 2011). A cost-effective method consisting of a flow injection-spectrophotometric system with a mini-column comprising of XAD-4 resin impregnated with nalidixic acid was designed for the pre-concentration and determination of scandium in different samples. The samples ranged from tap water to a complex matrix of synthetic seawater and certified reference material for lake

sediment. According to the authors, this method was rapid and straightforward, having reasonable detection limits and enrichment factors (Shahida et al*.,* 2013).

Scandium has also attracted the attention of nuclear researchers and physicians over the last decade due to the existence of matched radionuclides for the possibility of theranostic applications (Müller et al*.,* 2018). The radioisotopes can be produced via two main production routes using different target materials, including natural titanium and enriched titanium, natural calcium and enriched calcium (Müller et al*.,* 2018). Good chemical separation from its target material is necessary to increase the radioisotope and radiochemical purity of the produced radioactive scandium.

The separation of ^{47}Sc from a proton-irradiated titanium target was investigated using liquid-liquid extraction and ion-exchange chromatography. The authors indicated that the ^{47}scandium radioisotope was produced via irradiation of natural titanium, and the separation of scandium from titanium and other produced radionuclide was done using the Dowex 50W-X8 cation exchange resin. The results showed a separation efficiency of 90% from the target and the separation process time was sufficient for the reservation of the activity (Deilami-Nezhad et al*.,* 2016). After neutron irradiation of a titanium target, the radioactive scandium was separated from the irradiated titanium using a silica gel column. More than 95% of the radioactive scandium was recovered with this method, having a very low chemical impurity of titanium in the final product (Bokhari et al*.,* 2010).

Calcium, a non-toxic element, can be present in the preparations of radiopharmaceuticals. However, calcium could influence the yield of the radio-labelling process and should thus be removed as far as possible before the synthesis of radiopharmaceuticals (Pyrzyńska et al*.,* 2019). A fast and straightforward method for separating scandium from calcium targets was developed using chelating resin Chelex 100. The weakly bound ^{44}Ca and other metal ions were eluted using 30 mL of 0.01 M HCl. Scandium was recovered using 2 mL of 1 M HCl, having a yield of ^{44}Sc greater than 70% (Krajewski et al*.,* 2013). A novel separation method, using UTEVA extraction resin, was used to obtain ^{44}Sc from the proton irradiation of calcium targets. The method produced excellent yields of over 80% and high chemical and radiochemical purities (Valdovinos et al*.,* 2015). A two-column system has also been used for the separation of scandium from the calcium target material. After dissolving the target material in 3 M HCl, it was transferred directly onto a DGA column to remove the Ca^{2+} ions. The ^{44}Sc was eluted with 0.1 M HCl, and the eluant was transferred directly onto a second column, the SCX cation resin, for pre-concentration (van der Meulen et al*.,* 2015).

2.7 Adsorption process

Adsorption is the process whereby the accumulated solutes (adsorbate) are collected on the surface of the adsorbents to form a film of solutes (adsorbate). Additionally, adsorption is a

function of the solute concentration. The adsorption process can be categorised as either physisorption or chemisorption, depending on the type of interaction between the solute (adsorbate) and the adsorbent.

Physisorption is when the attraction between the adsorbed molecules and the adsorbent is of a physical nature. It is caused mainly by weak intermolecular forces (Van de Waals forces) and the electrostatic forces between the solute and the atoms comprising the adsorbent surface. The resulting adsorption is easily reversible as a result of the weak interaction.

Chemisorption is when the attraction forces between the adsorbed molecules and the absorbent result from chemical bonding. The bonding in chemisorption is strong and becomes difficult to reverse. The interaction in chemisorption is much stronger than that of physisorption.

2.7.1 Adsorption isotherms

Adsorption equilibrium information is fundamental for a proper understanding of an adsorption process. To allow for the overall improvement of adsorption mechanisms pathways and the design of effective adsorption systems, the knowledge and interpretation of adsorption isotherms are of fundamental importance (El-Khaiary, 2008). Adsorption isotherms are used to describe the equilibrium relationship between concentration in the liquid phase and the concentration of sorbent particles at a given temperature (Gökmen & Serpen 2002). The isotherms also provide information on whether the sorption process occurs via a chemical reaction (chemisorption) or due to weak van der Waals forces between the adsorbent and the sorbate species (physisorption).

The two-parameter isotherm models most commonly used are Langmuir and Freundlich isotherm models, while others include Temkin and Dubinin-Radushkevich isotherms (Abdullah et al*.,* 2009).

2.7.1.1 Langmuir isotherm model

The Langmuir model is the simplest theoretical model for monolayer adsorption onto a surface with a finite number of identical sites (Abdullah et al*.,* 2009). This model represents the equilibrium distribution of metal ions between the sorbent and the aqueous phase (Dada et al*.,* 2012). The Langmuir model was developed on the following assumptions:

- molecules absorb to well-defined localised sites;
- each of the sites is allowed to hold only one adsorbate molecule;
- all sites have equal energy;
- molecules adsorbed on connecting sites do not interact (Abdullah et al*.,* 2009).

The linearised form of the Langmuir isotherm equation is expressed as:

$$\frac{C_e}{q_e} = \frac{\alpha_L C_e}{K_L} + \frac{1}{K_L}$$ *Eq. 2-5*

K_L and α_L are the equilibrium constants of Langmuir equation. The plot of Ce/qe against C_e yields a straight line with slope, $\alpha L/K_L$, and intercept $1/K_L$ (Abdullah et al., 2009).

The essential characteristic of the Langmuir isotherm model can be explained in terms of a dimensionless separation factor or an equilibrium parameter that predicts whether a sorption system is favourable or unfavourable, which is R_L is defined by:

$$R_L = \frac{1}{1 + bC_o}$$ *Eq. 2-6*

where C_o (mg/L) is the initial metal ion concentration and b (L/mg) is the Langmuir constant. The R_L value indicates whether the Langmuir isotherm is to be irreversible ($R_L = 0$), linear (R_L = 1), favourable ($0 < R_L < 1$) and unfavourably ($R_L > 1$).

When experimental data fit the Langmuir isotherm model, it may be an indication of the uniform distribution of the extractant molecules on the surface of the polymeric support (Hosseini-Bandegharaei et al., 2016).

2.7.1.2 Freundlich isotherm model

The Freundlich isotherm is relevant to the adsorption process that occurs on heterogeneous surfaces. The isotherm is an expression of the surface heterogeneity and the exponential distribution of active sites and their energies (Nimibofa et al., 2017). This model assumes that the logarithmic form of the Freundlich isotherm equation is expressed as:

$$log\ q_e = log\ K_f + \frac{1}{n} log\ C_e$$ *Eq. 2-7*

where K_f (mg/g) is the binding energy constant reflecting the affinity of the adsorbents to the metal ions and $\frac{1}{n}$ is the constant indicating the intensity of the adsorption (Bao et al., 2016).

As soon as data fit the Freundlich isotherm model, it can be assumed that the adsorption of the metal ions occurs on a heterogeneous or uneven surface by monolayer sorption (Van Nguyen et al., 2013).

2.7.1.3 Temkin isotherm model

The Temkin model considers the effects of adsorbent/adsorbate interactions on the adsorption process. The model further assumes the decrease in the heat of adsorption of all molecules in the layer is linear owing to increase surface coverage (Nimibofa et al., 2015). The linear form of the Temkin isotherm is expressed as follows:

$$qe = \frac{Rt}{b}(ln\ KT + ln\ Ce\ ) \qquad \text{Eq. 2-8}$$

where b is the Temkin constant which is related to the heat of sorption (J/mol), and KT is the Temkin isotherm constant (L/g) (Samarghandi et al*.,* 2009).

2.7.1.4 Dubinin-Radushkevich isotherm model

The Dubinin-Radushkevich isotherm model is an empirical adsorption model generally applied to express the adsorption mechanism with Gaussian energy distribution onto heterogeneous surfaces (Nimibofa et al*.,* 2017). This isotherm is only suitable for an intermediate range of adsorbate concentrations. The model is a semiempirical equation in which adsorption follows a pore-filling mechanism. It presumes a multilayer character involving Van Der Waal's forces, applicable to physical adsorption processes (Nimibofa et al*.,* 2017). The Dubinin-Radushkevich isotherm is expressed as follows:

$$ln\ qe\ =\ ln\ qm\ \beta\varepsilon 2 \qquad \text{Eq. 2-9}$$

where Ɛ = RT ln(1+1/Ce) is the Polanyi potential, where R is gas constant (8.31 $Jmol^{-1}\ k^{-1}$), T is the absolute temperature, and Ce is the equilibrium concentration. β is the Dubinin-Radushkevich constant, and qm is the sorption capacity.

The Dubinin-Radushkevich constant (β) could be used to estimate the mean sorption energy E, the energy released per mole of sorbate as it approaches the sorbent from an infinite distance in the bulk solution. The value of E is applied to differentiate between the chemical and physical sorption of metal ions, calculated as follows:

$$E = \frac{1}{\sqrt{2\beta}} \qquad \text{Eq. 2-10}$$

When the magnitude of E in the range 8 – 16 $kJ{\cdot}mol^{-1}$ signifies chemisorption as a sorption mechanism, whereas E < 8 $kJ{\cdot}mol^{-1}$ suggests physisorption (Chabani et al*.,* 2006; Memon et al*.,* 2006).

2.7.2 Adsorption kinetics

The design of sorption systems is very much dependent on adsorption kinetic information. Kinetic models aid in gaining insight into the sorption mechanisms and the potential rate-controlling steps (Tan & Hameed, 2017). Several mathematical models can be used to describe adsorption data and generally consider adsorption reaction models and adsorption diffusion models. Both models are used to describe the kinetics of the adsorption process but differ in nature (Qiu et al*.,* 2009).

Several diffusion processes can define adsorption diffusion models: (i) diffusion across the liquid film surrounding the adsorbent particles, i.e. film diffusion; (ii) diffusion in the liquid contained in the pores and/or along the pore walls, which is so-called internal diffusion or intra-

particle diffusion; and (iii) adsorption and desorption between the adsorbate and active sites, i.e., mass action (Qiu et al*.,* 2009), as illustrated in Figure 2.4. One of these processes offers greater diffusion resistance than the others and can thus be considered the rate-controlling step of the sorption process (Cortina et al*.,* 2003).

However, adsorption reaction models are based on the whole process of adsorption, not taking into account the steps mentioned as part of adsorption diffusion models. Pseudo-first-order and pseudo-second-order equations are commonly used to model adsorption reaction kinetics, and the Weber-Morris Model describes adsorption diffusion kinetics.

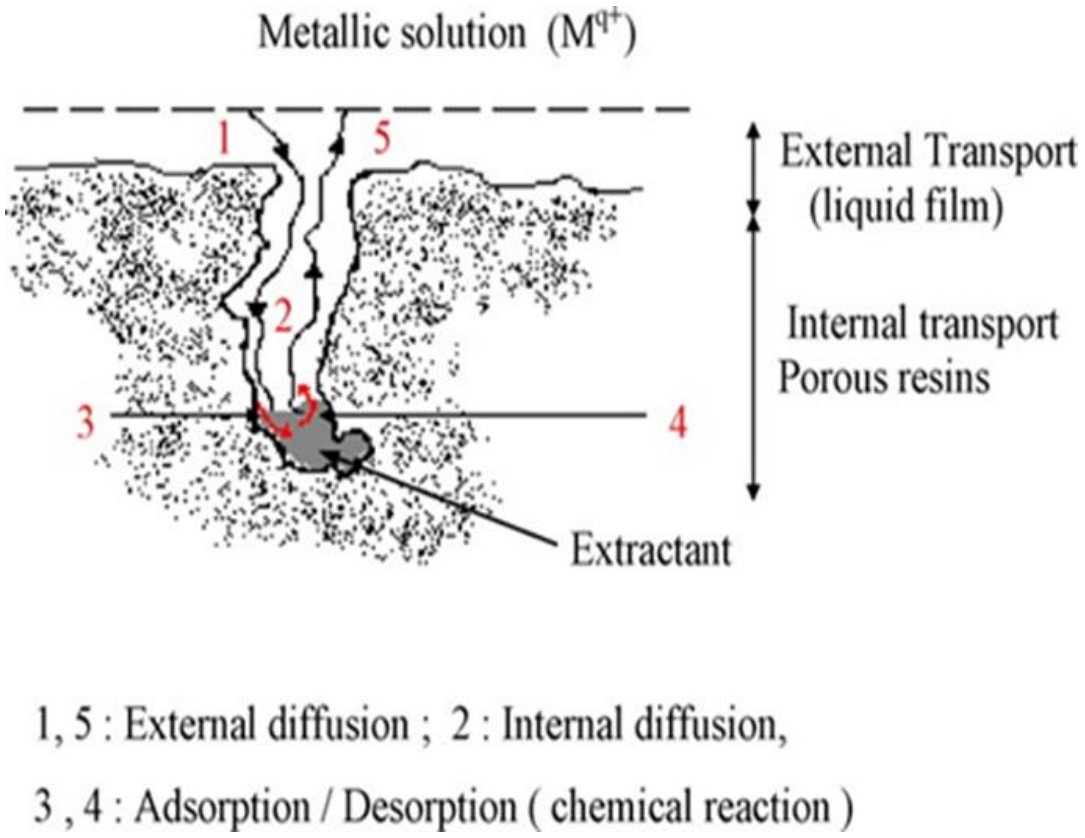

Figure 2.4: Processes involved in determining the rate-controlling step of the adsorption process

Source: Qiu et al., 2009

2.7.2.1 Adsorption reaction models

2.7.2.1.1 Pseudo-first order model

The Pseudo-First-Order model was first presented by Lagergren in 1898 to describe the kinetics of a liquid-solid phase system (Qiu et al*.,* 2009). However, to differentiate kinetic equations based on adsorption capacity from solution concentration, Lagerfren's first-order

rate equation has been termed pseudo-first-order. The integrated form of the pseudo-first-order model is illustrated as follows:

$$log\ (q_e - q_t)\ =\ log\ q_e\ \frac{k1.t}{2.303} \qquad \textit{Eq. 2-11}$$

where qe (mg/g) and qt (mg/g) are the amount of metal sorbed at equilibrium time and the amount of metal sorbed at any time, respectively. The pseudo-first-order rate constant, k_1 (min^{-1}), can be obtained from the slope of the linear plot of log (qe-qt) against time (t)

2.7.2.1.2 Pseudo-second order model

The first mathematical form of the Pseudo-Second-Order equation was proposed to describe the kinetics of heavy metal removal using neutral zeolites. The relevance of this model is explained based on the assumption that the overall sorption rate is limited by the rate of sorbate diffusion of sorbent (Plazinski et al*.,* 2013). The pseudo-second-order model is illustrated as follows:

$$\frac{d_q}{d_t} = k_2\,(q_e\text{-}q)^2 \qquad \textit{Eq. 2-12}$$

where q_e (mg/g) and q_t (mg/g) are the amount of metal sorbed at equilibrium and the amount of metal sorbed at any time, and k_2 is the pseudo-second-order rate constant (Ho & McKay 2000).

After integration with the initial concentration, the equation can be expressed as follows:

$$\frac{t}{q_t} = \frac{1}{k_2 q_e^2} + \frac{t}{q_e} \qquad \textit{Eq. 2-13}$$

where k_2 (g/mg.min) and q_e can be obtained from the plot between t/q_e versus t (Qu et al*.,* 2009).

2.7.2.1.3 Elovich equation

This model is based on a kinetic principle that assumes that adsorption sites increase exponentially with adsorption; this implies multilayer adsorption. The equation was first developed to describe the kinetics of the chemisorption of gas onto solids. The linear forms of the Elovich model are expressed as follows:

$$\frac{q_e}{q_m} = K_E C_e e\,\frac{q_e}{q_m} \qquad \textit{Eq. 2-14}$$

but the linear form is expressed as follows:

$$ln\,\frac{q_e}{C_e} = ln\ K_e q_m - \frac{q_e}{q_m} \qquad \textit{Eq. 2-15}$$

Elovich maximum adsorption capacity and Elovich constant can be calculated from the slope

and intercept of the plot of ln(qe/Ce) versus qe (Hamdaoui & Naffrechoux, 2007; Nimibofa et al*.,* 2017).

2.7.2.2 Adsorption diffusion models

2.7.2.2.1 Weber Morris model

The adsorption of metal ions on porous adsorbent using batch experiments can be defined by a number of diffusion processes, of which one of these processes offers greater diffusion resistance over the others and can thus be considered as the rate-controlling step of the sorption process. The dominant diffusion resistance for adsorption using synthetic resins is expected to be either film or interparticle diffusion. The Weber-Morris equation, derived from Fick's law for adsorbent diffusing in spherical sorbent particles, can be applied to evaluate the effect of film and interparticle diffusion on adsorption kinetics by assessing the relationship between the adsorbent uptake (q) and the square root of adsorption time ($t^{1/2}$) according to the following equation:

$$q = kt^{1/2} + I \qquad \text{Eq. 2-16}$$

where k is the diffusion rate parameter (mg L^{-1} $s^{-1/2}$), and the value of I can be calculated from the intercept from the plot of q versus $t^{1/2}$ (Zhu et al*.,* 2016).

2.8 Analytical techniques used in this study

Various analytical techniques have been applied to characterise the modified Amberlite XAD-4 resin to evaluate its chemical and structural properties. Powder X-Ray Diffraction (PXRD) was used to identify the resin's crystalline phase and unit cell dimension. Fourier Transform Infrared Spectroscopy (FTIR) was used to identify the functional groups present before and after modification. The resin's specific area and pore size were determined using Brunauer-Emmett-Teller (BET) nitrogen adsorption isotherms and Barrett-Joyner-Halenda (BJH), respectively. Scanning Electron Microscope – Elemental Dispersive Spectrometer (SEM-EDS) was used to confirm the elemental composition. SEM images were also collected, and Transmission Electron Microscopy (TEM) was used to determine the morphological changes of the modified resin before and after application.

2.8.1 Powder X-Ray Diffraction (PXRD)

X-ray powder diffraction (XRD) is a rapid analytical technique primarily used to phase identification of a crystalline material and provide information on unit cell dimensions. The analysed material is finely ground, homogenised, and the average bulk composition is determined. X-ray diffraction is now a common technique for studying crystal structures and atomic spacing (Guinier, 1994).

X-ray diffraction is based on the constructive interference of monochromatic X-rays and a

crystalline sample. These X-rays are generated by a cathode ray tube, filtered to produce monochromatic radiation, collimated to concentrate, and directed toward the sample. The interaction of the incident rays with the sample produces constructive interference (and a diffracted ray) when conditions satisfy Bragg's Law (nλ = 2d sin θ). This law relates the wavelength of electromagnetic radiation to the diffraction angle and the lattice spacing in a crystalline sample. These diffracted X-rays are then detected, processed and counted. By scanning the sample through the range of 2θ angles, all possible diffraction directions of the lattice should be attained due to the random orientation of the powdered material. Conversion of the diffraction peaks to d-spacing allows the identification of the mineral because each material has a set of unique d-spacing. Typically, this is achieved by comparison of d-spacing with standard reference patterns (Valente et al*.,* 2009; Chakrapani et al*.,* 2010).

2.8.2 Fourier Transform Infrared Spectroscopy (FTIR)

Fourier-transform infrared spectroscopy (FTIR) exploits the fact that molecules that absorb specific frequencies from the electromagnetic spectrum (EMS) are characteristic of their structure. The absorbed frequencies are directly proportional to vibrational energies and dependent on Hooke's law, where v, c, k, and μ is a vibrational frequency, speed of light, force/spring constant and reduced mass of bonding atoms, respectively (Mirabella, 1992). Factors that influence the exact IR absorption band of a covalent bond are the shape of the molecular potential energy surface, the mass of absorbing atoms and associated vibrational coupling. The vibrational frequency equation is as follows:

$$\nu = \frac{1}{2\pi c}\sqrt{\frac{k}{\mu}} \qquad \textit{Eq. 2-17}$$

Where ν is the vibrational frequency, c is the speed constancy (c = $3x10^{10}$ cm/sec), k is the molecular force constant, and μ is the reduced mass given by the following equation:

$$\mu = m_A m_B/(m_A + m_B) \qquad \textit{Eq. 2-18}$$

Where m_A and m_B are the atomic masses A and B, respectively.

When a sample interacts with infrared light, selected, IR vibrational frequencies are absorbed. Examination of transmitted light reveals how much energy is absorbed in each frequency. The technique is commonly used to analyse samples containing covalent bonds (non-metals) (Murphy et al*.,* 2015). IR absorption occurs when the incoming light frequency matches the bond's vibrational frequency, enabling the researchers to identify specific functional groups in molecules in the sample. When the bond is strong, the frequency where atoms vibrate becomes stronger (the shorter the wavelength, the higher the energy). Light can be detected through transmission (%T) - the amount of light that passes through the sample. It can also be seen by reflection - the amount of light that bounces off the sample. High transmittance at a frequency means few bonds absorb that "colour" light in the sample. Low transmittance means

a high bond population has vibrational energies corresponding to the incident light.

2.8.3 Brunauer-Emmett-Teller (BET)

The Brunauer-Emmett-Teller (BET) technique is commonly used to measure the specific surface area of materials. The BET theory is related to the adsorption of a gas on the material's surface. BET theory is used in systems of counter-layer adsorption and typically employs inquisitive gases. The boiling temperature of nitrogen gas is the commonly used gas because N_2 does not chemically respond with material surfaces as adsorbates to compute the specific surface area (Lowell et al*.*, 2006; Che & Védrine, 2012; Hiemenz & Rajagopalan, 2016). Specific surface area is a scale-dependent property, with no single actual value of a particular surface area definable. Thus quantities of a specific surface area determined through BET theory may depend on the adsorbate molecule utilised and its adsorption cross-section.

As seen in Figure 2.5 below, six BET isotherms have been reported in the literature (Thommes et al*.*, 2015).

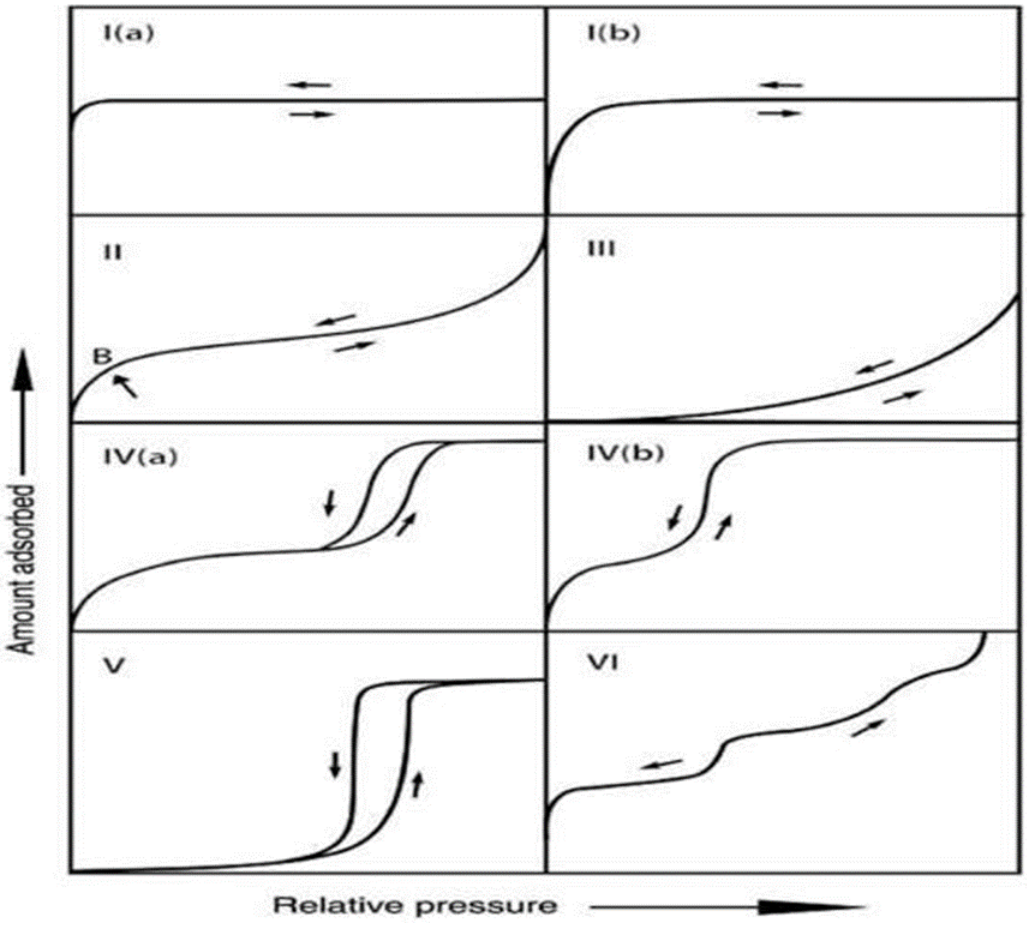

Figure 2.5: International Union of Pure and Applied Chemistry (IUPAC) classification of BET isotherm

Source: Thommes et al. (2015)

A Type I isotherm (Ia and Ib) is concave to the P/P° axis and the amount adsorbed approaches a limiting value. This limiting uptake is governed by the accessible micropore volume rather than by the internal surface area. A steep uptake at very low P/P° is due to enhanced adsorbent-adsorptive interactions in narrow micropores (micropores of molecular dimensions), resulting in micropore filling at very low P/P°. Reversible type I isotherm, which is typical for microporous solids, has two patterns. For nitrogen and argon adsorption at 77 K and 87 K, Type I(a) isotherms are microporous materials and are mainly composed of narrow micropores (of width $<\sim$ 1 nm). The pore size distributions of Type I(b) isotherms are narrow mesopores ($< \sim$ 2.5 nm) and wider micropores (Thommes et al*.,* 2015).

Reversible Type II isotherm represents mono-porous and microporous materials. The gradual change in curvature demonstrates the multilayer adoption (monolayer coverage overlaps). In contrast, if the monolayer coverage (Point B on the isotherm) is elucidated, the difference in curvature will be sharp. Type III isotherm indicates weak interaction between the adsorbent and adsorbate. Type IVa isotherm depends on the size of the width and the critical width. For example, suppose the width's size is larger than the required width corresponding to the material's adsorption characteristics and temperature, Type IVa isotherm. In 39 comparisons, Type IVb isotherm is only obtained for mesoporous materials of smaller widths. Type V isotherms can be detected at lower P/P° ranges and have a similar shape as Type III isotherms, which may be credited to the weak adsorbent-adsorbate relations. However, hysteresis, such as obtained in Type IV(a), can be detected at higher P/P° ranges due to pores filled by molecular clustering. Type VI isotherm represents multilayer adsorption materials with highly uniform nonporous surfaces. The stepwise curve of the isotherm depends on the material, gas, and temperature at which it is operated.

Figure 2.6 below illustrates five types of hysteresis loops as reported in the original IUPAC classification of 1985, which is now extended in light of more recent findings.

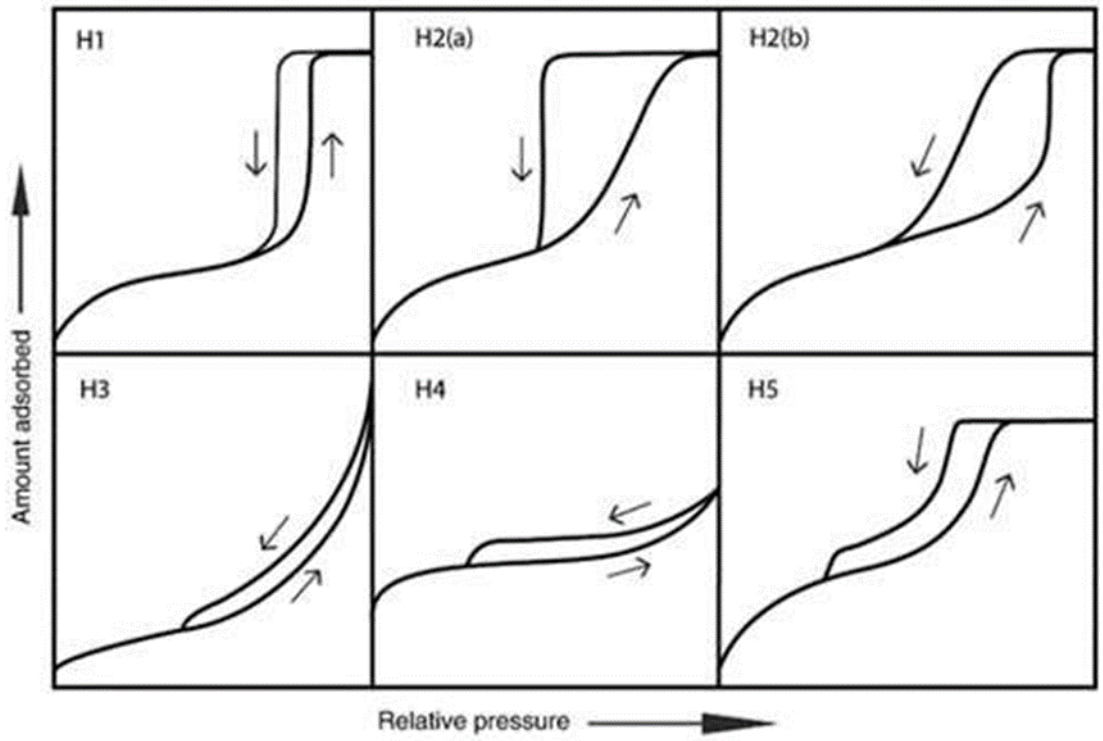

Figure 2.6: Classification of hysteresis loop

Source: Thommes et al. (2015)

Each of these five distinct types is reasonably closely related to particular pore structure features and underlying adsorption mechanisms. The Type H1 loop is found in materials that exhibit a narrow range of uniform mesopores (Thommes & Cychosz, 2014). Hysteresis loops of Type H2 are given by more complex pore structures in which network 40 effects are significant. The very steep desorption branch, a characteristic feature of H2(a) loops, can be attributed to pore-blocking/percolation in a narrow range of pore necks cavitation-induced evaporation. The Type H2(b) loop is also associated with pore blocking, but the size distribution of neck widths is now much more prominent. There are two distinctive features of the Type H3 loop: (i) the adsorption branch resembles a Type II isotherm (ii) the lower limit of the desorption branch usually is located at the cavitation-induced P/P°. For the H4 loop, the adsorption branch is a composite of Types I and II, the more pronounced uptake at low P/P° being associated with the filling of micropores. Type H5 loop is unusual, but it has a distinctive form related to specific pore structures containing both open and partially blocked mesopores.

2.8.4 Scanning Electron Microscope (SEM)

The scanning electron microscope (SEM) was developed in the early 1950s. The SEM is a microscope that uses electrons instead of light to form an image. It also describes the physics of electron-probe formation and electron-specimen interactions. Prints are produced by scanning the beam while displaying the signal from an electron detector on a computer

monitor. By choosing the appropriate detection mode, information about the sample, such as external morphology (texture), chemical composition, and crystalline structure and orientation of materials that make up the sample, can be obtained (Reimer, 2013). The ‘composition’ here refers to the mean atomic number, as the individual elements cannot be distinguished.

2.8.5 Transmission Electron Microscopy (TEM)

Electron microscopy techniques use a beam of accelerated electrons as a source of illumination as against visible light photons used in light microscopes. Since the wavelength of electrons is 100,000 times shorter than that of the photons in visible light, electron microscopes can produce images with a magnification 5,000 times better than visible light. In a transmission electron microscope (TEM), high voltage electrons, typically accelerated from a tungsten anode at + 100eKv (with respect to the cathode), are focused on and transmitted through an ultra-thin film sample. Electron beams emerging from the sample convey information about the structure of the sample.

CHAPTER 3
MATERIALS AND METHODOLOGY

This chapter outlines the reagents, apparatus, analytical instrumentation and separation methods used in this study. The experimental procedures and parameters are directly related to the results presented in Chapter 4 and Chapter 5.

3.1 Reagents and solutions

The 65% HNO_3, CaO (64%), Di-(2-Ethylhexyl) phosphoric acid (D2EHPA) (>95%), diethyl ether and methanol were purchased from Sigma Aldrich; the 48% HBr and $ScCl_3.6H_2O$ (18%), Amberlite XAD-4 (a polystyrene-based and nonpolar resin) were purchased from Industrial Analytical. The Dowex 50W-X8 (hydrogen form) cation exchange resin was purchased from BioRad SA.

All the acids and chemicals used for all experiments were of analytical grade. All these reagents were used without further purification.

The Sc ($ScCl_3.6H_2O$) and Ca (CaO) metal ion solutions were prepared from their respective salts. All stock solutions were 1000 mg/L for each metal ion (Sc and Ca) and were prepared in 250 mL volumetric flasks. The 1000 mg/L stock aqueous solutions of Sc and Ca were further diluted to a working stock solution of 50 ppm for ICP-OES calibration.

3.2 Sorption and separation studies using the Extraction Chromatography method

In the process of assessing the efficient method between the selected chromatographic methods (discussed in Section 3.3 above and in this Section) for the separation of Sc from Ca in an aqueous mixture solution, Amberlite XAD-4 resin impregnated with Di-2-Ethylhexyl phosphoric acid (D2EHPA) was used as absorbent. Di-2-Ethylhexyl) phosphoric acid (D2EHPA) was used as an extractant. Amberlite XAD-4 was used as an sorbent. All the conducted experiments are outlined below, ranging from the preparation of D2EHPA – XAD-4 impregnated resin (1.1.1), batch sorption studies (3.2.2), and the structural and morphological characterization of the materials (3.2.3).

3.2.1 Preparation of the Di-2-Ethylhexyl phosphoric acid - Amberlite XAD-4 impregnated resin

The di-2-Ethylhexyl phosphoric acid - Amberlite XAD-4 impregnated resin (D2EHPA – XAD-4 impregnated resin) was prepared using the dry method by impregnating di-2-Ethylhexyl phosphoric acid (D2EHPA) onto the Amberlite XAD-4 resin. Amberlite XAD-4 was pre-treated successively with 50 mL of 2 mol/L HNO_3 and 50 mL of 2 mol/L NaOH, followed by distilled water until neutralised to remove impurities. The resin was then dried at 60 ^oC in a vacuum oven for 24 hours and stored in a polyethylene bottle before use.

After the pre-treatment of the Amberlite XAD-4 resin, as described in 3.2.1, a desired amount of D2EHPA was dissolved in 13 mL of diethyl ether. 1g of Amberlite XAD 4 resin was added, and the mixture was shaken for 2 hours on an automatic mechanical shaker (Labotec model 262) at 150 rpm. The mixture was filtered under vacuum, and the resin was dried in a vacuum oven at 40 ^oC overnight to remove the solvent (diethyl ether). The amount of D2EHPA impregnated was determined after washing 0.5 g of the impregnated resin with 10 mL ethanol, followed by titration with 0.1 M NaO (Draa et al*.,* 2004).

3.2.2 Batch sorption studies

The sorption capacity of the D2EHPA-XAD-4 resin towards Sc^{3+} and Ca^{2+} in metal ion solutions was investigated by batch sorption experiments. In this investigation, synthetic metal ion solutions were used. All the batch sorption experiments were carried out in 50 mL plastic bottles on a mechanical shaker. The effect of pH, adsorbent dosage, contact time and initial concentration of Sc^{3+} ions and Ca^{2+} ions on the adsorption of these elements were evaluated.

Sample blanks (reference standards) without the adsorbent were prepared for each batch experiment and used as the initial concentration for each experiment. The metal ion concentration for Sc^{3+} and Ca^{2+} in the solutions after sorption was measured by ICP-OES.

The amount of metal ion sorbed (q, mg/g) and percent sorption (% A) was calculated as shown by Equation 3-1 and Equation 3-2, respectively.

$$q = \frac{Co - Cf \; X \; V}{M} \qquad \textit{Eq. 3-1}$$

$$Sorption\% = \frac{Co - Cf \; X \; 100}{Co} \qquad \textit{Eq. 3-2}$$

Where q is the amount of metal ion sorbed (mg/g), Co is the initial metal ion concentration (mg/L), Cf is the final metal ion concentration (mg/L), V is the volume of the solution (L), and M is the sorbent mass (g) (Sang et al*.,* 2008).

3.2.2.1 Effect of pH

To evaluate the effect of pH on the adsorption of Sc^{3+} ions and the Ca^{2+} ions, samples of 1,0 g of D2EHPA-XAD 4 resin were mixed with 25 mL of 2,0 mg/L Sc^{3+} ion and 10,0 mg/L Ca^{2+} solutions, respectively, at different pH values, ranging from pH=2 to pH=8, for a period of 4hours. The pH of the individual solutions was adjusted using 0.1 M HCl and 0.1 M NaOH, using a Basic 20+ CRISON digital pH meter prior to the addition of the sorbent. The 2,0 mg/L Sc^{3}+ stock solution was prepared by dissolving 0.0057 g of $ScCl_3.6H_2O$ in 500 mL of deionised water. The 10 mg/L Ca^{2+} stock solution was prepared by dissolving 0.0138 g of $CaCl_2$ in 500 mL of deionised water. After equilibration (4 hours), the resin was separated from the aqueous phase by filtration using 0.45 µm filter paper. The amount of Sc^{3+} and Ca^{2+} was determined in the aqueous phases by ICP-OES. All the samples were run in triplicate. The calibration standards were prepared from a 50 mg/L stock solution for each metal ion which was prepared from 1000 mg/L ICP standard solutions. The working calibration standard range was 0.1, 0.5, 1.0, 2.5 and 5 mg/L for scandium and 0.1, 0.5, 1.0, 2.5, 5.0 and 10 mg/L for calcium.

3.2.2.2 Effect of metal ion concentration

The effect of scandium and calcium concentrations was performed using Sc^{3+} and Ca^{2+} solutions at different initial concentrations (*0*.5, 1.0, 1.5, 2.0, 2.5, 3.0, 3.5 and 4 mg/L) for both metal ions. Both experiments were performed over a period of four hours. The respective concentrations were prepared from 10 mg/L stock solutions. The 10 mg/L Ca^{2+} stock solution was prepared by dissolving 0.0138 g of $CaCl_2$ in 500 mL of deionised water, and the 10 mg/L Sc^{3+} stock solution was prepared by dissolving 0.0285 g of $ScCl_3.6H_2O$ in 500 mL of deionised water. After the completion of equilibrium, the resin was separated from the aqueous phase by filtration using 0.45 µm filter paper. The amount of Sc^{3+} and Ca^{2+} was determined in the aqueous phases by ICP-OES. All the samples were run in triplicate. The obtained data were applied to determine the sorption capacity of the adsorbent.

3.2.2.3 Effect of contact time (Sorption Kinetics)

The contact time experiments were performed using 1 g of D2EHPA-XAD 4 resin contacted with 25 mL of 2,0 mg/L Sc^{3+} ion solutions and 10 mg/L Ca^{2+} ion solutions, respectively, at different time intervals (2, 4, 6, 8, 10, 30, 60, 120, 180,240 min). The 2,0 mg/L Sc^{3+} stock solution was prepared by dissolving 0.0043 g of $ScCl_3.6H_2O$ in 500 mL of deionised water. The 10 mg/L Ca^{2+} stock solution was prepared by dissolving 0.0138 g of $CaCl_2$ in 500 mL of deionised water. After the specified time, the resultant filtrates were analysed by ICP-OES. All the samples were run in triplicate. The calibration standards were prepared from a 50 mg/L stock solution for each metal ion which was prepared from 1000 mg/L ICP standard solutions. The working calibration standard range was 0.1, 0.5, 1.0, 2.5 and 5 mg/L for scandium and 0.1, 0.5, 1.0, 2.5, 5.0 and 10 mg/L for calcium**.**

3.2.2.4 Effect of adsorbent dosage

The optimum adsorbent dosage was investigated using different masses of the impregnated resin (0.1, 0.25, 0.5, 1.0, 1.5, 2.0, 2.5 and 3.0 g). The different masses were contacted with 25 mL of 2.0 mg/L Sc^{3+} ion and 10 mg/L Ca^{2+} ions solutions, respectively, for a period of 4 hours. The 2.0 mg/L Sc^{3+} stock solution was prepared by dissolving 0.0114 g of $ScCl_3.6H_2O$ in 500 mL of deionised water. The 10,0 mg/L Ca^{2+} stock solution was prepared by dissolving 0.0138 g of $CaCl_2$ in 500 mL of deionised water. After equilibration, the resin was separated from the aqueous phase by filtration using 0.45 µm filter paper. The amount of Sc^{3+} and Ca^{2+} was determined in the aqueous phases by ICP-OES. All the samples were run in triplicate. The calibration standards were prepared from a 50 mg/L stock solution for each metal ion which was prepared from 1000 mg/L ICP standard solutions. The working calibration standard range was 0.1, 0.5, 1.0, 2.5 and 5 mg/L for scandium and 0.1, 0.5, 1.0, 2.5, 5.0 and 10 mg/L for calcium.

3.2.3 Structural and morphological characterization of the materials

3.2.3.1 Powder X-Ray Diffraction (PXRD)

X-ray diffraction was used to identify the crystalline phase of the Amberlite XAD-4 resin, D2EHPA-XAD-4 impregnated resin and the metal-loaded D2EHPA-XAD-4 impregnated resin. The diffraction patterns were collected with a powder diffractor (Bruker, D8 Advance) equipped with a Lynexe detector, Cu tube at 1.54A°, 30 kV and 10 Amp current, over the range of 2θ from 0° to 90°, in steps of 0.034° 2θ, with a measuring time of 25 min.

3.2.3.2 Fourier Transform Infrared (FTIR)

The infrared spectra of Amberlite XAD-4 resin, D2EHPA, D2EHPA-XAD-4 impregnated resin and the metal-loaded D2EHPA-XAD-4 impregnated resin was collected using a Perkin Elmer UATR spectrum two. Adsorption bands were collected in the range of 4000 – 400 cm^{-1} to identify the present functional groups in the materials.

Prior to the analysis, the diamond crystal and the arm were cleaned using iso-propanol. A background spectrum was recorded. No sample preparation was required. A small amount of each sample was added to the plate to cover the crystal. The pressure arm was lowered onto the sample until a pressure limit of 50% was reached. This allowed for satisfactory contact between the sample and the diamond crystal.

3.2.3.3 Brunauer-Emmett-Teller (BET) Characterization

Specific surface area and pore size were analysed using Brunauer-Emmett-Teller (BET) nitrogen adsorption isotherms and Barrett-Joyner-Halenda (BJH), respectively. 0.1 g of the samples were weighed and transferred into a pre-weighed BET tube and then de-gassed at 130 ˚C for 24 hours in nitrogen gas to remove possible impurities and moisture in the sample. The mass of the BET tube

plus the mass of the material after the de-gassing were weighed, and the de-gassed sample was then analyzed using the BET surface area instrument (3Flex (version 5.00) Surface Characterization Analyzer, from Micrometirics). The BET adsorptive analysis was performed using the adsorption of nitrogen gas at 77 K, ambient free spacing of 15.6543 cm^3 and equilibration interval of 10s.

3.2.3.4 Scanning Electron Microscope (SEM) Characterization

The morphologies and surface texture of individual particles and the elemental composition of the unimpregnated Amberlite XAD-4, D2EHPA, D2EHPA-XAD-4 impregnated resin and the metal-loaded D2EHPA-XAD-4 impregnated resins samples were analysed using Zeiss Auriga Field-Emission Gun Scanning Electron Microscopy (FEG-SEM) (Auriga Instrument, USA), equipped with secondary electron detectors coupled with energy dispersive spectroscopy (EDS). Samples for FEG-SEM-EDS analysis were prepared by sprinkling a representative portion of materials onto double-sided carbon tape mounted on an SEM stub. The samples were then coated with a thin layer of gold-palladium (Au-Pd) using a Q150T Turbo-Pumped Sputter Coater (Q150T ES) equipped with an Edwards vacuum pump to eliminate the charging artefacts that may be caused by a build-up electron. The metal coating assures sample conductivity while lessening electron influx.

3.2.3.5 Transmission Electron Microscopy (TEM) Characterization

The surface morphology of unimpregnated Amberlite XAD-4, D2EHPA, D2EHPA-XAD-4 impregnated resin and the metal-loaded D2EHPA-XAD-4 impregnated resins were examined using a transmission electron microscope (TEM, Tecnai TF20 thermionic, FEI, Switzerland) equipped with a LaB6 filament and a Gatan GIF energy filter). Images were captured at 200 keV in bright field mode.

3.3 Equilibrium distribution coefficients (K_d) and separation studies using ion exchange chromatography method

3.3.1 Equilibrium distribution coefficients (K_d) for extraction of Sc^{3+} and Ca^{2+} from aqueous mixture solution

Equilibrium distribution coefficient determinations for Ca^{2+} and Sc^{3+} were performed by equilibrating a 50 mL mixture of HBr and methanol solution (with specific concentration ratios).

Briefly, 0.05 mmol per 50 mL Ca^{2+} with 0.50 g of dry Dowex 50W-X8 (in the hydrogen form) were added to the 50 mL mixture of HBr and methanol solution and shaken for 24 hours on a mechanical shaker. For Sc^{3+}, the equilibrium distribution coefficient determination was prepared by equilibrating a 50 mL mixture of HBr and methanol solution containing 0.33 mmol per 50 mL of Sc^{3+} with 0.50 g of dry Dowex 50W-X8 (in the hydrogen form). The solution mixture (HBr + methanol + Sc^{3+} + Dowex 50W-X8) was shaken for 24 hours on a mechanical shaker.

After equilibration, the resins were separated from the aqueous phase by vacuum filtration. The

filtrates were collected in 100 mL volumetric flasks and made up to the mark with deionised water. The amounts of Sc^{3+} and Ca^{2+} were determined in the aqueous phases (solutions) using Inductively Coupled Plasma-Optical Emission Spectroscopy (ICP-OES). The equilibrium distribution coefficients were calculated according to the following equations:

$$K_d = \frac{M_{ERR}}{mass\ of\ element\ in\ solution}\ X\ 100 \qquad \textit{Eq. 3-3}$$

$$M_{ERR} = Aver.of\ the\ reference\ standards - a\ mass\ of\ an\ element\ in\ a\ solution \qquad \textit{Eq. 3-4}$$

Thus, $K_d = \frac{Aver.of\ reference\ standards - mass\ of\ element\ in\ solution}{mass\ of\ element\ in\ solution}$ *X100* *Eq. 3-5*

Where M_{ERR} is the mass of the element retained on the resin. The distribution coefficient experimental conditions for both scandium and calcium, with the varying HBr-methanol ratios, are illustrated in Table 3-1.

3.3.1.1 Calibration studies of ICP-OES

Four reference standards were prepared for each of Sc^{3+} and Ca^{2+}, containing the same concentration of the elements as used for the distribution coefficient experiments. The calibration standards were prepared from a 50 mg/L working stock solution for each metal ion prepared from 1000 mg/L ICP standard solutions. The working calibration standard range was 0.1, 0.5, 1.0, 2.5 and 5.0 mg/L for scandium and 0.1, 0.5, 1.0, 2.5, 5.0 and 10.0 mg/L for calcium.

Table 3.1: HBr-methanol solution for scandium and calcium Kd batch studies

M HBr	% methanol	mL 8,9 M HBr	mL Sc stock solution	mL methanol	mL water	Total volume (mL)
0,5	20	2,8	5,0	10	32,1	50,0
0,5	40	2,8	5,0	20	22,2	50,0
0,5	60	2,8	5,0	30	12,2	50,0

M HBr	% methanol	mL 8,9 M HBr	mL Sc stock solution	mL methanol	mL water	Total volume (mL)
1,0	20	5,6	5,0	10	29,4	50,0
1,0	40	5,6	5,0	20	19,4	50,0
1,0	60	5,6	5,0	30	9,4	50,0

M HBr	% methanol	mL 5.0 M HBr	mL Sc stock solution	mL methanol	mL water	Total volume (mL)
2.0	20	20.0	2.0	10.0	18.0	50.0
2.0	40	20.0	2.0	20.0	8.0	50.0

		mL 6.0 M HBr				
2.0	60	16.7	2.0	30.0	1.3	50.0
M HBr	% methanol	mL 6.0 M HBr	mL stock solution	mL methanol	mL water	Total volume (mL)
3.0	20	25.0	2.0	10.0	13.0	50.0
3.0	40	25.0	2.0	20.0	3.0	50.0
		mL 8.9 M HBr				
3.0	60	16.9	2.0	30.0	1.2	50.0

3.3.2 Separation studies of Sc^{3+} from Ca^{2+} in an aqueous binary mixture solution

Elemental separation (elution curves) were obtained by equilibrating 15 mL Dowex 50W-X8 (dry resin) with 50 mL of 2.0 M HBr-60% methanol. The loading solution was made up of 0.3 mg Sc and 0.0035 g Ca dissolved in 50 mL 3.0 M HBr-20% methanol. The solution mixture was passed through the column at a flow rate of 5.0 ± 0.5 mL/min. Fractions (10 mL) were collected from the loading (sorption) step.

Ca was eluted with 200 mL of 3.0 M HBr-20% methanol, and the fractions (10 mL) were collected in 15 mL plastic vials. Sc was eluted with 200 mL of 5M HCl, and the fractions (10mL) were collected in 15 mL plastic vials All the fractions (Ca and Sc) were determined using ICP-OES.

3.4 Apparatus

An automatic mechanical shaker (Labotec model 262) with speed control was used for all batch equilibrium studies for both methods.

A Basic 20+ CRISON digital pH meter was used to adjust the pH values.

A Gilson MINIPULS Evolution peristaltic pump was used in all column experiments.

A Spectro ARCOS ICP-OES spectrometer with Smart Analyzer Vision installed software, coupled with a Certac ASX-520 Autosampler was used to determine metal ion concentrations. The operating parameters are listed in Table 3.2.

Table 3.2: Operating parameters of the ICP-OES spectrometer

Parameter Name	Parameter Value
RF Power	1400 W
Argon Flow	12 L/min
Auxiliary Flow	1.0 L/min
Nebuliser Flow	0.8 L/min
Peristaltic Pump Speed	63 rpm

3.5 Flow Diagram for the two methods

Below is a flow diagram illustrating the fixed and varied parameters for each of the experimental methods in this study.

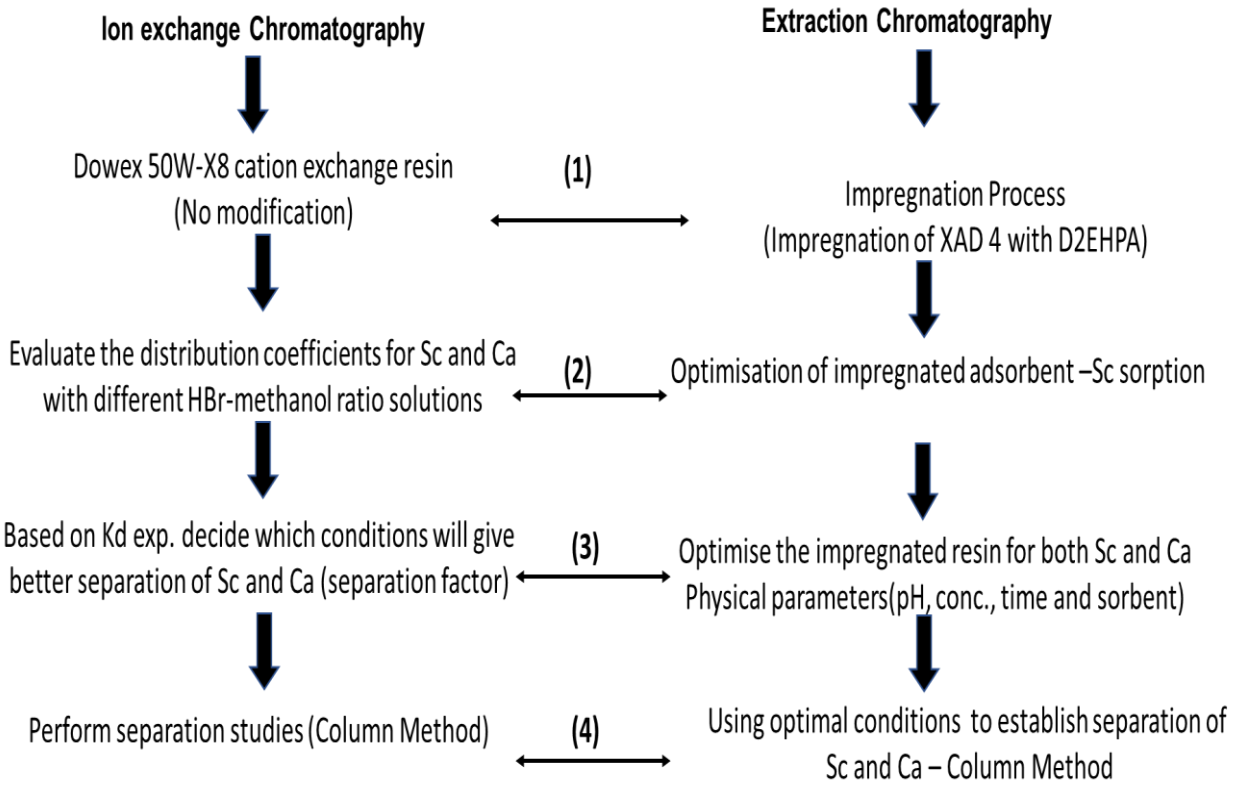

CHAPTER 4
RESULTS AND DISCUSSION: EXTRACTION CHROMATOGRAPHY

4.1 Preparation of impregnated resin

The efficiency of the impregnation process of the D2EHPA – XAD-4 impregnated resin prepared using a dry method was evaluated by determining the loading capacity of the resin. Firstly, the degree of D2EHPA loading onto the resin by contacting the resin with a series of solutions of different volumes of D2EHPA, ranging from 1,0 mL to 25,0 mL of D2EHPA. The loading capacity for each solution was calculated by titration with 0.1M NaOH. Typically, it would be expected that the interaction of D2EHPA loading onto the XAD-4 resin reaches an equilibrium at the “optimal” volume of D2EHPA. However, this was not the case in this study, as evident in Figure 4.1a. The results showed a continuous increase in loading capacity as the volume of D2EHPA increased.

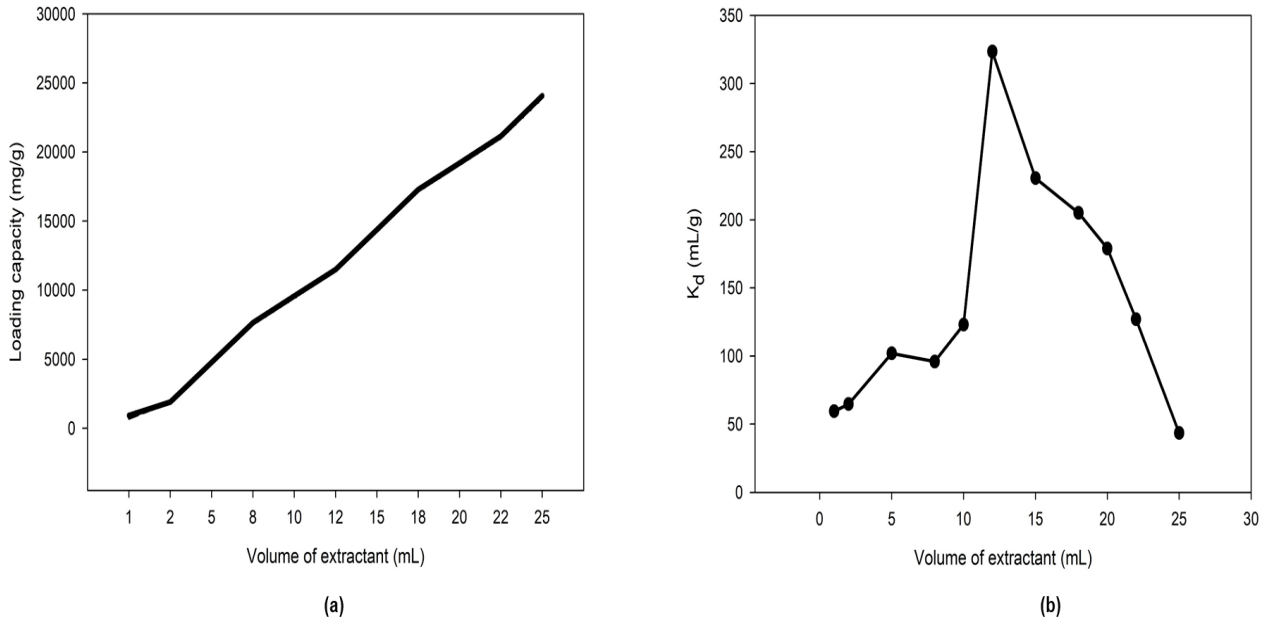

Figure 4.1: (a) Loading capacity of resin for the extractant and (b) distribution coefficient values at varying extractant volumes

Since no plateau was reached, adsorption performance tests were conducted to evaluate the effect of loading ratios on the adsorption performances of the adsorbent for scandium.

The distribution coefficient (K_d) was calculated by Eq.4.1 equation:

$$K_d = \frac{conc.of\ metal\ in\ resin}{conc.of\ metal\ in\ solution} \times \frac{mL\ of\ solution}{grams\ of\ resin} \quad \textbf{Eq. 4.1}$$

The distribution coefficients of the adsorbent for the different loading ratios are shown below in Figure 4.1b. Evident in Figure 4.1b, and presented in Table 4.1, the maximum value for the distribution coefficient was observed at a volume of 12 mL of extractant (loading capacity of 11,500 mg D2EHPA/g XAD 4). Again, the adsorption performance generally increases proportionally to the loading capacity (Moon et al*.,* 2006); however, a different scenario was observed in this study. The evident deviation from the expected trend could be due to the leaching of the extractant from the SIR at higher loading. This study defines K_d as the quantity of analyte that is retained in the solid phase divided by the quantity of analyte retained in the aqueous phase, thus the magnitude of the K_d value is directly proportional to the analyte's affinity for a given chromatographic resin under a given set of conditions (Snow and Ward 2020). Based on the experimental results and K_d calculations, it was concluded that 12 mL of D2EHPA per 1g of Amberlite XAD-4 resin is the optimal parameter for preparing the impregnated resin, and it was used for all further experiments.

Table 4.1: Loading capacity of Amberlite XAD-4 with varying D2EHPA concentrations and time

Mass of resin (g)	Volume of D2EHPA (mL)	Loading capacity (mg D2EHPA/ g resin)	Loading capacity (mg D2EHPA/ g resin)	Loading capacity (mg D2EHPA/ g resin)
		1 hour	2 hours	24 hours
1.0	1	937	943	725
1.0	2	1898	1902	1902
1.0	5	4773	4772	4788
1.0	8	7655	7633	7666
1.0	10	9589	9568	9592
1.0	12	11508	11502	11535
1.0	15	14395	14380	14436
1.0	18	17290	17274	17322
1.0	20	19211	19200	19240
1.0	22	21154	21135	21175
1.0	25	24079	24036	24069

4.2 Characterisation of impregnated resin

The characterisations of the impregnated resin are presented here from a comparative point of view

using the following methods: Powder X-Ray diffraction (PXRD), Fourier Transform Infra-Red (FT-IR) spectroscopy, Brunauer-Emmett-Teller (BET), Scanning Electron Microscopy (SEM) and Transmission Electron Microscopy (TEM).

4.2.1 Powder X-Ray diffraction (PXRD)

The XRD spectra in Figure 4.2 show a comparison of unimpregnated Amberlite XAD-4, impregnated Amberlite XAD-4 with D2EHPA and impregnated Amberlite XAD 4 with D2EHPA after the application (adsorption of scandium). These are presented as XAD-4, XAD-4/D2EHPA, and XAD-4/D2EHPA_Sc on the below graphs, respectively. As shown in Figure 4.2, a sharp prominent peak and a broader hump were observed at 2θ of 5.0° and 18.0°, which may indicate the polymer matrix (Amberlite XAD-4) with an amorphous nature-like structure. After impregnation with D2EHPA, a reduction in peak areas at 2θ of 5.0° and 18.0° was observed. There were no significant changes observed after the scandium adsorption. Therefore, these reductions could be ascribed to the resin and extractant interaction.

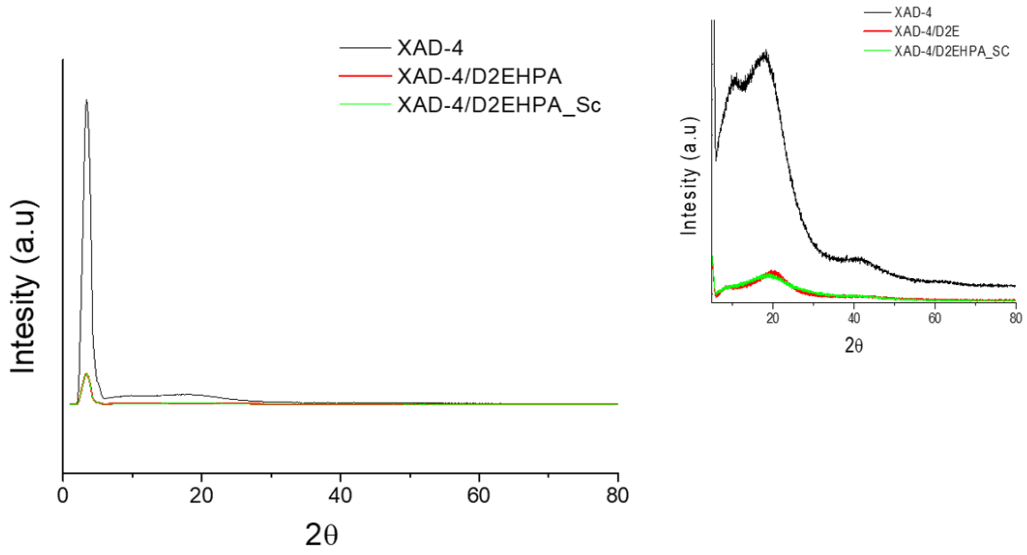

Figure 4.2: Diffractograms of unimpregnated Amberlite XAD-4, XAD/D2EHPA impregnated resin and Sc loaded D2EHPA-XAD-4/D2EHPA impregnated resin

4.2.2 Fourier Transform Infra-Red (FT-IR)

The FT-IR spectra of unimpregnated Amberlite XAD-4, pure D2EHPA, the impregnated XAD-4/D2EHPA resin and impregnated XAD-4/D2EHPA after Sc adsorption (XAD-4/D2EHPA_Sc) are represented in Figure 4.3.

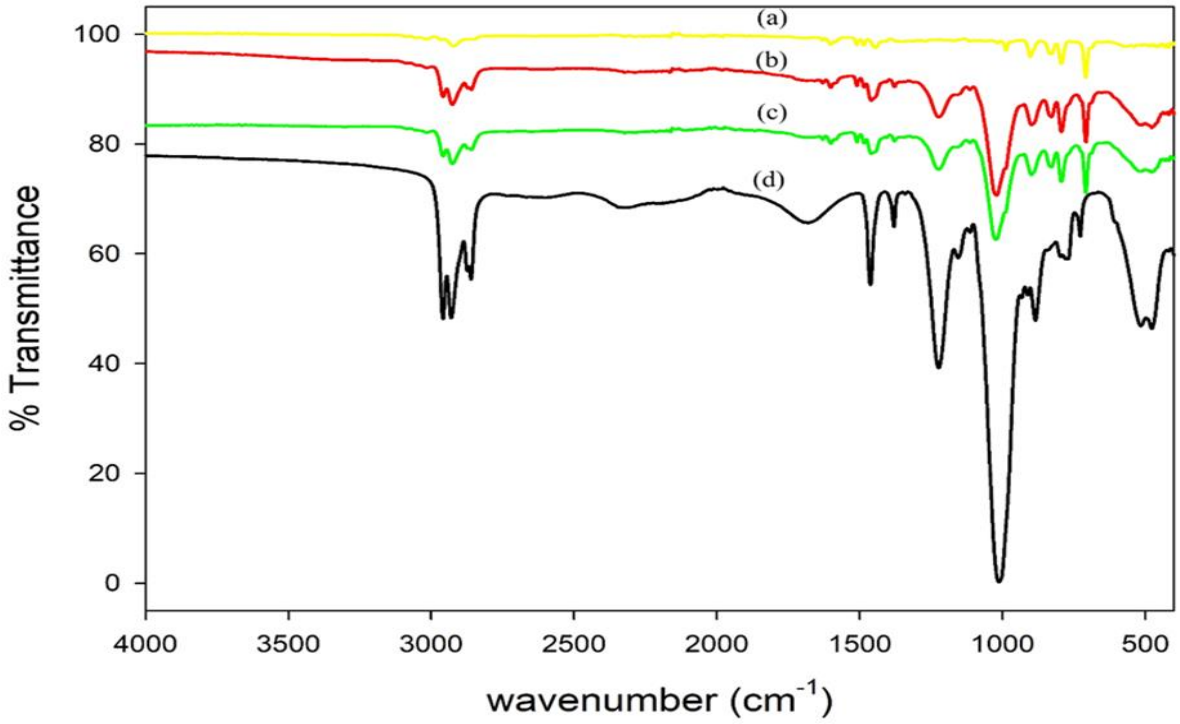

Figure 4.3: FTIR spectra of (a) unimpregnated Amberlite XAD-4, (b) impregnated XAD-4/D2EHPA, (c) impregnated XAD-4/D2EHPA_Sc and (d) pure D2EHPA in the region 400 -4000 cm^{-1}

Amberlite XAD-4 is a polystyrene-based and nonpolar resin with aliphatic C-H stretching = 2923 cm^{-1}; C=C ring stretching = 1606, 1485, 1446 cm^{-1}; ring substitution = 903 cm^{-1}. The characteristic IR bands of neat D2EHPA appear at 1224 cm^{-1} for the stretching vibrational band of the P=O bond, the P-O-C stretching vibration at 1012 cm^{-1}, and the P-OH vibration at 2323 cm^{-1}. Slight changes are observed in the P=O bond and the P-O-C stretching from 1224 cm^{-1} to 1225 cm^{-1} 1012 cm^{-1} to 1024 cm^{-1}, respectively, for the XAD-4/D2EHPA-impregnated resin. These frequency shifts may indicate an effective interaction between D2EHPA and Amberlite XAD-4 resin (Abderrahim et al*.,* 2008).

The FT-IR spectra of D2EHPA–XAD-4 impregnated resin loaded with scandium show a reduction and shift in the P=O vibration from 1225 cm^{-1} to 1224 cm^{-1}, which indicates that the oxygen atom of P=O is involved in complex formation with scandium. The P-O-C stretching vibration in the XAD-4/D2EHPA-impregnated resin shifts from 1024 cm^{-1} to 1021 cm^{-1} when scandium is loaded on the resin, indicating that the H^+ ion of D2EHPA is replaced by the Sc^{3+} ions in solution as a result of the cation exchange process (Mishra & Devi, 2020).

4.2.3 Brunauer-Emmett-Teller (BET)

Table 4.2: BET surface area and BJH adsorption average pore size and pore volume

Sample	BET Surface Area (m^2/g)	Pore Volume (cm^3/g)	Average pore size (nm)
Amberlite XAD 4	981.11	1.55	7.86
Amberlite XAD 4 + D2EHPA	71.91	0.37	17.4
Amberlite XAD 4 + D2EHPA +Sc	69.67	0.38	18.5

The BET surface areas, pore volume, and average pore size of unimpregnated Amberlite XAD-4, impregnated XAD-4/D2EHPA resin and impregnated XAD-4/D2EHPA resin after the adsorption of Sc is shown in Table 4.2. Their nitrogen adsorption-desorption isotherms are presented in Figure 4.4.

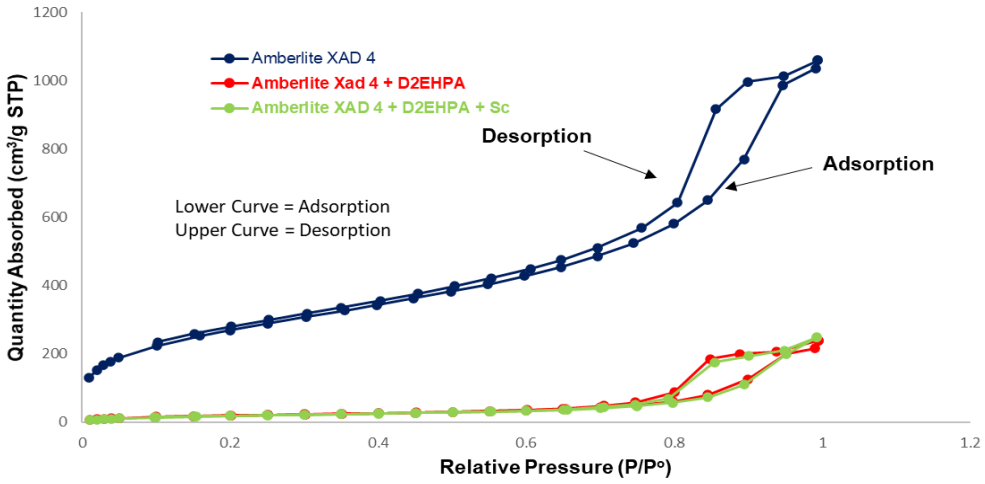

Figure 4.4: Nitrogen adsorption-desorption isotherm of unimpregnated Amberlite XAD-4, impregnated XAD-4/D2EHPA and impregnated XAD-4/D2EHPA after the adsorption of scandium

The BET surface areas ranged between 69.67 m^2 /g to 981.11 m^2 /g, and the BHJ average pore size adsorption ranged from 7.87 nm to 18.56 nm (Table 4.2). The surface area of the impregnated Amberlite XAD-4/D2EHPA resin decreased, and the pore size increased due to the impregnation of extractant (D2EHPA) into the resin pores. After the adsorption of scandium using the impregnated Amberlite XAD-4/D2EHPA resin, a further decrease in the surface area and an increase in the pore size of the XAD-4/D2EHPA resin was observed. This shows the exchange of H^+ ions on the modified resin with Sc^{3+} ions decreases. The pore sizes ranged from approximately 8 nm to about 18 nm, and according to IUPAC nomenclature, the resins can be classified as mesoporous materials (Cyganowski et al., 2015).

The nitrogen adsorption-desorption isotherms (Figure 4.4) of impregnated XAD-4/D2EHPA resin compared with unimpregnated Amberlite XAD-4 resin can be categorised as a type IV isotherm, indicating the presence of mesoporous structure, with H-2(b) type hysteresis loop at the relative pressure (P/P^o) ranging between 0.8 and 1.0, which can be associated with pore blocking.

4.2.4 Scanning Electron Microscope (SEM)

SEM images of unimpregnated Amberlite XAD-4 resin, impregnated XAD-4/D2EHPA resin, impregnated XAD-4/D2EHPA resin after scandium adsorption and impregnated XAD-4/D2EHPA resin after calcium adsorption are presented in Figure 4.5.

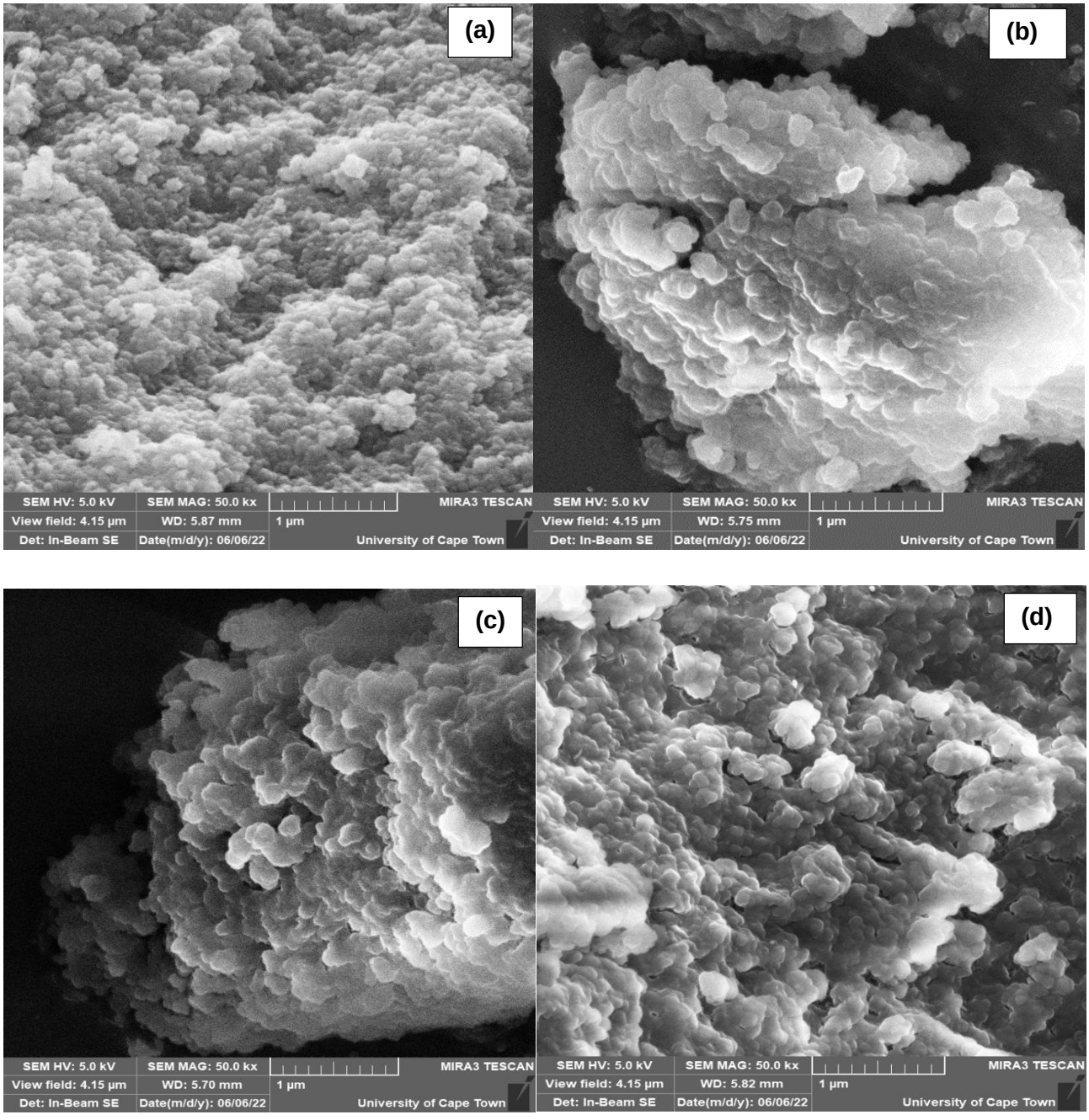

Figure 4.5: SEM images of (a) unimpregnated Amberlite XAD-4 resin, (b) Impregnated XAD-4/D2EHPA resin, (c) Impregnated XAD-4/D2EHPA resin after scandium adsorption, and (d) Impregnated XAD-4/D2EHPA resin after calcium adsorption

From the unimpregnated resin Figure 4.5(a), the spherical shape of the resin particles is evident, with a uniform size distribution. The aggregated morphology of the unimpregnated resin appears more agglomerated after impregnation with D2EHPA (Figure 4.5b). It could be an indication that the pores were filled with D2EHPA. The agglomerated morphology of the impregnated resin increases the strength of the resin to avert physical degradation during the adsorption process (Iqbal & Datta 2022). No apparent change in the resin's external surface can be seen after the adsorption of scandium (Figure 4.5c) and calcium (Figure 4.5d). Similar results have been reported in the literature (Kaur et al., 2011; Iqbal & Datta, 2022).

The EDS analysis of the unimpregnated Amberlite XAD-4, the impregnated XAD-4/D2EHPA resin and impregnated XAD-4/D2EHPA after Sc adsorption (XAD-4/D2EHPA_Sc) are represented in Table 4.3. As evident in Table 4.3, there were changes observed in the elemental composition of the unimpregnated Amberlite XAD-4, the impregnated XAD-4/D2EHPA resin and impregnated XAD-4/D2EHPA after Sc adsorption (XAD-4/D2EHPA_Sc). No phosphorus was present in the unimpregnated Amberlite XAD-4 resin, compared to the impregnated XAD-4/D2EHPA resin having a phosphorus weight percentage of 3.71, indicating the impregnation of D2EHPA.

Table 4.3: Weight% of elemental composition of the unmodified, modified and used resins

Sample	Wt% Carbon	Wt% Oxygen	Wt% Phosphorus
Amberlite XAD 4	94.97	5.03	*
XAD 4/D2EHPA	80.08	16.21	3.71
XAD 4/D2EHPA_Sc	80.04	16.23	3.73

4.2.5 Transmission Electron Micrscopy (TEM)

Figure 4.6 (a and b) shows the TEM images of unimpregnated and impregnated resins. The white sections in Figure 4.6(a) can be considered to be the pores of the polymeric resin, and the darker sections the polymer surrounding the pores. The unimpregnated Amberlite XAD-4 consisted of more agglomerated pores, indicating a developed mesoporosity. This observation agrees well with the results of the adsorption-desorption isotherm of N_2 reported in the literature (Li et al., 2010). From the TEM image for D2EHPA impregnated Amberlite XAD-4 resin Figure 4.6(b), it is evident that the mesopores of the resin have been filled by the extractant (D2EHPA), as fewer pores are visible. These results correspond with the increase in pore size observed in the BET analysis. The TEM analysis corresponds with the SEM characterisation observations.

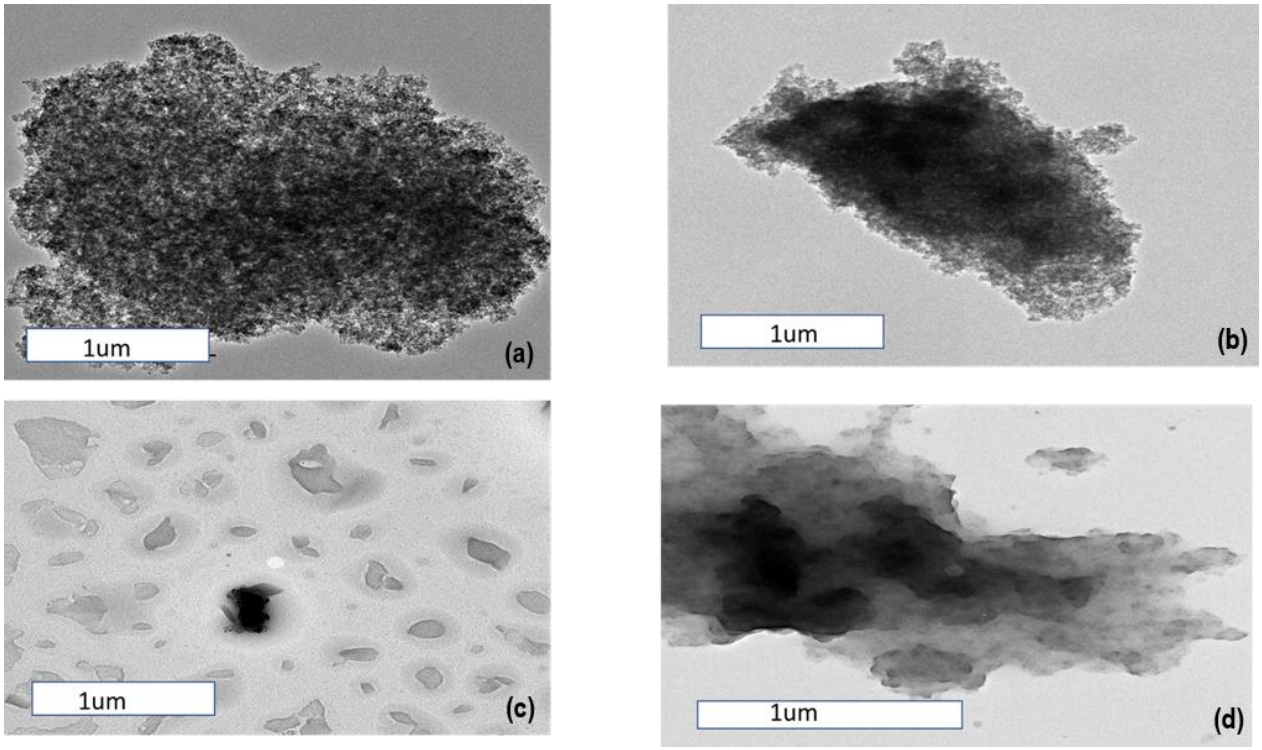

Figure 4.6: TEM images of unimpregnated Amberlite XAD-4 resin, (b) D2EHPA impregnated Amberlite XAD-4 resin, (c) Impregnated XAD-4 resin after scandium adsorption and (d) Impregnated XAD-4 resin after calcium adsorption

4.3 Batch adsorption experiments

Synthetic solutions were prepared for the batch sorption experiments of scandium and calcium. The XAD-4/D2EHPA-impregnated resin was used as an absorbent to perform the batch sorption experiments. Different physicochemical parameters (pH, sorbent dosage, contact time, and initial metal ion concentration), equilibrium isotherms, and sorption kinetics were evaluated for the sorption of scandium (Sc^{3+}) and calcium (Ca^{2+}).

4.3.1 Effect of pH on scandium (Sc^{3+}) and calcium (Ca^{2+})

4.3.1.1 Effect of pH on Scandium

The effect of solution pH on the sorption of scandium was evaluated over a pH range of pH=2 to pH=8 using a contact time of 2 hours and a concentration of 2 ppm. The obtained results are presented in Table 4.4 and Figure 4.7.

Table 4.4: Effect of pH on Sc^{3+} sorption

pH	Sc^{3+} Sorption (%)
2	100
3	94
4	91
5	94
6	100
7	99
8	99
9	97

The percentage removal of scandium was rapid at a pH=2. The maximum sorption was observed at pH=2, with a maximum sorption capacity of 0.050 mg/g. The increased scandium sorption observed at pH=5 could be ascribed to the precipitation of $Sc(OH)_3$ (s), based on the Eh-pH and speciation diagrams of a study by (Van Nguyen et al*.,* 2016).

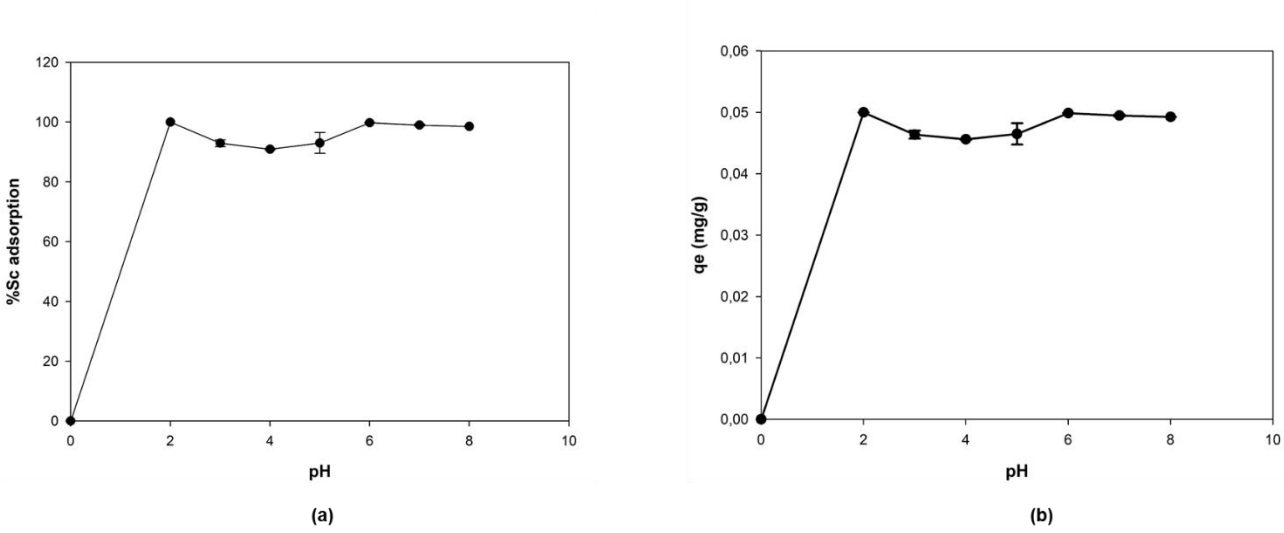

Figure 4.7: Scandium sorption efficiency as a function of pH and (b) Scandium Sorption capacity as a function of pH.

Scandium can be hydrolysed to $ScOH^{2+}$ (aq), $Sc(OH)_2^{+}$ (aq), or $Sc(OH)_4^{-}$ (aq) with an increase in solution pH (Schweitzer and Pesterfield 2010). Scandium mostly exists as Sc^{3+} in an aqueous acidic solution. The extractant, D2EHPA, can form a strong complex with Sc^{3+}. This result is in agreement with a study done by (Van Nguyen et al*.,* 2016).

Generally, evaluating the effect solution pH has on the sorption process could give a better understanding of the mechanism involved in the uptake of the metal ions onto the surface of the resin. The metal ions in aqueous solutions are inclined to exchange with H^+ ions which come from the extractant that is impregnated on the adsorbent.

The percentage of scandium removal remained above 90% over the pH range (pH=2 to pH=8) used in this study. It can be concluded that the solution pH significantly impacts the sorption of scandium from aqueous solutions.

4.3.1.2 Effect of pH on Calcium

The effect of solution pH on the sorption of calcium was evaluated over a pH range of pH=2 to pH=8, a contact time of 2 hours and a concentration of 10 ppm was used. The obtained results are presented in Table 4.5 and Figure 4.8.

Table 4.5: The effect of pH on Ca^{2+} sorption efficiency

pH	Ca^{2+} Sorption (%)
2	79
3	98
4	99
5	97
6	98
7	99
8	98
9	99

The Ca^{2+} sorption is strongly pH-dependent (Table 4.5, Figure 4.8). The maximum sorption (0.2428 mg/g) occurs at pH=4, with a sorption efficiency of 99%. No significant change in sorption is observed upon a further increase in pH. With the addition of more NaOH to increase the solution pH, an acid-base neutralisation reaction possibly occurred forming Na-D2EHPA species, followed by a cation exchange process, forming a Sc-D2EHPA complex after contact with Sc^{3+}, resulting in a plateau in Ca^{2+} sorption (Shi et al*.,* 2020).

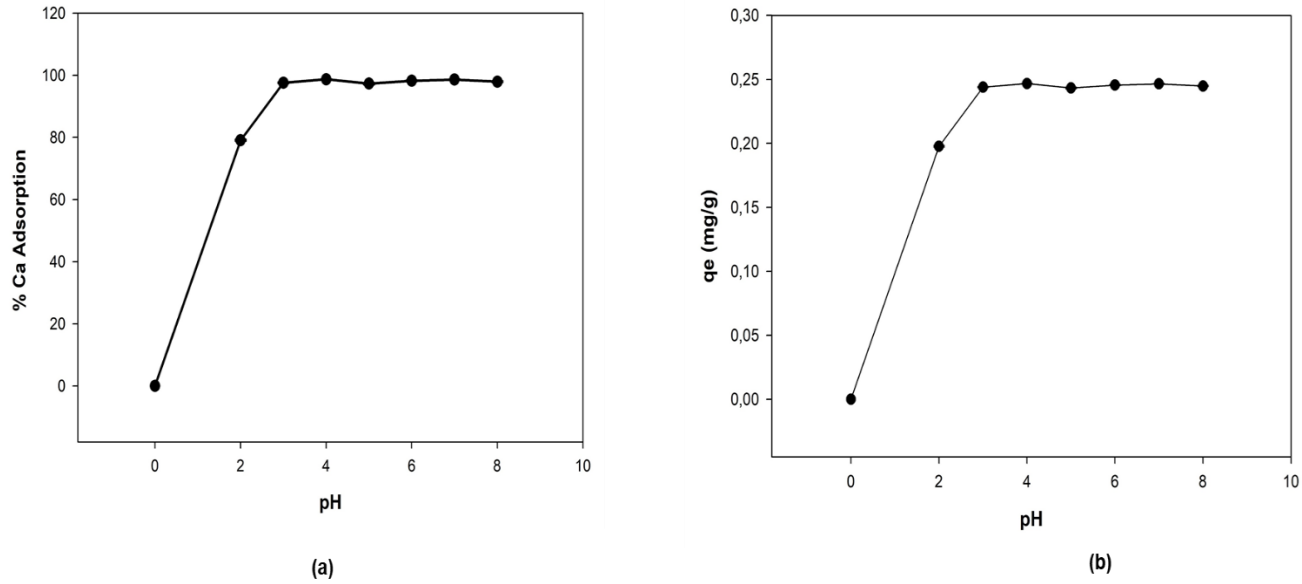

Figure 4.8: Calcium sorption efficiency as a function of (a) pH and (b) sorption capacity of calcium as a function of pH

4.3.2 Effect of initial metal ion (Sc^{3+} and Ca^{2+}) concentration

4.3.2.1 Effect of initial scandium (Sc^{3+}) concentration

The effect on initial metal ion concentration was studied at a pH=4, contact time of 2 hours and a concentration of 0.5 mg/L to 4.0 mg/L and the obtained results are depicted in Figure 4.9.

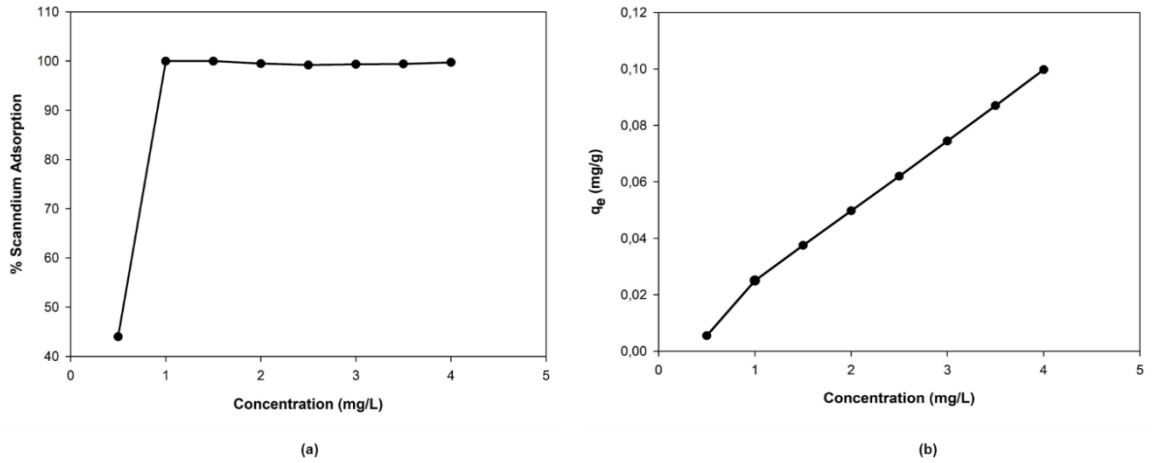

Figure 4.9: Scandium sorption efficiency with varying (a) initial concentration and (b) Scandium sorption efficiency as a function of concentration

Figure 4.9 (a and b) depicts the results of the effect concentration has on the percentage removal and the sorption capacity of scandium using the impregnated resin. A steady and linear increase in the amount of scandium adsorbed per unit mass (0.006 mg/g to 0.10 mg/g) was observed over the concentration range (Figure 4.9b). The linear increase could be due to the saturation of available sites. A sharp rise in the percentage removal of scandium from the solution was observed (Figure

4.9a) from 0 to 100% as the initial concentration increased from 0.5 to 1.0 mg/L, with a sorption capacity of 0.025 mg/g. The percentage of scandium sorption remains constant thereafter. This supports the fact that available sorption sites become occupied with increasing Sc^{3+} concentration until saturation is reached. The sorption capacity at 2.0 mg/L (0.050 mg/g) is in agreement with the maximum sorption capacity obtained from the pH studies. Based on this, it was decided to use the 2.0 mg/L as the optimal initial scandium concentration for the rest of the studies.

4.3.2.2 Effect of initial calcium (Ca^{2+}) concentration

The effect on initial Ca^{2+} concentration was studied at a pH=4, a contact time of 2 hours using a concentration range of 0.5 mg/L to 4.0 mg/L. Calcium sorption increased linearly with increasing initial ion concentration, and no sorption plateau was reached (Figure 4.10). The sorption capacity at 10 mg/L compares well with the maximum sorption capacity obtained from the pH studies (0.2428 mg/g).

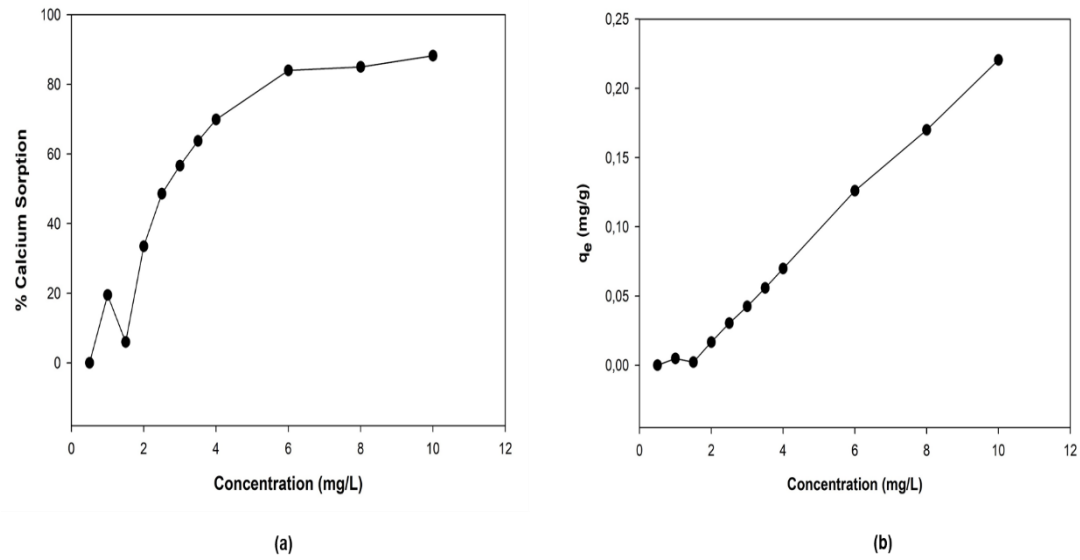

Figure 4.10: (a) Effect of initial concentration on calcium sorption efficiency and (b) Calcium sorption capacity as a function of initial concentration

4.3.3 Time dependence

4.3.3.1 Time dependence on the sorption of Scandium

Table 4.6 and Figure 4.11 present the obtained results of the effect of time on the scandium sorption studied over a range of 2 min to 30 min, using an initial concentration of 2.0 mg/L at a pH=4.

Table 4.6: Effect of time on Sc^{3+} sorption efficiency

Time (min)	Sc Conc (mg/L)	% Sorption	Qe (mg/g)
0.00	2.10	0	0.00
2.00	1.79	41	0.06
4.00	1.73	73	0.07
6.00	1.67	100	0.09
8.00	1.42	100	0.14
10.00	1.24	100	0.17
15.00	1.14	100	0.19
30.00	0.60	100	0.30
60.00	0.66	100	0.29
120.00	0.10	100	0.40
180.00	0.10	100	0.40
240.00	0.10	100	0.40

As shown in Figure 4.11(a), a rapid increase in the adsorption of scandium was observed within the first 6 minutes, having a sorption efficiency of 100%. The sorption remained constant thereafter. The optimal reaction time of 30 min was selected for sorption equilibrium to be attained.

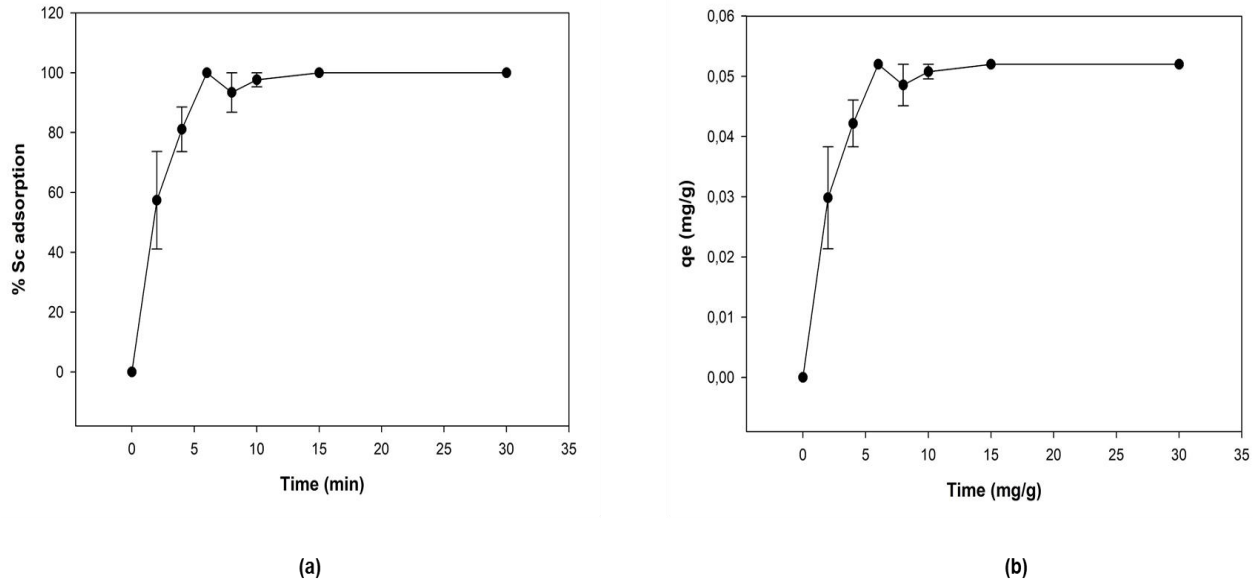

Figure 4.11: (a) Effect of contact time on scandium sorption efficiency and (b) Scandium sorption capacity over time.

4.3.3.2 Time dependence on the sorption of Calcium

The time-dependence studies of calcium sorption were carried out at a pH=4, 10 ppm Ca^{2+} concentration, over a range of 10 min to 4 hours. The results are demonstrated in Table 4.7 and Figure 4.12. The results showed the Ca^{2+} ion sorption occurred within 60 min. After 60 min, the maximum sorption capacity of 0.248 mg/g was reached. The sorption capacity at 60 min agrees with the maximum sorption capacities obtained from the pH and concentration studies.

Table 4.7: Effect of time on Ca sorption efficiency

Time	Ca Conc (mg/L)	% Sorption	Qe (mg/g)
0	0	0	0
10	0.84	91	0.229
30	0.24	97	0.244
60	0.085	99	0.248
120	0.155	98	0.246
180	0.33	96	0.242
240	0.14	98	0.247

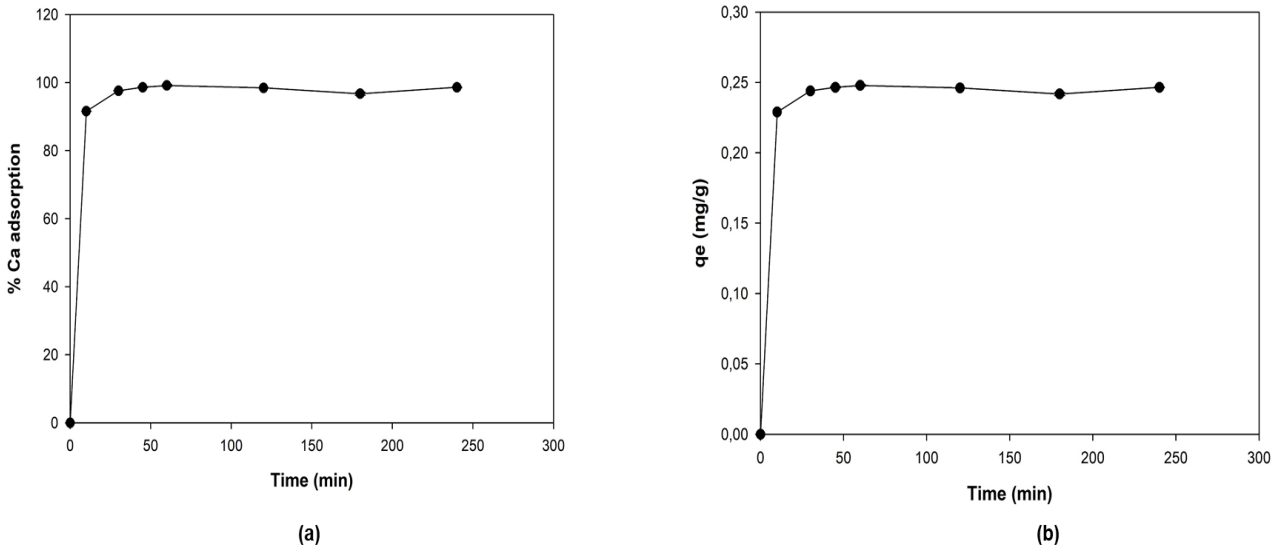

Figure 4.12: (a) Effect of contact time on calcium sorption efficiency and (b) Calcium sorption capacity over time.

4.3.4 Effect of the sorbent dosage on the sorption of Sc and Ca

The sorbent mass is an important parameter because it determines the capacity of the sorbent for the sorption of metal ions.

4.3.4.1 Sorbent dose on the sorption of Scandium

The effect sorbent mass has on the sorption of Sc^{3+} was evaluated, and the results are illustrated in Figure 4.13. The mass was varied between 0.1 g to 3.0 g using a concentration of 2.0 mg/L Sc^{3+} aqueous solution. The sorption of Sc^{3+} increased from 56% and 91% with an increase in sorbent dosage.

This increase in% sorption can be ascribed to the increase in the available sites for metal ion adsorption, leading to increased sorption of metal ions. It was observed that by increasing the amount of adsorbent from 0.1 g to 1.0 g, the% sorption remained constant with further increases up to 3.0 g. This can be a result of sorption sites overlapping, as opposed to the overfilling of adsorbent particles. Based on these results, the optimal sorbent mass used for Sc^{3+} sorption studies was 1.0 g.

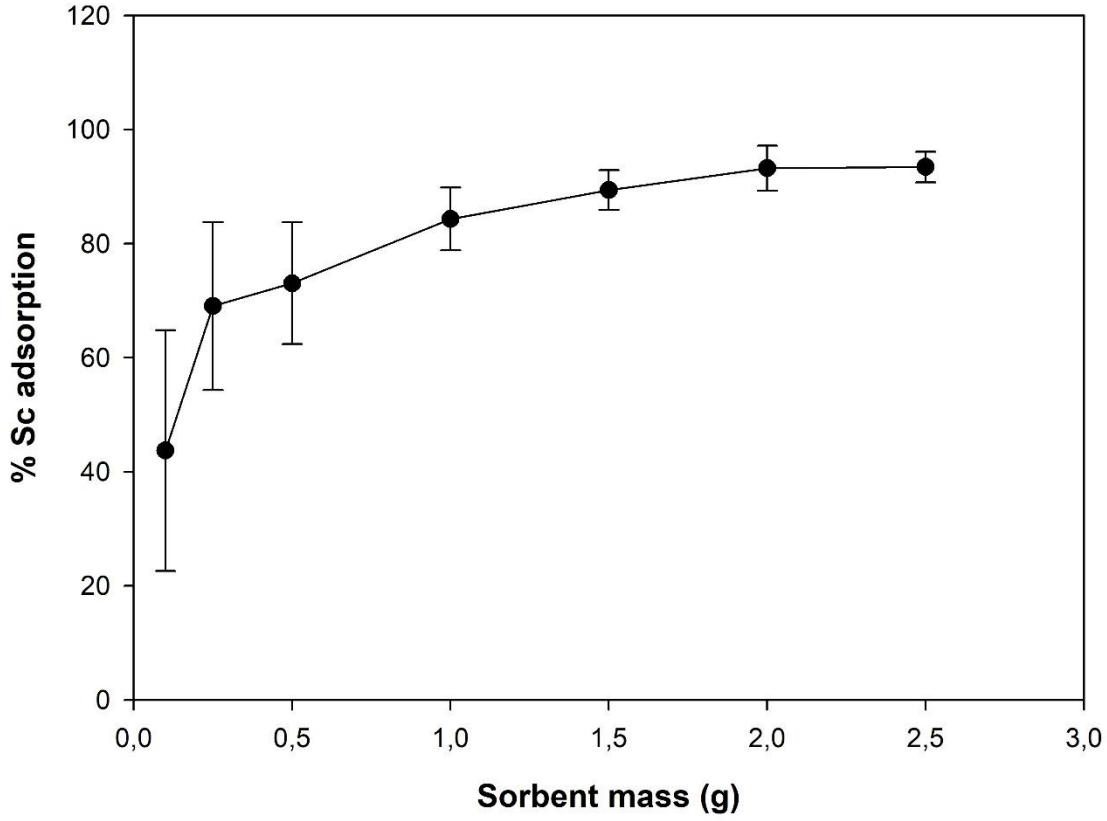

Figure 4.13: Effect of sorbent dosage on Sc^{3+} sorption

4.3.4.2 Sorbent dose on the sorption of Calcium

Ca^{2+} sorption capacity with a varying sorbent mass was evaluated, and the results are demonstrated in Figure 4.14. The sorbent mass was varied from 0.1 g to 3.0 g. The concentration of Ca^{2+} solutions was 10.0 mg/L. With increasing sorbent dosage, the sorption of Ca^{2+} ions increased from 91% to 100%. Based on these results, the optimal sorbent mass used for all sorption studies for Ca^{2+} was 1.0 g.

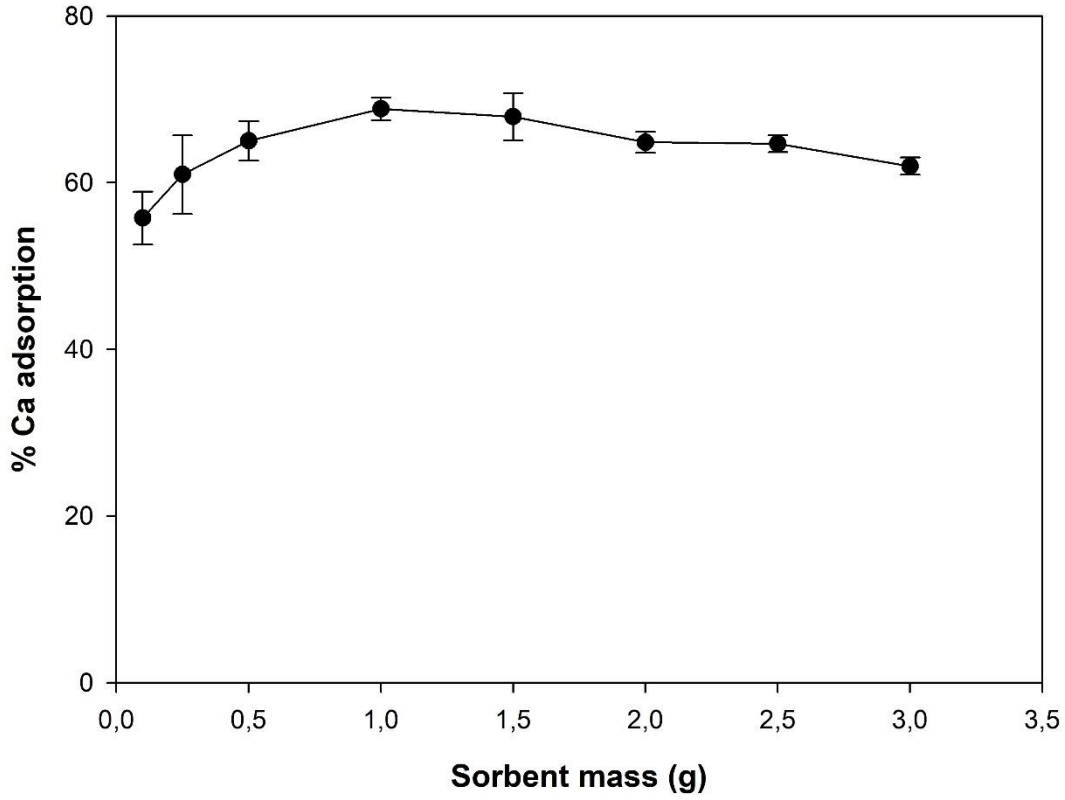

Figure 4.14: Effect of sorbent dosage on Ca^{2+} sorption

4.3.5 Adsorption isotherm

Adsorption isotherms are useful and important for understanding the relationship between metal ions (sorbate) and sorbent during adsorption. Experimental equilibrium data obtained from this study for both scandium and calcium were subjected to four adsorption equilibrium isotherm models (Langmuir, Freundlich, Temkin and Dubinin-Radushkevich).

4.3.5.1 Scandium

A summary of the characteristic parameters for each of the four isotherms is presented in Figure 4.15(a-d) and Table 4.8. Of the four isotherms, the Langmuir isotherm provided the best fit to the experimental data, with a high linear regression coefficient of R^2=0.9934 Figure 4.15(a). The other three isotherms—Freundlich (Figure 4.15b), Temkin (Figure 4.15c), and

Dubinin-Radushkevic (Figure 4.15d) had very low regression coefficients, and their calculated capacities poorly correlate to the experimental value. The mean sorption energy (E) obtained from the Dubinin-Radushkevic plot was 158 kJ/mol, which signifies chemisorption as the sorption mechanism involved in Sc sorption using the impregnated resin.

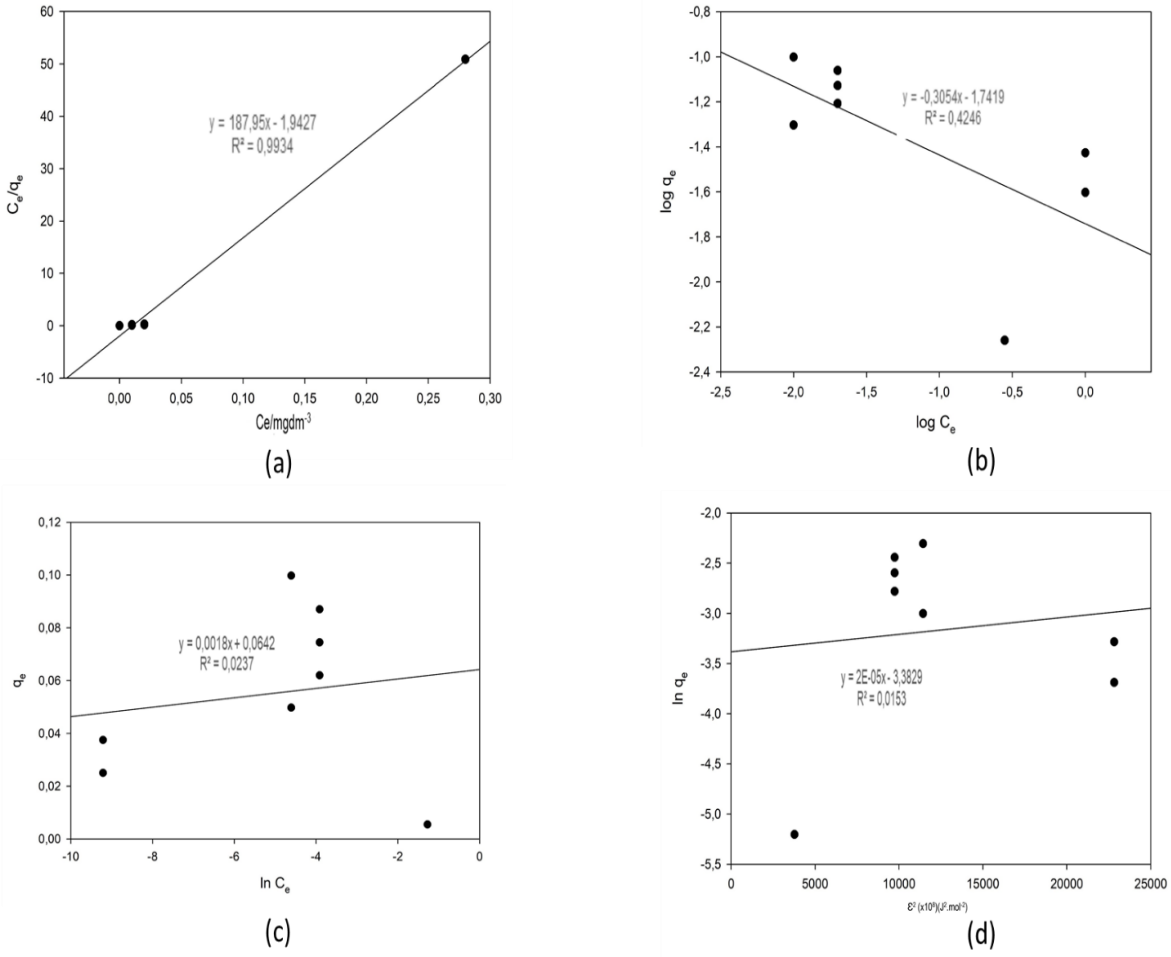

Figure 4.15: Adsorption isotherms of Sc^{3+}, (a) Langmuir isotherm, (b) Freundlich isotherm, (c) Temkin isotherm and (d) Dubinin-Radushkevich

The linearized form of the Langmuir isotherm equation is expressed as:

$$\frac{C_e}{q_e} = \frac{\alpha_L C_e}{K_L} + \frac{1}{K_L} \qquad \textbf{Eq.4.2}$$

K_L and α_L are the equilibrium constants of Langmuir equation. The plot of Ce/qe against C_e yields a straight line with a slope, $\alpha L/K_L$, and intercept $1/K_L$ (Abdullah et al*.,* 2009). The essential feature of the Langmuir isotherm can be expressed in terms of a separation factor that can be calculated from the following equation (Bouhamed et al*.,* 2012):

$$R_L = \frac{1}{(1+K_L C_o)} \qquad \textbf{Eq. 4.3}$$

The value of R_L was calculated to be $6.8x10^{-3}$. It falls within the range of 0-1 at optimum pH, confirming the favourable adsorption of Sc^{3+} ions on the impregnated resin (Kalal et al*.,* 2012).

Table 4.8: Characteristic parameters of Sc^{3+} sorption isotherms

Isotherm	Correlation coefficient	Parameters
Langmuir	0.9934	q_m = 0.00532 mg/g K_L = 96.757 dm^3/mg
Temkin	0.0237	RT/b = 0.0018 J/mol $K_T = 3.1x10^{12}$
Freundlich	0.4246	K_F = 0.4949 mg/g n =1.7419
Dubinin-Radushkevich	0.0153	X_m = 29.456 mg/g $\beta = 2x10^{-5}$ mol^2/kJ^2 E = 158.1 kJ/mol

4.3.5.2 Calcium

A summary of the characteristic parameters for each of the four isotherms is presented in Figure 4.16 (a-d) and Table 4.9. When the data was applied to all four isotherms, the data fitted the Dubinin-Radushkevich isotherm best, with R^2 = 0.3571 (Figure 4.16d). This adsorption model follows a pore-filling mechanism, presumes a multi-layer character, and is typically associated with physical adsorption processes (Nimibofa et al., 2017). The other three isotherms, Langmuir (Figure 4.16a), Freundlich (Figure 4.16b), and Temkin had varying correlation coefficients ranging from 0.3366 to 0.0966. The Langmuir model is generally associated with monolayer sorption, while the Freundlich model is related to multi-layer sorption. However, these models cannot primarily be used to distinguish whether the sorption process is governed by either a chemical or physical process. Hence, the sorption energy can be used to give information regarding the mechanism involved in the sorption process. From the Dubinin-Radushkevic plot (Figure 4.16d) for Ca, the mean sorption energy (E) of 14.7 kJ/mol was calculated, concluding that Ca^{2+} sorption occurred via the chemical sorption process. The value of the constant indicating the intensity of sorption (n) calculated from the slope of the Freundlich plot was between and 10, thus implying the sorption of Ca onto the impregnated resin was favourable.

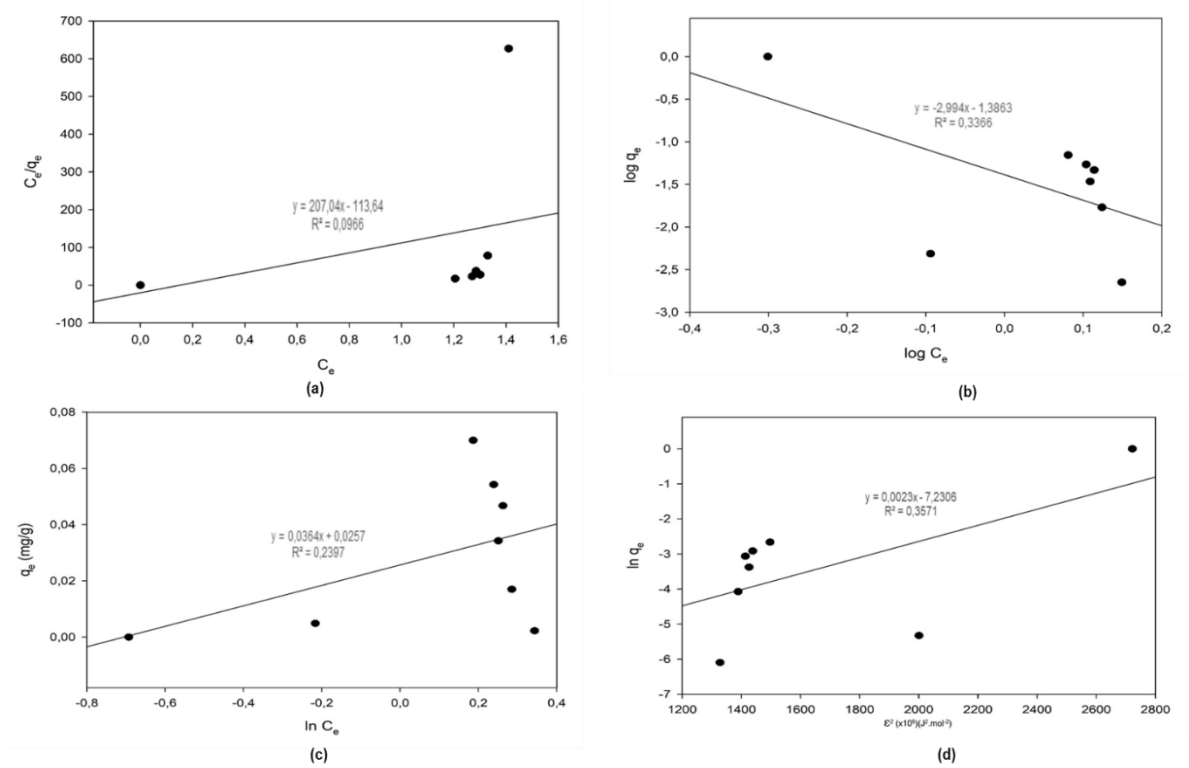

Figure 4.16: Adsorption isotherms of Ca^{2+}, (a) Langmuir isotherm, (b) Freundlich isotherm, (c) Temkin isotherm and (d) Dubinin-Radushkevich.

Table 4.9: Characteristic parameters for Ca^{2+} sorption isotherms

Isotherm	Correlation Coefficient	Parameters
Freundlich	0.3366	K_F = 0.0010 mg/g n =1.3863
Dubinin-Radushkevich	0.3571	X_m = 1423.1 mg/g β = 0.0023 mol^2/kJ^2 E = 14.744 kJ/mol
Temkin	0.2397	RT/b = 0.0364 J/mol K_T = 2.03x10-3 kL/mol
Langmuir	0.0966	q_m = 0.00483 mg/g K_L = 1.82 L/mg

4.3.6 Sorption kinetics

4.3.6.1 Adsorption reaction kinetics

4.3.6.1.1 Scandium

The Pseudo-First-order, Pseudo-Second order, and Elovich models were applied to analyse

the sorption data for scandium. The plots are shown in Figure 4.17, and their parameters are presented in Table 4.10.

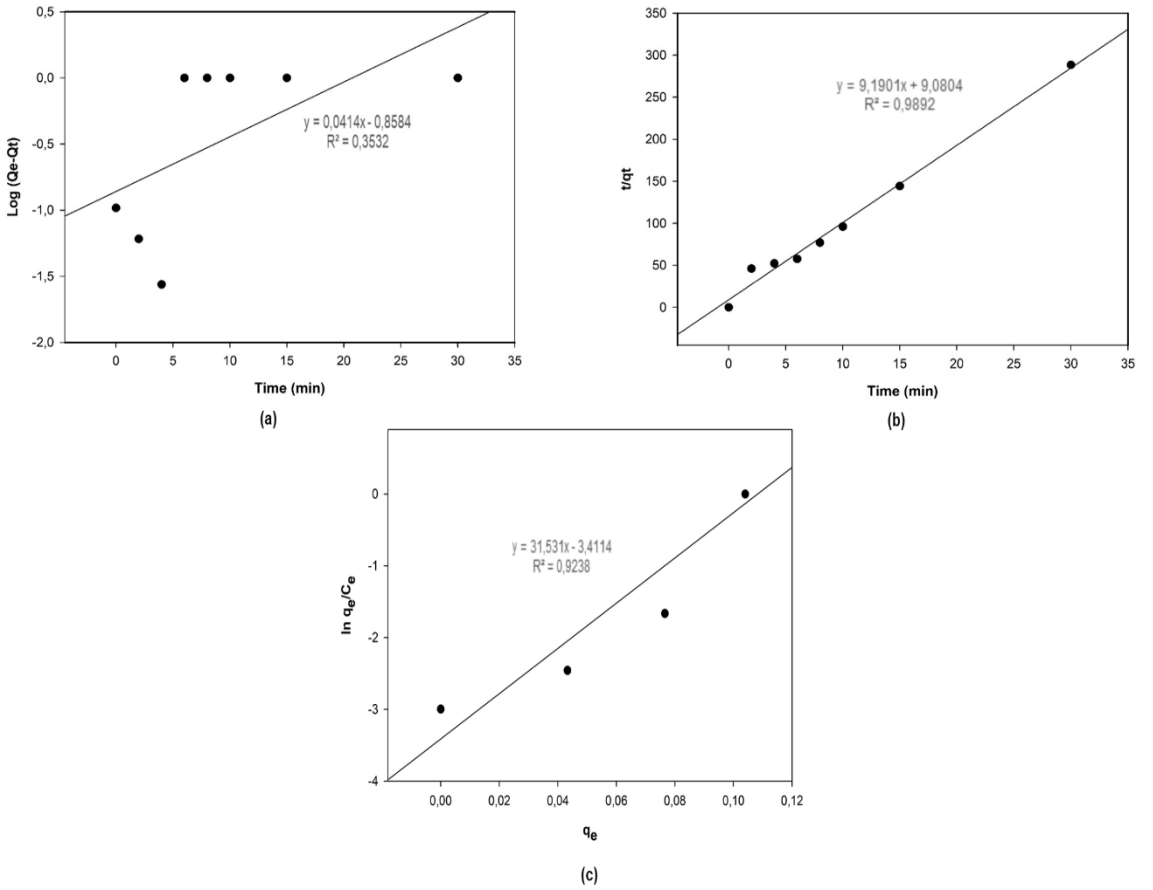

Figure 4.17: Adsorption kinetics of Sc^{3+}, (a) Pseudo first-order model, (b) Pseudo second-order model and (c) Elovich model

The correlation coefficients (R^2) were 0.9892 > 0.9238 > 0.0287 for Pseudo Second-order, Elovich, and Pseudo-First-order models, respectively. The Pseudo-Second-order graph (Figure 4.17b) gave a higher correlation between the experimental parameters compared to the other models, a suggestion the experimental scandium data is best modelled by the Pseudo-Second-order kinetics.

A theoretically predicted adsorption capacity (0.109 mg/g) closely compared to the experimental value (0.100 mg/g) serves as confirmation that the Pseudo-Second-order kinetics model is the better fit and that the sorption is occurring via a chemical process (Kumar et al., 2011). A summary of the kinetics parameters for scandium is presented in Table 4.10.

Table 4.10: Kinetics parameters for scandium for pseudo-first-order model, pseudo-second-order model and Elovich model

Models			Parameters	
Pseudo-First-order	Qe (expt.)	Qe (calc.)	R^2	K_1
	0.10	0.1385	0.3532	0.095
Pseudo-Second-order	Qe (expt.)	Qe (calc.)	R^2	K_1
	0.10	0.109	0.9892	9.269
Elovich	Qe (expt.)	Qe (calc.)	R^2	K_1
	0.10		0.9238	

The calculated sorption capacity (qe) and First-Order rate constant (k_1) were calculated from the intercept and slope of the corresponding graph, respectively, as follows:

$$\frac{k_1}{2.303} = 0.0414 \qquad \textbf{Eq. 4.4}$$

$$k_1 = 0.095$$

The calculated sorption capacity (q_e) and the second order rate constant (k_2) was derived from the slope and the intercept of the graph, respectively, and calculated according to the following equations:

$$\frac{1}{qe,calc} = \quad 9.1901 \qquad \textbf{Eq. 4.5}$$

$$\therefore \; qe,calc = 0.109\ mg/g$$

$$\frac{1}{h} = \frac{1}{k_2\, qe^2} = 9.0804 \qquad \textbf{Eq. 4.6}$$

$$k_2 = 9.269$$

4.3.6.1.2 Calcium

The Pseudo-First-order, Pseudo-Second order, Elovich models were applied to analyse the sorption data for calcium, and the obtained plots and their parameters are presented in Figure 4.18(a-c) and Table 4.11, respectively. The Pseudo-First-order graph (Figure 4.18a) has a correlation coefficient (0.8255), and the calculated sorption capacity (0.327 mg/g) obtained from the slope differed significantly from the experimental value. The Pseudo-Second-order graph (Figure 4.18b) showed an excellent correlation between experimental conditions.

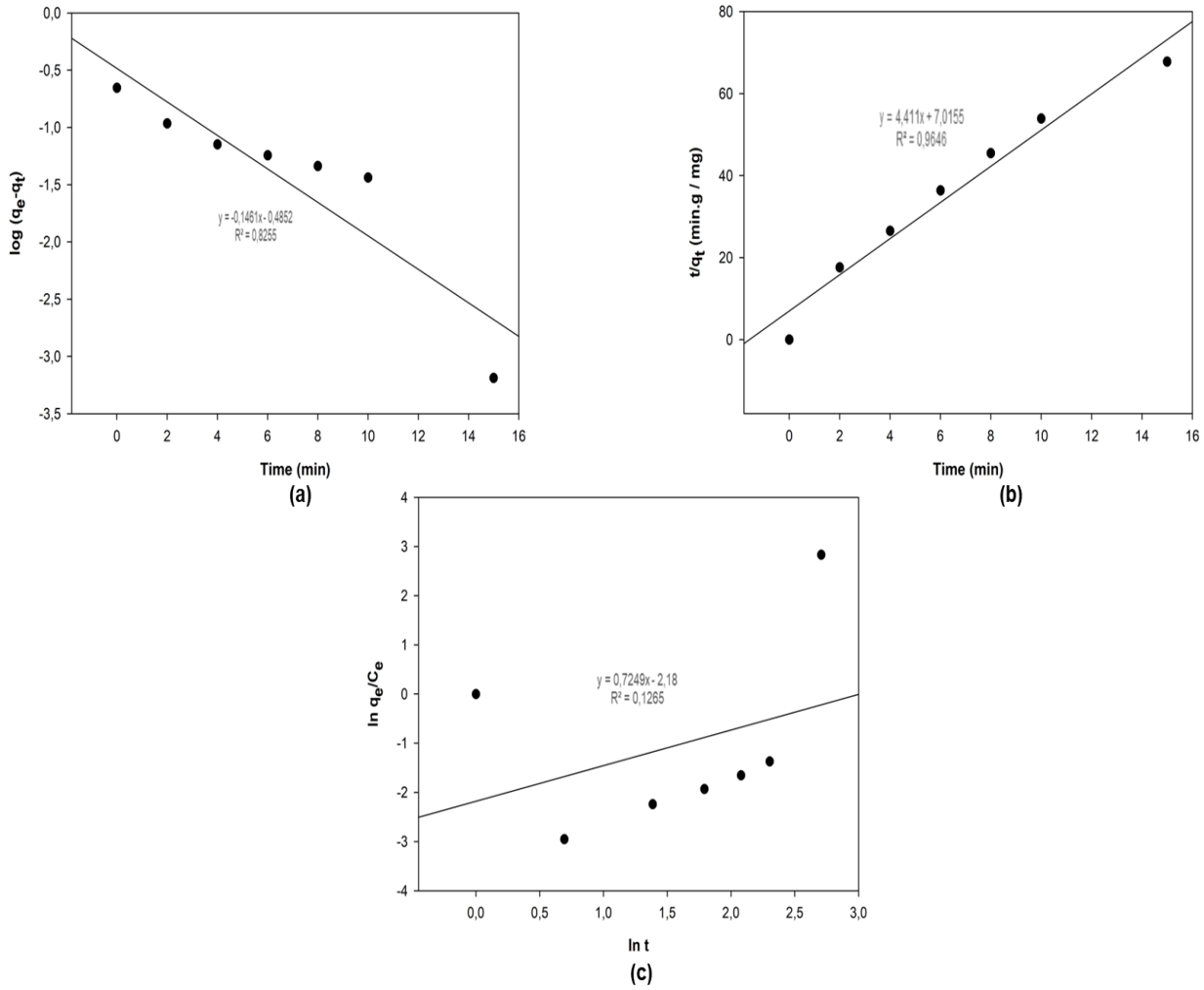

Figure 4.18: Adsorption kinetics of Ca^{2+}, (a) Pseudo first-order model, (b) Pseudo second-order model and (c) Elovich model

The calculated sorption capacity (0.227 mg/g) from the Pseudo-Second-order (Figure 4.18c, Table 4.11) was in good agreement with the practical value. The good correlation and sorption capacity suggest Ca^{2+} sorption on the impregnated resin occurred via chemisorption. The correlation coefficients (R^2) were 0.9645 > 0.8255 > 0.1265 for Pseudo-Second-order, Pseudo-First-order models and Elovich model, respectively.

Table 4.11: Kinetics parameters for calcium for pseudo-first-order model, pseudo-second-order model and Elovich model

Models			Parameters	
Pseudo-First-order	Qe (expt.)	Qe (calc.)	R^2	K_1
	0.22	0.327	0.8255	0.336
Pseudo-Second-order	Qe (expt.)	Qe (calc.)	R^2	K_1
	0.22	0.227	0.9645	2.766
Elovich Model	Qe (expt.)	Qe (calc.)	R^2	K_1
	0.22		0.1265	

4.3.6.2 Reaction-diffusion

4.3.6.2.1 Weber Morris model

The Weber-Morris diffusion model was used to describe the sorption of scandium and calcium onto D2EHPA-impregnated resin. This model is based on the assumption that the overall sorption process is controlled by either one or a combination of factors, for example, film diffusion, pore diffusion, surface diffusion, and sorption onto the adsorbent pore surface (Fierro et al*.,* 2008; Asuquo et al*.,* 2017).

The equation for this model is expressed as:

$$q = kt^{1/2} + I \qquad \textbf{Eq. 4.7}$$

where k is the diffusion rate parameter (mg L^{-1} $s^{-1/2}$), and the value of I can be calculated from the intercept from the plot of q versus $t^{1/2}$ (Zhu et al., 2016). The plots for scandium and calcium are presented in Figure 4.19.

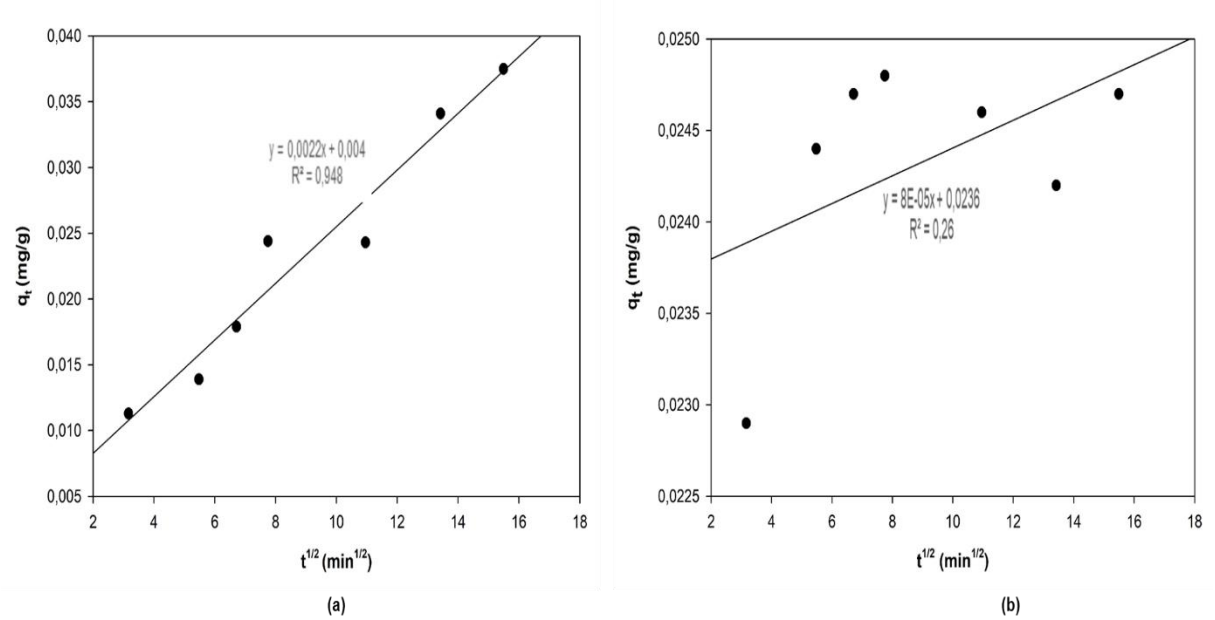

Figure 4.19: Weber Morris diffusion kinetics plots for (a) scandium sorption and (b) calcium sorption

Intraparticle diffusion is normally considered the rate-controlling step when the linear plot of qe against $t^{1/2}$ passes through the origin. The plots of qe against $t^{1/2}$ for both graphs did not pass through the origin nor did it produce a straight, suggesting intra-particle diffusion was not the only diffusion mechanism involved, and that sorption diffusion kinetics may be controlled by film diffusion and pore diffusion (Qiu et al., 2009). The plots for both scandium and calcium show multi-linearity over the sorption period (Figure 4.20).

Multi-linearity suggests both diffusion mechanisms are present and can thus control the sorption process. Multi-linearity also implies that varying pore sizes influenced the diffusion of Sc^{3+} ions through the resin structure, as was confirmed by the SEM images for the impregnated resin.

Based on the results from the batch sorption studies, separations from binary mixtures were conducted using the column method. The separation of Sc from Ca is significant to the isolation of the Sc-47 isotope, which is among the radioisotopes with attractive theranostic effects for targeted radionuclide therapy of small tumours and cancer metastasis (Gizawy et al., 2021).

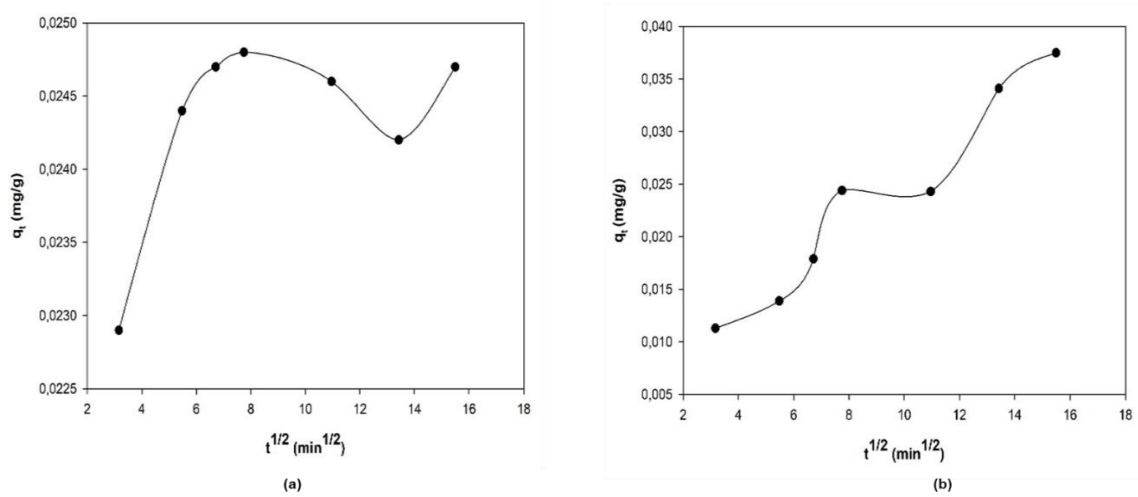

Figure 4.20: Intraparticle diffusion kinetics for (a)scandium and (b) calcium removal using the impregnated resin

The impregnated resin has a high selectivity for Sc at a pH=2. The concentration of each element in the mixture was 1.0 mg/L (Sc^{3+}) and 10.0 mg/L (Ca^{2+}). The pH of the influent solution was maintained at pH=2. The breakthrough curve for each element is presented in Figure 4.21.

From Figure 4.21 it can be observed that Sc cannot be separated with great efficiency from Ca. Both Sc and Ca began to break through the column in the first few eluate fractions.

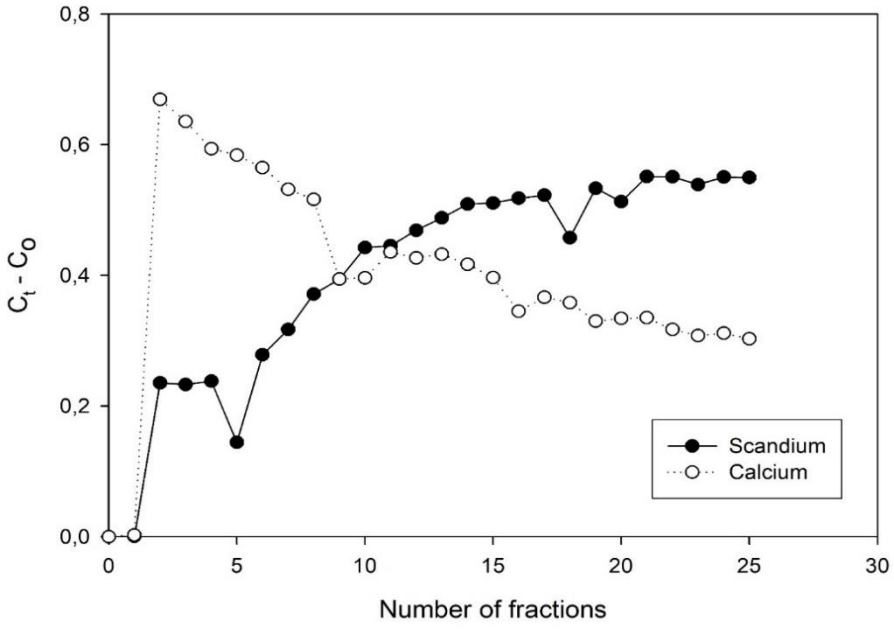

Figure 4.21: Breakthrough curve for D2EHPA-XAD-4 for scandium and calcium

4.3.7 Statistical analysis

A *t*-test is a type of statistical test that is used to compare the means of two groups. It is one of the most widely used statistical hypothesis tests in pain studies . There are two types of statistical inference: parametric and nonparametric methods. Parametric methods refer to a statistical technique in which one defines the probability distribution of probability variables and makes inferences about the parameters of the distribution. In cases in which the probability distribution cannot be defined, nonparametric methods are employed. T tests are a type of parametric method; they can be used when the samples satisfy the conditions of normality, equal variance, and independence.

T-tests can be divided into two types. There is the independent t test, which can be used when the two groups under comparison are independent of each other, and the paired t test, which can be used when the two groups under comparison are dependent on each other. The independent *t*-test is also known as Student's t test. It is a statistical analysis technique that was developed by William Sealy Gosset in 1908 as a means to control the quality of dark beers. A t test used to test whether there is a difference between two independent sample means is not different from a t test used when there is only one sample.

The results for the t-test for the batch adsorption experiments (pH, time dependence and sorbent dosage) for scandium and calcium are shown in Table 4.12.

Table 4.12: Independent t test

Parameter	Scandium		Calcium				
	Mean	SD	Mean	SD	*t*-value	*p*-value	*df*
pH	0.0735	0.070	0,463	0.666	-1,427	0,179	12
Time Dependance	0,443	0,682	1,491	3,224	-0.841	0.414	14
Sorbent Dosage	0.493	0.331	3.626	0.411	-15.75	$7.5x10^{-10}$	13

CHAPTER 5
RESULTS AND DISCUSSION: ION EXCHANGE CHROMATOGRAPHY

5.1 Equilibrium distribution coefficient determination

The addition of a water-miscible organic solvent to aid in the formation of chloride complexes and to improve the cation exchange separation of metals was first explored by (Kember et al*.,* 1955). The distribution coefficients and cation exchange behaviour of various elements, using both HCl-acetone and HCl-methanol mixtures, have previously been studied by (Strelow et al*.,* 1971; Strelow 1984). This chapter focuses on the sorption behaviour of scandium and calcium on the Dowex 50W-X8 cation exchange resin in HBr-methanol mixtures. The equilibrium distribution coefficients of scandium and calcium were investigated on the cation exchange resin in various HBr-methanol mixtures. Using the findings from the distribution coefficients studies, a two-component binary separation on the cation exchange resin was investigated. The results of the experimental determination of the distribution coefficients are presented in Table 5.1 and Table 5.2, as well as Figure 5.1.

Table 5.1: Distribution coefficients (K_d) for scandium

% Methanol	0.5 M HBr	1.0 M HBr	2.0 M HBr	3.0 M HBr
20	4607	601	164	55
40	10463	1521	386	142
60	23779	6821	2139	702

Table 5.2: Distribution coefficients (Kd) for calcium

% Methanol	0.5 M HBr	1.0 M HBr	2.0 M HBr	3.0 M HBr
20	369	76	13	2
40	592	156	23	11
60	1063	336	78	54

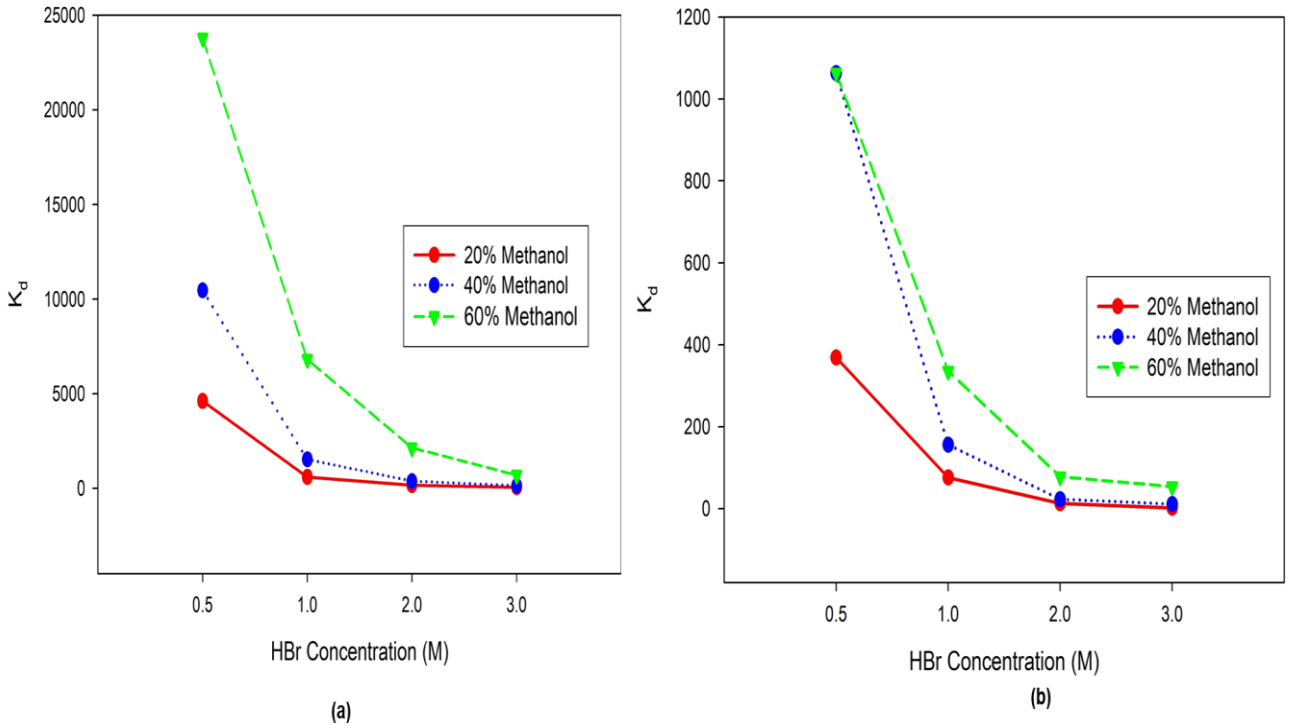

Figure 5.1: Distribution coefficients (K_d) for (a) scandium and (b) calcium

In general, the greater the K_d value, the stronger the metal ion is retained by the resin and the more difficult it would be to elute. The charge and the valencies of the metal ion also play an important role in the Kd value. Elements with higher ionic charge, tend to be stronger retained by the resin. From the results obtained, it is evident that the resin has a greater affinity for Sc^{3+} ion than for Ca^{2+} over the concentration range of 0.5 M HBr to 3 M HBr, with various methanol ratios. As indicated in 2.6.1.2.6, a separation factor greater than 10 between two ions normally implies efficient separation. Based on the results, separation of Sc^{3+} and Ca^{2+} is possible for all HBr- methanol mixtures. The separation factors for scandium and calcium for all the HBr-methanol mixtures are illustrated in Table 5.3 and Figure 5.2.

Table 5.3: Separation factors for Sc and Ca

% Methanol	0.5 M HBr	1.0 M HBr	2.0 M HBr	3.0 M HBr
20	12.5	8.0	10.2	27.5
40	17.7	9.8	16.8	7.4
60	22.4	20.3	27.4	12.9

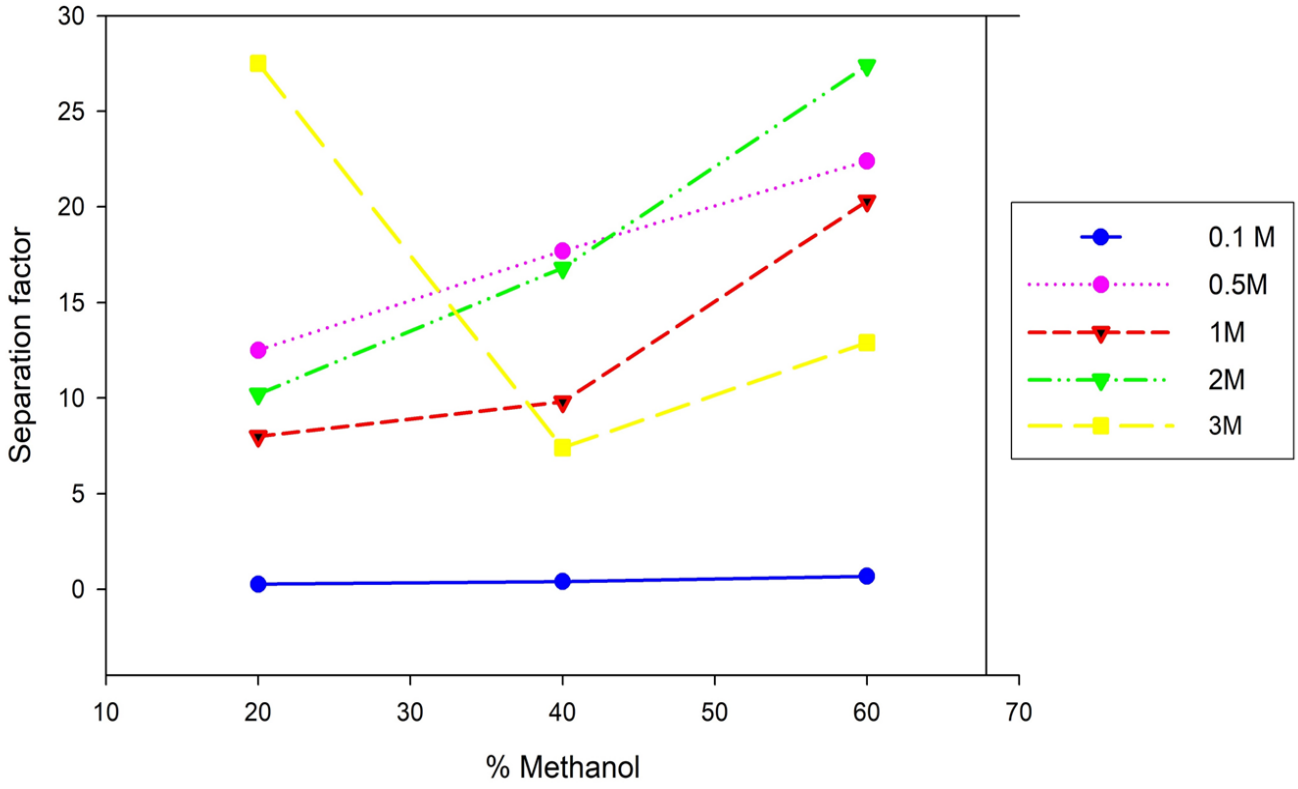

Figure 5.2: Separation factors plot for scandium and calcium

5.2 Elution curves for elemental separation

Based on the experimental distribution coefficients and separation factors, a two-component separation of scandium and calcium was investigated in a 3.0 M HBr – 20% methanol mixture, having a separator factor of 27.5. A 5 mL resin column was equilibrated with 50 mL of 3.0 M HBr-20% methanol. A solution containing 0.05 mg Sc^{3+} and 5 mg Ca^{2+} in 50 mL of 3.0 M HBr-20% methanol was prepared and passed through the column. The Ca^{2+} was eluted with a total of 200 mL of 3.0 M HBr-20% methanol solution. Any remaining Sc^{3+} on the resin was then eluted with 200 mL of 5 M HCl. A flow rate of 5.0 ± 0.5 mL/min was maintained throughout, and 10 mL fractions were collected from the start of the loading (sorption) step. All fractions collected, were treated, and analysed as described in 3.3.2.

From Figure 5.3, it follows that the Sc^{3+} ions were retained on the resin and the Ca^{2+} ions passed through the column during the first ten fractions. This confirms the K_d values obtained from the batch studies.

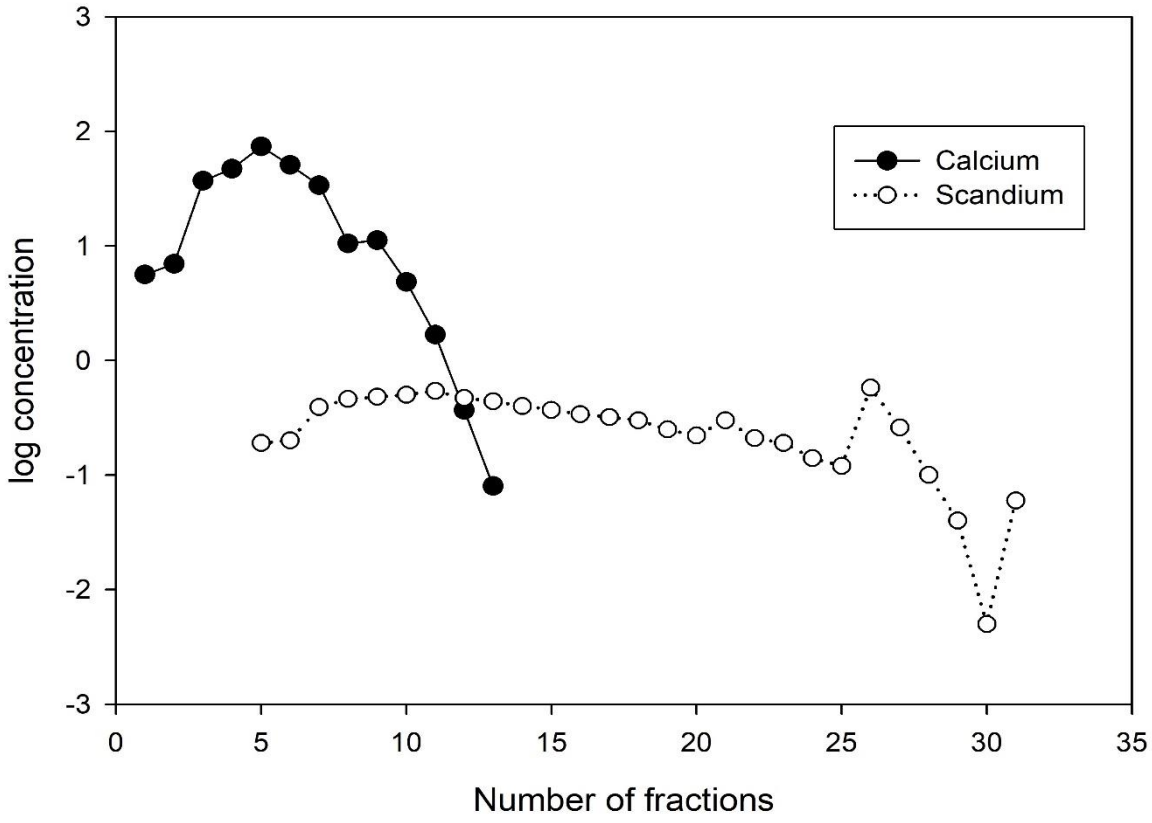

Figure 5.3: Breakthrough curve for Ca^{2+} and Sc^{3+} on a Dowex 50W-X8 cation resin column in 3.0 M HBr – 20% methanol. The sorption step and eluting step of Ca^{2+} with 3.0 M HBr – 20% methanol mixture, followed by 5.0 M HCl to elute Sc^{3+}.

Based on the results from the column studies, it is conspicuous that ion exchange chromatography is the more efficient method for the separation of Sc from Ca. To optimise this method, attention was focused on column length and flow rate.

Three different column lengths were investigated (3mL, 5mL and 10mL). Each of the columns were equilibrated by passing 50mL 3.0 M HBr-20% methanol solution. A solution containing 0.05 mg Sc^{3+} and 5 mg Ca^{2+} in 50 mL of 3.0 M HBr-20% methanol was prepared and passed through the column at a flow rate of 5mL/min. The columns were eluted as described above (5.1.2). Experimental data for these are presented in Figure 5.4.

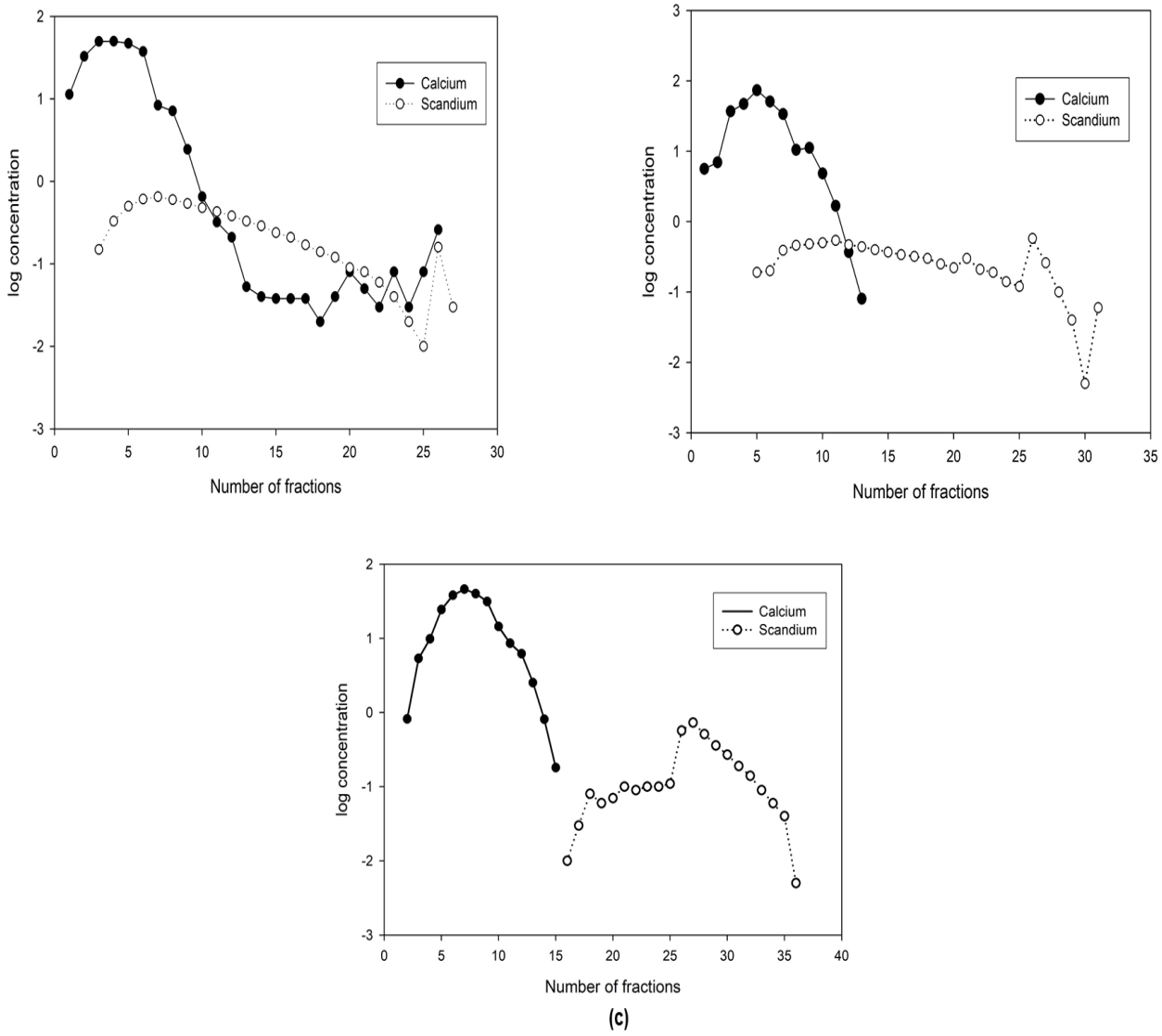

Figure 5.4: Elution curve for Ca^{2+} and Sc^{3+} on a Dowex 50W-X8 cation resin column in 3.0 M HBr – 20% methanol. The sorption step and eluting step of Ca^{2+} with 3.0 M HBr – 20% methanol mixture, followed by 5.0 M HCl to elute Sc^{3+} at a column length of (a) 3 mL, (b) 5 mL and (c) 10 mL

It is evident from Figure 5.4(c) that the 10mL column showed better separation. Both Sc and Ca were effectively eluted from the column. Ca was effectively eluted after the 16 fraction, with the 3.0 M HBr-20% methanol solution, and Sc was effectively eluted after the 12 fraction with 5M HCl. Two flow rates (5 mL/min and 7 mL/min) were evaluated. The 10mL column at a flow rate of 5 mL/min Figure 5.5(a) had in a more efficient separation for Sc. Both Ca and Sc was completely eluted within the 10^{th} fraction using 3.0 M HBr-20% methanol and 5M HCl, respectively.

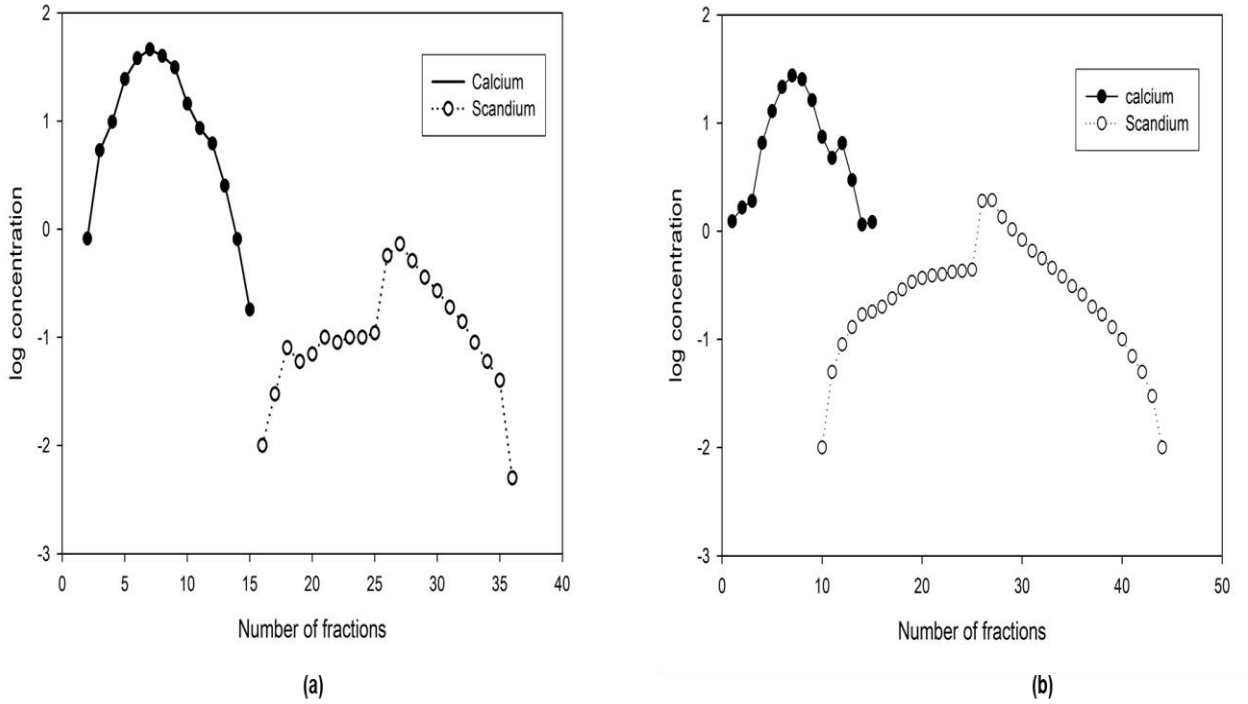

Figure 5.5: Elution curve for Ca^{2+} and Sc^{3+} on a Dowex 50W-X8 cation resin column in 3.0 M HBr – 20% methanol. The sorption step and eluting step of Ca^{2+} with 3.0 M HBr – 20% methanol mixture, followed by 5.0 M HCl to elute Sc^{3+} at a flow rate of (a) 5 mL/min and (b) 7 mL/min

CHAPTER 6
GENERAL DISCUSSION AND CONCLUSION

There has been an increased demand for scandium in the 21st century owing to its wide-ranging applications such as aerospace, special alloys, electronics and the nuclear industry. The growing application of scandium in new technologies raised concerns about its accumulation in the environment following anthropogenic inputs (Pyrzyńska et al*.,* 2019). As a result, the recovery and separation of scandium have attracted a lot of attention (Yagmurlu et al*.,* 2018).

Several methods have been employed to separate and purify scandium for different applications (Pyrzyńska et al*.,* 2019). The separation and purification of scandium from aqueous solutions are customarily executed using precipitation, solvent extraction, and ion exchange chromatography. The downside of these methods includes but is not limited to:

The low scandium purity yields from precipitation due to the co-precipitation of other metals present (Wang & Cheng, 2011). In addition, a large volume of organic reagents is required, sediment generation, and inefficiency for low concentrations (Van Nguyen, et al*.,* 2016; Shi, et al*.,* 2017).

Solvent extraction and ion exchange were the most widely used methods for collecting scandium from various resources (Wang & Cheng, 2011). Solvent extraction, however, uses large amounts of solvent, which poses an environmental risk. Other shortcomings of solvent extraction, such as loss of extractant, phase separation, and third-phase formation, cannot always be easily overcome (Van Nguyen et al*.,* 2013).

Ion exchange chromatography has certain benefits over solvent extractions, such as high adsorption capacity, less complex operations and lower maintenance costs (Fadel et al*.,* 2016).

Extraction chromatography offers an easy-to-use and effective method for separating various metal ions. It serves as a bridge between solvent extraction and the conventional ion exchange processes. As the demand for new scandium sources exists, developing environmentally friendly and cost-effective methods for the separation and purification of scandium is required.

Scandium-44 is a medically interesting positron and gamma emitting radionuclide. It is commonly produced using a cyclotron in a calcium or sometimes a titanium based irradiation target. As the radiopharmaceutical use of scandium radionuclides commonly requires chelation, scandium needs to be separated from the target matrix. This is most often carried out either via extraction chromatography using a suitable solid phase or ion exchange chromatography.

Consequently, this study focused on optimizing and evaluating the efficiency of an extraction chromatography method and ion exchange chromatography method for separating milligram amounts of scandium from gram amounts of calcium. The following objectives have been proposed and achieved:

For extraction chromatography:

Prepared and optimized a solvent-impregnated resin (SIR) using Amberlite XAD-4 impregnated with di-(2-Ethylhexyl) Phosphoric Acid (DEHPA).

Physical characterization of SIR using PXRD, FTIR, BET, SEM and TEM.

Optimised the metal ion sorption for scandium and calcium by investigating the following parameters:

- adsorbent mass
- pH
- contact time
- initial ion concentration

For ion exchange chromatography:

Determined the distribution coefficients (K_d) for scandium and calcium on cation exchange resin, Dowex 50W-X8, with different HBr-methanol mixtures.

Performed column studies for the separation of scandium from calcium from the obtained Kd values (Elution curves).

The experimental results attained from this study are presented in Chapters 4 and 5.

Chapter 4 details the impregnation of the Amberlite XAD-4 resin with the organophosphorus extractant, di-2-Ethylhexyl phosphoric acid. The loading capacity of the resin was evaluated, and the surface morphologies of the resin were characterized using PXRD, FTIR, BET, SEM and TEM. The loading capacity of the resin showed an increase with increasing D2EHPA volume without a plateau, which is not generally the case with similar studies. This deviation from the expected trend could be due to the leaching of the extractant from the SIR at higher loading. After conducting adsorption performance tests to evaluate the effect of loading ratios on the sorption performance of the sorbent for scandium. From the data, 12 mL of D2EHPA per 1 g of Amberlite XAD-4 resin was used for all further experiments. The results obtained from the morphological characterisation of the resin before and after impregnation confirmed successful impregnation. Slight shifts were observed in P=O and P-O-C stretchings of the FTIR result, which confirms the interaction between D2EHPA and Amberlite XAD-4 resin.

The sorption of scandium and calcium was studied under varying pH conditions, initial metal ion concentration, time, and sorbent mass. The optimum scandium sorption occurred at a pH of 2, while the maximum sorption of calcium occurred at a pH of 4. The high K_d value for scandium obtained at pH=2 serves as confirmation that the impregnated resin has a strong affinity for scandium at this pH.

An increase in scandium sorption was observed when the sorbent dosage was increased from 0.1 g to 0.5 g. It can be concluded that this is due to sorption sites overlapping, as opposed to the overfilling of adsorbent particles. The sorption of calcium was considerably high at 0.1 g and remained relatively constant over the mass range. Based on these results, the optimal sorbent mass used for both scandium and calcium sorption studies was 1.0 g. Scandium was quantitively adsorbed at a low initial concentration (1 mg/L). Calcium, however, adsorbed a higher concentration initial concentration (10.0 mg/L). The optimum initial concentration for both metals was concluded to be 1.0 mg/L for Sc and 10.0 mg/L for Ca.

Both scandium and calcium followed Pseudo-Second order reaction kinetics. Chemisorption is customarily associated with second-Order kinetics. Theoretical data had a good correlation with experimental data, hence confirming the data obtained from the batch equilibrium studies. The Weber-Morris diffusion model was used to describe the sorption of scandium and calcium onto the impregnated resin. The multi-linearity shown by both metals suggests both pore and film diffusion mechanisms are present and can thus control the sorption process. Varying pore sizes influenced the diffusion of metal ions through the resin structure, as was confirmed by the SEM images for the impregnated resin.

The sorption of scandium and calcium was driven by both physical and chemical mechanisms. Scandium sorption was governed by a chemical process. Sorption energy obtained from the Dubinin-Radushkevic plot was used to confirm that chemisorption was the mechanism in the scandium sorption process. The equilibrium data for calcium best fitted the Dubinin-Radushkevich isotherm, indicating calcium sorption occurred via a physical adsorption process. The sorption energy data from the Dubinin-Radushkevic plot was 14.7 kJ/mol, concluding that Ca^{2+} sorption occurred via the chemical sorption process. Hence, calcium sorption was governed by both physical and chemical mechanisms. The column separation studies for Sc from Ca were conducted under the optimal condition from the batch studies. From the breakthrough curve, it was observed that both Sc and Ca breaks through the column in the first few eluate fractions. This would make the separation of these two elements very difficult,if at all possible. As much as extraction chromatography is a more convenient and efficient separation method, it is unfortunately not applicable for the separation of scandium from calcium.

Chapter 5 reports on the equilibrium distribution coefficients (K_d) of scandium and calcium that were investigated on Dowex 50W-X8 cation exchange resin in various HBr-methanol mixtures. Based on the findings of these studies, it was concluded that the 3M – 20% HBr mixture was the better eluent for the efficient separation of scandium and calcium on the resin. Separation was conducted by the column method (elution curves). The resin strongly retained scandium, and calcium was eluted very early in the elution. Scandium was eluted with 5M HCl.

The ion exchange chromatography method resulted in the efficient separation of Sc from Ca. This method was further investigated and maximised by optimising column length and flow rate. A column length of 10 mL at a flow rate of 5 mL/min more efficiently separated Sc from Ca.

Ion exchange chromatography has good sorption capacity and low maintance, compared to extraction chromatography having greater separation efficiency. Unfortunately, extraction chromatography did not yield a more effient separation of scandium from calcium as was hypothesised.

6.1 Novelty of the thesis

In this study, a D2EHPA-Amberlite XAD-4 impregnated resin, and Dowex 50W-X8 cation exchange resin in various HBr-methanol mixtures was used for the separation of scandium from calcium. There is currently no literature reporting on D2EHPA-Amberlite XAD-4 impregnated resin and Dowex 50W-X8 in HBr-methanol in the application of scandium separation from aqueous solutions nor its application in the separation of radioactive isotopes of scandium. Findings from this study may be used for the separation and purification of scandium radioisotopes for medical applications in targeted radionuclide therapy of small tumours and cancer metastasis. Additionally, both these methods have the added benefits of ease of operation, higher selectivity and lower maintenance costs.

6.2 Recommendations

In this study, ion exchange chromatography gave a better separation of scandium from calcium, and was identified as the more efficient method for the separation of Sc from Ca. Only column length and flow rate were considered to maximise the efficiency of this method. It is recommended that the reusability of the ion exchange column be investigated as well. The application of this method for the separation of Sc radioisotope did not fall within the scope of this study. For further studies, it is thus recommended that this method be applied in the separation of Sc-47 or Sc-44 radioisotopes from a Ca target material.

REFERENCES

Abderrahim, O., Didi, M.A. & Villemin, D. 2008. Extraction of cation mixture with Di (2-ethylhexyl) phosphoric acid immobilized on amberlite resins. *Environmental Science: An Indian Journal*, 3(1):125-133.

Abdullah, M., Chiang, L. & Nadeem, M. 2009. Comparative evaluation of adsorption kinetics and isotherms of a natural product removal by Amberlite polymeric adsorbents. *Chemical Engineering Journal,* 146(3): 370-376.

Achmad, A., Kassim, J., Tong, K.S., Rozaini, C.A. & Tan, L.S. 2012. Equilibrium, kinetic and thermodynamic studies on the adsorption of direct dye onto a novel green adsorbent developed from Uncaria gambir extract. *Journal of Physical Science*, 23(1): 1-13.

Ahmad, Z. 2003. The properties and application of scandium-reinforced aluminum. *JOM*: *The Journal of the Minerals, Metals & Materials Society*, 55(2): 35-39.

Akcil, A., Akhmadiyeva, N., Abdulvaliyev, R., Abhilash & Meshram, P. 2018. Overview on extraction and separation of rare earth elements from red mud: Focus on scandium. *Mineral Processing and Extractive Metallurgy Review*, 39(3): 145-151.

Akelah, A. 2013. Polymeric materials: preparation and properties. In *Functionalized polymeric materials in agriculture and the food industry*. Boston, MA: Springer: 1-61.

Akita, S., Maeda, T. & Takeuchi, H. 1994. Metal sorption characteristics of a macromolecular resin containing D2EHPA. *Journal of Chemical Engineering of Japan*, 27(1): 126-129.

An, Y., de Ridder, D.J., Zhao, C., Schoutteten, K., Vanden Bussche, J., Zheng, H. Chen, G. & Vanhaecke, L. 2016. Adsorption and photocatalytic degradation of pharmaceuticals and pesticides by carbon doped-TiO2 coated on zeolites under solar light irradiation. *Water Science and Technology*, 73(12): 2868-2881.

Asuquo, E., Martin, A., Nzerem, P., Siperstein, F. & Fan, X. 2017. Adsorption of Cd (II) and Pb (II) ions from aqueous solutions using mesoporous activated carbon adsorbent: Equilibrium, kinetics and characterisation studies. *Journal of Environmental Chemical Engineering*, 5(1): 679-698.

Avdibegović, D., Zhang, W., Zu, J., Regadio, M., Koivula, R. & Binnemans, R. 2019. Selective ion-exchange separation of scandium (III) over iron (III) by crystalline α-zirconium phosphate platelets under acidic conditions. *Separation and Purification Technology*, 215: 81-90.

Nimibofa, A., Ebelegi, A.N., & Wankasi, D. 2017. Modelling and interpretation of adsorption isotherms. *Journal of Chemistry*, 2017: Art. 3039817.

Baba, Y., Fukami, A., Kubota, F., Noriho, K. & Masahiro, G. 2014. Selective extraction of scandium from yttrium and lanthanides with amic acid-type extractant containing alkylamide and glycine moieties. *RSC Advances*, 4(92): 50726-50730.

Badei, M.A., Khalifa, S., Dessouky, H.A., Aly, H.M. & Aly, H.F. 1989. Extraction chromatographic performance of uranium using XAD-4 loaded with di-2-ethylhexylphosphoric acid and nitrate solutions. *Isotopenpraxis Isotopes in Environmental and Health Studies*, 25(5): 211-214.

Badwal, S., Ciacchi, F. & Milosevic, D. 2000. Scandia–zirconia electrolytes for intermediate temperature solid oxide fuel cell operation. *Solid State Ionics,* 136: 91-99.

Balaram, V. 2019. Rare earth elements: A review of applications, occurrence, exploration, analysis, recycling, and environmental impact. *Geoscience Frontiers*, 10(4): 1285-1303.

Bao, S., Hawker, W. & Vaughan, J. 2018. Scandium loading on chelating and solvent impregnated resin from sulfate solution. *Solvent Extraction and Ion Exchange*, 36(1): 100-113.

Bao, S., Tang, Y., Zhang, Y. & Liang, L. 2016. Recovery and separation of metal ions from aqueous solutions by solvent-impregnated resins. *Chemical Engineering & Technology*, 39(8): 1377-1392.

Batra, S., Awasthi, A., Iqbal, M. & Datta, D. 2022. Solvent impregnated resins for the treatment of aqueous solutions containing different compounds: A review. *Reviews in Chemical Engineering*, 38(2): 209-242.

Belkhouche, N.-E. & Didi, M.A.. 2010. Extraction of Bi (III) from nitrate medium by D2EHPA impregnated onto Amberlite XAD-1180. *Hydrometallurgy*, 103(1-4): 60-67.

Benamor, M., Bouariche, Z., Belaid, T. & Draa, M.T. 2008. Kinetic studies on cadmium ions by Amberlite XAD7 impregnated resins containing di (2-ethylhexyl) phosphoric acid as extractant. *Separation and Purification Technology*, 59(1): 74-84.

Binnemans, K., Jones, P.T., Blanpain, B., van Gerven, T., Yang, Y., Walton, A. & Buchert, M. 2013. Recycling of rare earths: A critical review. *Journal of Cleaner Production*, 51: 1-22.

Bokhari, T.H., Mushtaq, A. & Khan, I.U. 2010. Separation of no-carrier-added radioactive scandium from neutron irradiated titanium. *Journal of Radioanalytical and Nuclear Chemistry*, 283(2): 389-393.

Bouhamed, F., Elouear, Z. & Bouzid, J. 2012. Adsorptive removal of copper (II) from aqueous solutions on activated carbon prepared from Tunisian date stones: Equilibrium, kinetics and thermodynamics. *Journal of the Taiwan Institute of Chemical Engineers*, 43(5): 741-749.

Calmon, C. 1981. Specific and chelate exchangers: New functional polymers for water and wastewaster treatment. *Journal American Water Works Association*, 73(12): 652-656.

Celebi, O., Üzüm, Ç., Shawan, T. & Erten, H.N. 2007. A radiotracer study of the adsorption behavior of aqueous Ba2+ ions on nanoparticles of zero-valent iron. *Journal of Hazardous Materials*, 148(3): 761-767.

Chabani, M., Amrane, A., & Aicha, B. 2006. Kinetic modelling of the adsorption of nitrates by ion exchange resin. *Chemical Engineering Journal*, 125(2): 111-117.

Chakrapani, C., Babu, C., Vani, K.N.K. & Rao, K.S. 2010. Adsorption kinetics for the removal of fluoride from aqueous solution by activated carbon adsorbents derived from the peels of selected citrus fruits. *E-Journal of Chemistry*, 7(S1): S419-S427.

Chanda, M. 2017. *Plastics technology handbook*. Boca Raton, FL: CRC Press.

Che, M. & Védrine, J.C. 2012. Characterization of solid materials and heterogeneous catalysts: From structure to surface reactivity. Hoboken, NJ: John Wiley & Sons.

Ciopec, M., Negrea, A., Lupa, L., Davidesc, C.M. & Negrea, P. 2014. Studies regarding As (V) adsorption from underground water by Fe-XAD8-DEHPA impregnated resin. Equilibrium sorption and fixed-bed column tests. *Molecules,* 19(10): 16082-16101.

Cortina, J., Miralles, N., Aguilar, M. & Sastre, A.M. 1994. Solvent impregnated resins containing di (2-ethyl-hexyl) phosphoric acid. II. Study of the distribution equilibria of Zn (II), Cu (II) and Cd (II). *Solvent Extraction and Ion Exchange*, 12(2): 371-391.

Cortina, J., Miralles, N., Sastre, A.M. & Aguilar, M. 1995. Solid-liquid extraction studies of Zn (II), Cu (II) and Cd (II) from chloride media with impregnated resins containing mixtures of organophosphorus compounds immobilized on to Amberlite XAD2. *Hydrometallurgy,* 37(3): 301-322.

Cortina, J., Warshawsky, A., Kahana, N. & Kampel, V. 2003. Kinetics of goldcyanide extraction using ion-exchange resins containing piperazine functionality. *Reactive and Functional Polymers,* 54(1-3): 25-35.

Cortina, J.L. & Warshawsky, A. 2021. Developments in solid-liquid extraction by solvent-impregnated resins. In *Ion Exchange and Solvent Extraction.* Abingdon, UK: Routledge: 195-293.

Cyganowski, P., Jermakowicz-Bartkowiak, D., Chęcmanowski, J. & Kujawska, M.E. 2015. New core-shell type polymeric supports based on the Amberlite XAD-4 adsorbent: A novel synthesis procedure. *Chinese Journal of Chemistry*, 33(5): 594-600.

Dada, A., Olalekan, A. & Olatunya, A. 2012. Langmuir, Freundlich, Temkin and Dubinin–Radushkevich isotherms studies of equilibrium sorption of Zn2+ unto phosphoric acid modified rice husk. *IOSR Journal of Applied Chemistry*, 3(1): 38-45.

Das, N. & Das, D. 2013. Recovery of rare earth metals through biosorption: An overview. *Journal of Rare Earths*, 31(10): 933-943.

Davidescu, C.M., Ciopec, M., Adina, N. & Popa, A. 2011. Use of di-(2-ethylhexyl) phosphoric acid (DEHPA) impregnated XAD7 copolymer resin for the removal of chromium (III) from water. *Revista de Chimie Bucharest,* 62: 712-717.

De Lima, I.B. & Leal Filho, W. 2015. Rare earths industry: Technological, economic, and environmental implications. Amsterdam: Elsevier.

Deilami-Nezhad, L., Moghaddam-Banaem, L., Sadeghi, M. & Asgari, M. 2016. Production and purification of Scandium-47: A potential radioisotope for cancer theranostics. *Applied Radiation and Isotopes*, 118: 124-130.

Dietz, M.L., Horwitz, E.P. & Bond, A. 1997. *Extraction chromatography: Progress and opportunities.* Argonne, IL: Argonne National Lab.

Dorfner, K. (ed). 2011. *Ion exchangers*. Berlin: Walter de Gruyter.

Dorfner, K. 1972. Ion exchangers; properties and applications. In *Ann Arbor Science, Newton*. Diepoldsau, Switzerland: YUMPU Publishing: 177.

Dostal, J. 2017. Rare earth element deposits of alkaline igneous rocks. *Resources*, 6(3): 34.

Draa, M., Belaid, T. & Benamor, M. 2004. Extraction of Pb (II) by XAD7 impregnated resins with organophosphorus extractants (DEHPA, IONQUEST 801, CYANEX 272). *Separation and Purification Technology*, 40(1): 77-86.

El-Khaiary, M.I. 2008. Least-squares regression of adsorption equilibrium data: Comparing the options. *Journal of Hazardous Materials*, 158(1): 73-87.

Emmanuel, E.C., Ananthi, T., Anandkumar, B. & Maruthamuthu, S. 2012. Accumulation of rare earth elements by siderophore-forming Arthrobacter luteolus isolated from rare earth environment of Chavara, India. *Journal of Biosciences*, 37(1): 25-31.

Fadel, D., El-Bahy, S. & Abdelaziz, Y.A. 2016. Heavy metals removal using iminodiacetate chelating resin by batch and column techniques. *Desalination and Water Treatment*, 57(53): 25718-25728.

Fierro, V., Torne, V., Montane, D. & Celzard, A. 2008. Adsorption of phenol onto activated carbons having different textural and surface properties. *Microporous and Mesoporous Materials*, 111(1-3): 276-284.

Fritz, J.S. 2004. Early milestones in the development of ion-exchange chromatography: A personal account. *Journal of Chromatography*, 1039(1-2): 3-12.

Gökmen, V. & Serpen, A. 2002. Equilibrium and kinetic studies on the adsorption of dark colored compounds from apple juice using adsorbent resin. *Journal of Food Engineering,* 53(3): 221-227.

Guo, F., Nishihama, S. & Yoshizuka, K. 2013. Selective recovery of valuable metals from spent Li-ion batteries using solvent-impregnated resins. *Environmental technology*, 34(10): 1307-1317.

Gwenzi, W., Mangori, L., Danha, C., Chaukura, N., Dunjana, N. & Sanganyado, E. 2018. Sources, behaviour, and environmental and human health risks of high-technology rare earth elements as emerging contaminants. *Science of the Total Environment*, 636: 299-313.

Hamdaoui, O. & Naffrechoux, E. 2007. Modeling of adsorption isotherms of phenol and chlorophenols onto granular activated carbon: Part I. Two-parameter models and equations allowing determination of thermodynamic parameters. *Journal of Hazardous Materials*, 147(1-2): 381-394.

Haque, N., Hughes, A., Lim, S. & Vernon, C. 2014. Rare earth elements: Overview of mining, mineralogy, uses, sustainability and environmental impact. *Resources*, 3(4): 614-635.

Harland, C.E. 1994. *Ion exchange: Theory and practice*. London: Royal Society of Chemistry.

Hiemenz, P.C. & Rajagopalan, R. 2016. *Principles of colloid and surface chemistry, revised and expanded*. Boca Raton, FL: CRC Press.

Ho, Y. & McKay, G. 2000. The kinetics of sorption of divalent metal ions onto sphagnum moss peat. *Water Research,* 34(3): 735-742.

Horwitz, E.P., McAlister, D.R. & Dietz, M.L. 2006. Extraction chromatography versus solvent extraction: How similar are they? *Separation Science and Technology*, 41(10): 2163-2182.

Hosseini-Bandegharaei, A., Allahabadi, A., Sani, A.R. & Rastegar, A. 2016. Thorium removal from weakly acidic solutions using titan yellow-impregnated XAD-7 resin beads: Kinetics, equilibrium and thermodynamic studies. *Journal of Radioanalytical and Nuclear Chemistry*, 309(2): 761-776.

Huynh, H.T. & Tanaka, M. 2003. Removal of Bi, Cd, Co, Cu, Fe, Ni, Pb, and Zn from an aqueous nitrate medium with bis (2-ethylhexyl) phosphoric acid impregnated kapok fiber. *Industrial & Engineering Chemistry Research,* 42(17): 4050-4054.

Iqbal, M. & Datta, D. 2020. Competitive removal of malachite green and Rhodamine-B using Amberlite-XAD-4 impregnated with Aliquat 336: Experimental and modelling studies. *Separation Science and Technology,* 55(3): 537-553.

Iqbal, M. & Datta, D. 2022. Rhodamine-B dye removal using aliquat-336 modified amberlite XAD-4 resin in fixed-bed columns in series. *Water Science and Technology*, 85(1): 1-15.

Jha, M.K., Kumari, A., Panda, R. & Jyothi, R.K. 2016. Review on hydrometallurgical recovery of rare earth metals. *Hydrometallurgy*, 165: 2-26.

Jiyan, C., Ruidong, Y., Wei, H. & Gao, J. 2013. Rare earth element geochemistry of Cambrian phosphorites from the Yangtze Region. *Journal of Rare Earths*, 31(1): 101-112.

Juang, R.S. & Lin, H.C. 1995. Metal sorption with extractant-impregnated macroporous resins. 1. Particle diffusion kinetics. *Journal of Chemical Technology & Biotechnology: International Research in Process, Environmental and Clean Technology*, 62(2): 132-140.

Juang, R.S. & Su, J.Y. 1992. Separation of zinc and copper from aqueous sulfate solutions using bis (2-ethylhexyl) phosphoric acid-impregnated macroporous resin. *Industrial & Engineering Chemistry Research,* 31(12): 2779-2783.

Kalal, H.S., Panahi, H.A., Hoveidi, H., Taghiof, M. & Menderjani, M.T. 2012. Synthesis and application of Amberlite xad-4 functionalized with alizarin red-s for preconcentration and adsorption of rhodium (III). *Iranian Journal of Environmental Health Science & Engineering*, 9(1): 1-9.

Karve, M. & Vaidya, B. 2008. Selective separation of scandium (III) and yttrium (III) from other rare earth elements using Cyanex302 as an extractant. *Separation Science and Technology*, 43(5): 1111-1123.

Kaur, H., Shah, D. & Pal, U. 2011. Resin encapsulated palladium nanoparticles: An efficient and robust catalyst for microwave-enhanced Suzuki–Miyaura coupling. *Catalysis Communications*, 12(14): 1384-1388.

Kember, N., Macdonald, P. & Wells, R. 1955. The selective elution of metals adsorbed on cation-exchange resins by organic solvents. Part I. *Journal of the Chemical Society (Resumed)*: 2273-2280.

Kim, T.K. & McClintic, R.P. 1988. *Process for recovering scandium from waste material.* Patent. Washington, DC: U.S. Department of Energy.

Kobayashi, S. & Manabe, K. 2000. Green Lewis acid catalysis in organic synthesis. *Pure and Applied Chemistry*, 72(7): 1373-1380.

Korkisch, J. 2017. Handbook of ion exchange resins: Their application to inorganic analytical chemistry. Abingdon-on-Thames, UK: Routledge.

Krajewski, S., Cydzik, I., Abbas, K., Bulgheroni, A., Simonelli, F., Holzwarth, U. & Bilewicz, A. 2013. Cyclotron production of 44Sc for clinical application. *Radiochimica Acta*, 101(5): 333-338.

Kumar, B.N., Radhika, S., Kantam, M.L. & Reddy, B.R. 2011. Solid–liquid extraction of terbium from phosphoric acid solutions using solvent-impregnated resin containing TOPS 99. *Journal of Chemical Technology & Biotechnology,* 86(4): 562-569.

Kumar, S. & Jain, S. 2013. History, introduction, and kinetics of ion exchange materials. *Journal of Chemistry*, 2013: Art. 957647

Lazaridis, N. & Asouhidou, D. 2003. Kinetics of sorptive removal of chromium (VI) from aqueous solutions by calcined Mg–Al–CO3 hydrotalcite. *Water Research*, 37(12): 2875-2882.

Lee, M-S., Lee, J-Y., Kim, J-S. & Lee, G.S. 2005. Solvent extraction of neodymium ions from hydrochloric acid solution using PC88A and saponified PC88A. *Separation and Purification Technology*, 46(1-2): 72-78.

Li, D. & Wang, C. 1998. Solvent extraction of Scandium (III) by Cyanex 923 and Cyanex 925. *Hydrometallurgy*, 48(3): 301-312.

Li, G., Ye, Q., Deng, B., Luo, J., Rao, M., Peng, Z. & Jiang, T. 2018. Extraction of scandium from scandium-rich material derived from bauxite ore residues. *Hydrometallurgy*, 176: 62-68.

Li, Q., Li, Z., Sun, P. & Zhang, G.Q. 2016. Purifying scandium chloride solution by ion exchange. *Journal of Northeastern University (Natural Science),* 37(10): 1410.

Li, X., Chen, Z., Cheng, Z. & Zhang, Y. 2013. A human health risk assessment of rare earth elements in soil and vegetables from a mining area in Fujian Province, Southeast China. *Chemosphere*, 93(6): 1240-1246.

Li, Y., Long, C., Tao, W., Li, A. & Zhang, Q. 2010. Fractal dimensions of macroporous and hypercrosslinked polymeric adsorbents from nitrogen adsorption data. *Journal of Chemical & Engineering Data*, 55(9): 3147-3150.

Lieser, K. 1979. New ion exchangers, preparation, properties and application. *Pure and Applied Chemistry*, 51(7): 1503-1517.

Liu, R., Cai, G., Li, J., Zhao, C., Wang, S., Wen, T. & Wen, Z. 2010. Scandia-stabilized zirconia-impregnated (La, Sr) MnO 3 cathode for tubular solid oxide fuel cells. *Journal of Solid State Electrochemistry*, 14(10): 1923-1928.

Liu, W., Yang, J. Xiao, B. 2009. Review on treatment and utilization of bauxite residues in China. *International Journal of Mineral Processing*, 93(3-4): 220-231.

Liu, Z., Li, H., Jing, Q. & Zhang, M. 2017. Recovery of scandium from leachate of sulfation-roasted bayer red mud by liquid–liquid extraction. *JOM*: *The Journal of the Minerals, Metals & Materials Society*, 69(11): 2373-2378.

Lowell, S., Shields, J.E. & Thommes, M. 2006. *Characterization of porous solids and powders: Surface area, pore size and density*. Springer Science & Business Media.

Lu, Y., Haiqin, W., Zhang, Z. & Li, Y. 2016. Selective extraction and separation of thorium from rare earths by a phosphorodiamidate extractant. *Hydrometallurgy*, 163: 192-197.

Memon, S.Q., Bhanger, M., Hasany, S.M. & Khuhawar, M.Y. 2006. Sorption behavior of impregnated Styrofoam for the removal of Cd (II) ions. *Colloids and Surfaces A: Physicochemical and Engineering Aspects*, 279(1-3): 142-148.

Migaszewski, Z.M. & Gałuszka, A. 2015. The characteristics, occurrence, and geochemical behavior of rare earth elements in the environment: A review. *Critical Reviews in Environmental Science and Technology,* 45(5): 429-471.

Mishra, B.B. & Devi, N. 2020. Study on the extraction and separation of samarium from chloride medium using D2EHPA and [P 66614][D2EHP] and their application to monazite ore. *Transactions of the Indian Institute of Metals,* 73(9): 2247-2257.

Momen, M.A., Healy, M.R., Tsouris, C., Jansone-Popova, S., DePaoli, D.W. & Moyer, B.A. 2019. Extraction chromatographic materials for clean hydrometallurgical separation of rare-earth elements using diglycolamide extractants. *Industrial & Engineering Chemistry Research*, 58(43): 20081-20089.

Moon, J.-K., Han, Y.-J., Jung, C-H., Lee, E-H. (Lee, B-C. 2006. Adsorption of rhenium and rhodium in nitric acid solution by Amberlite XAD-4 impregnated with Aliquat 336. *Korean Journal of Chemical Engineering,* 23(2): 303-308.

Moon, J-Y., Takajo, C., Nishihama, S. & Yoshizuka, K. 2020. Separation and recovery of scandium and yttrium from aqueous chloride media by integrated ion exchange method. *Solvent Extraction Research and Development*, Japan 27(2): 91-97.

Müller, C., Domnanich, K.A., Umbricht, C.A. & van der Meulen, N.P. 2018. Scandium and terbium radionuclides for radiotheranostics: Current state of development towards clinical application. *The British Journal of Radiology*, 91(1091): 20180074.

Mumpton, F.A. 1999. La roca magica: Uses of natural zeolites in agriculture and industry. *Proceedings of the National Academy of Sciences,* 96(7): 3463-3470.

Murphy, B., Davis, M.E. & Xu, B. 2015. The effect of adsorbed molecule gas-phase deprotonation enthalpy on ion exchange in sodium exchanged zeolites: An in situ FTIR investigation. *Topics in Catalysis*, 58(7): 393-404.

Nash, K.L. & Jensen, M.P. 2000. Analytical separations of the lanthanides: Basic chemistry and methods. *Handbook on the Physics and Chemistry of Rare Earths*, 28: 311-371.

Nie, H., Wang, Y., Wang, Y. & Zhao, Z. 2018. Recovery of scandium from leaching solutions of tungsten residue using solvent extraction with Cyanex 572. *Hydrometallurgy,* 175: 117-123.

Ochsenkühn-Petropulu, M., Lyberopulu, T. & Parissakis, G. 1995. Selective separation and determination of scandium from yttrium and lanthanides in red mud by a combined ion exchange/solvent extraction method. *Analytica Chimica Acta*, 315(1-2): 231-237.

Olbrych-Śleszyńska, E., Brajter, K., Matuszewski, W., Trojanowicz, M. & Frenzel, W. 1992. Modification of nonionic adsorbent with eriochrome blue-black R for selective nickel (II) preconcentration in conventional and flow-injection atomic-absorption spectrometry. *Talanta*, 39(7): 779-787.

Onghena, B. & Binnemans, K. 2015. Recovery of scandium (III) from aqueous solutions by solvent extraction with the functionalized ionic liquid betainium bis (trifluoromethylsulfonyl) imide. *Industrial & Engineering Chemistry Research*, 54(6): 1887-1898.

Onghena, B., Borra, C.R., van Gerven, T. & Binnemans, K. 2017. Recovery of scandium from sulfation-roasted leachates of bauxite residue by solvent extraction with the ionic liquid betainium bis (trifluoromethylsulfonyl) imide. *Separation and Purification Technology*, 176: 208-219.

Pęgier, M., Kilian, K. & Pyrzyńska., K. 2018. Enrichment of scandium by carbon nanotubes in the presence of calcium matrix. *Microchemical Journal,* 137: 371-375.

Peng, Z., Li, V., Li, Z-Y., Zhang, G-Q., Cao, Z-y. & Guan, W-j. 2018. Removal of impurities from scandium solutions by ion exchange. *Journal of Central South University*, 25(12): 2953-2961.

Pietrelli, L., Kolsky, K. & Mausner, L. 1992. Separation of carrier-free47Sc from titanium targets. *Journal of Radioanalytical and Nuclear Chemistry,* 157(2): 335-345.

Plazinski, W., Dziuba, J. & Rudzinski, W. 2013. Modeling of sorption kinetics:the pseudo-second order equation and the sorbate intraparticle diffusivity. *Adsorption*, 19(5): 1055-1064.

Pyrzyńska, K., Kilian, K. & Pęgier, M. 2019. Separation and purification of scandium: From industry to medicine. *Separation & Purification Reviews*, 48(1): 65-77.

Qiu, H., Lv, L., Zhang, Q-j., Zhang, W-m. & Zhang, Q-x. 2009. Critical review in adsorption kinetic models. *Journal of Zhejiang University-Science A,* 10(5): 716-724.

Qu, Y., Zhang, C., Li, H. & Bo, X. 2009. Equilibrium and kinetics study on the adsorption of perfluorooctanoic acid from aqueous solution onto powdered activated carbon. *Journal of Hazardous Materials*, 169(1-3): 146-152.

Ramasamy, D.L., Puhakka, V., Repo, E. & Sillanpää, M. 2018. Selective separation of scandium from iron, aluminium and gold rich wastewater using various amino and non-amino functionalized silica gels–a comparative study. Journal of Cleaner Production, 170: 890-901.

Ramzan, M., Kifle, D. & Wibetoe, G. 2017. A rapid impregnation method for loading desired amounts of extractant on prepacked reversed-phase columns for high performance liquid chromatographic separation of metal ions. *Journal of Chromatography A*, 1500: 76-83.

Reimer, L. 2013. Transmission electron microscopy: Physics of image formation and microanalysis. Berlin/Heidelberg: Springer.

Ren, R., Wang, Y., Zhang, R., Gao, S., Zhang, H. & Yu, A. 2011. Solvent (ionic liquid) impregnated resin-based extraction coupled with dynamic ultrasonic desorption for separation and concentration of four herbicides in environmental water. *Talanta*, 83(5): 1392-1400.

Ringot, D., Lerzy, B., Chaplain, K., Bonhoure, J.P., Auclair, E. & Larondelle, Y. 2007. In vitro biosorption of ochratoxin A on the yeast industry by-products: Comparison of isotherm models. *Bioresource Technology*, 98(9): 1812-1821.

Rydberg, J. 2004. Solvent extraction principles and practice, revised and expanded. Boca Raton, FL: CRC Press.

Samarghandi, M., Hadi, M., Moayedi, S. & Askari, F.B. 2009. Two-parameter isotherms of methyl orange sorption by pinecone derived activated carbon. *Iranian Journal of Environmental Health Science and Engineering,* 6(4): 285-294

Sang, Y., Gu, Q., Sun, T., Li, F. & Liang, C. 2008. Filtration by a novel nanofiber membrane and alumina adsorption to remove copper (II) from groundwater. *Journal of Hazardous Materials*, 153(1-2): 860-866.

Schweitzer, G.K. & Pesterfield, L.L. 2010. *The aqueous chemistry of the elements*. Oxford, UK: OUP.

Shahida, S., Ali, A., Khan, M.H. & Saeed, M.M. 2013. On-line spectrophotometric determination of scandium after preconcentration on XAD-4 resin impregnated with nalidixic acid. *Journal of the Iranian Chemical Society*, 10(3): 461-470.

Shaoquan, X. & Suqing, L. 1996. Review of the extractive metallurgy of scandium in China (1978–1991). *Hydrometallurgy*, 42(3): 337-343.

Sharaf, M., Yoshida, W., Kubota, F. & Goto, M. 2018. A novel binary-extractant-impregnated resin for selective recovery of scandium. *Journal of Chemical Engineering of Japan,* 52(1).

Sherrington, D.C. 1998. Preparation, structure and morphology of polymer supports. *Chemical Communications*, 21: 2275-2286.

Shi, C., Jing, Y., Xiao, J. & Wang, X. 2017. Solvent extraction of lithium from aqueous solution using non-fluorinated functionalized ionic liquids as extraction agents. *Separation and Purification Technology*, 172: 473-479.

Shu, Q., Khayambashi, A. & Wang, X. 2018. Studies on adsorption of rare earth elements from nitric acid solution with macroporous silica-based bis (2-ethylhexyl) phosphoric acid impregnated polymeric adsorbent. *Adsorption Science & Technology*, 36(3-4): 1049-1065.

Silva, R.A., Hawboldt, K. & Zhang, Y. 2018. Application of resins with functional groups in the separation of metal ions/species–a review. *Mineral Processing and Extractive Metallurgy Review*, 39(6): 395-413.

Singh, R.K. & Dhadke, P.M. 2003. Extraction and separation of scandium (III) from perchlorate media, by D2EHPA and PC-88A. *Bulletin of the Chemists and Technologists of Macedonia*, 22: 1-11.

Smirnov, A., Titova, S., Rychkov, V. & Bunkov, G. 2017. Study of scandium and thorium sorption from uranium leach liquors. *Journal of Radioanalytical & Nuclear Chemistry,* 312(2).

Smirnov, D. & Molchanova, T. 1997. The investigation of sulphuric acid sorption recovery of scandium and uranium from the red mud of alumina production. *Hydrometallurgy*, 45(3): 249-259.

Smith-Jones, P., Strelow, F. & Böhmer, R.G. 1986. The separation of carrier-free 85Sr from a rubidium chloride cyclotron target. International Journal of Radiation Applications and Instrumentation. Part A. *Applied Radiation and Isotopes*, 37(3): 240-242.

Sokolova, Y.V. 2001. Sorption purification of scandium (III) to remove zirconium (IV) impurity in hydrochloric acid solutions. *Russian Journal of Applied Chemistry*, 74(3): 414-416.

Strelow, F.W. 1984. Distribution coefficients and cation-exchange behaviour of 45 elements with a macroporous resin in hydrochloric acid/methanol mixtures. *Analytica Chimica Acta*, 160: 31-45.

Strelow, F.W., Víctor, A.H., van Zyl, C.R. & Eloff, C. 1971. Distribution coefficients and cation exchange behavior of elements in hydrochloric acid-acetone. *Analytical Chemistry*, 43(7): 870-876.

Sun, X., Wu, D., Chen, J. & Li, D. 2007. Separation of scandium (III) from lanthanides (III) with room temperature ionic liquid based extraction containing Cyanex 925. *Journal of Chemical Technology & Biotechnology: International Research in Process, Environmental & Clean Technology,* 82(3): 267-272.

Tamang, A.M., Singh, N., Chandraker, S.K. & Ghosh, M.K. 2021. Solvent impregnated resin a potential alternative material for separation dyes, metal and phenolic compounds: A review. *Current Research in Green and Sustainable Chemistry*, p.100232.

Tan, K.L. & Hameed, B.H. 2017. Insight into the adsorption kinetics models for the removal of contaminants from aqueous solutions. *Journal of the Taiwan Institute of Chemical Engineers*, 74: 25-48.

Tanihara, K. 1995. Composite ion exchangers of redox type for cesium separation. Sorption-desorption-regeneration cycle with cupric ferrocyanide impregnated macroporous anion-exchange resins of strongly basic type. *Journal of Radioanalytical and Nuclear Chemistry*, 201(6): 509-519.

Taute, J.J., Sole, K.C. & Hardwick, E. 2013. Zinc removal from a base metal solution by ion exchange: process design to full-scale operation. In *Proceedings of* The Southern African Institute of Mining and Metallurgy Base Metals Conference 2013: 179-192.

Tavlarides, L., Bae, J. & Lee, C.K. 1987. Solvent extraction, membranes, and ion exchange in hydrometallurgical dilute metals separation. *Separation Science and Technology*, 22(2-3): 581-617.

Thommes, M. & Cychosz, K.A. 2014. Physical adsorption characterization of nanoporous materials: Progress and challenges. *Adsorption*, 20(2): 233-250.

Thommes, M., Kaneko, K., Neimark, A.V., Olivier, J.P., Rodriguez-Reinoso, F., Rouquerol, J. & Sing, K.S.W. 2015. Physisorption of gases, with special reference to the evaluation of surface area and pore size distribution (IUPAC Technical Report). Pure and Applied *Chemistry*, 87(9-10): 1051-1069.

Tranter, T. 2011. Solid-phase extraction technology for actinide and lanthanide separations in nuclear fuel reprocessing.In *Advanced separation techniques for nuclear fuel reprocessing and radioactive waste treatment.* Amsterdam: Elsevier: 377-413.

Valdovinos, H., Hernandez, R., Barnhart, T.E., Graves, S., Cai, W. & Nickleas, R.J. 2015. Separation of cyclotron-produced 44Sc from a natural calcium target using a dipentyl pentylphosphonate functionalized extraction resin. *Applied Radiation and Isotopes*, 95: 23-29.

Valente, J.S., Tzompantzi, F., Prince, J. & Cortez, J. 2009. Adsorption and photocatalytic degradation of phenol and 2, 4 dichlorophenoxiacetic acid by Mg–Zn–Al layered double hydroxides. *Applied Catalysis B: Environmental*, 90(3-4): 330-338.

Van der Meulen, N.P., Bunka, M., Domnanich, K.A., Müller, C., Haller, S., Vermeulen, C., Türler, A. & Schibli, R. 2015. Cyclotron production of 44Sc: From bench to bedside. *Nuclear Medicine and Biology*, 42(9): 745-751.

Van Hecke, K. & Goethals, P. 2006. *Research on advanced aqueous reprocessing of spent nuclear fuel: Literature study*. Mol, Belgium: Belgian Nuclear Research Centre.

Van Nguyen, N., Iizuka, A., Shibata, E. & Nakamura, T. 2015. Recovery of Scandium from chloride media using the novel ion exchange resin. *Proceedings of the World Congress on Mechanical, Chemical, and Material Engineering.* Barcelona, Spain, July 20-21, 2015.

Van Nguyen, N., Iizuka, A., Shibata, E. & Nakamura, T. 2016. Study of adsorption behavior of a new synthesized resin containing glycol amic acid group for separation of scandium from aqueous solutions. *Hydrometallurgy*, 165: 51-56.

Van Nguyen, N., Lee, J.-C., Jeong, J. & Pandey, B.D. 2013. Enhancing the adsorption of chromium (VI) from the acidic chloride media using solvent impregnated resin (SIR). *Chemical Engineering Journal*, 219: 174-182.

Vyas, C.K., Park, J.H., Hoon, J. & Dae, Y.S. 2016. Application of extraction chromatographic techniques for separation and purification of emerging radiometals 44/47Sc. *Journal of Radiopharmaceuticals and Molecular Probes,* Vol 2(2).

Wakui, Y., Matsunaga, H. & Suzuki, T.M. 1989. Selective recovery of trace scandium from acid aqueous solution with (2-ethylhexyl hydrogen 2-ethylhexylphosphonate)-impregnated resin. *Analytical Sciences*, 5(2): 189-193.

Wang, W. & Cheng, C.Y. 2011. Separation and purification of scandium by solvent extraction and related technologies: A review. *Journal of Chemical Technology & Biotechnology*, 86(10): 1237-1246.

Wang, W., Pranolo, Y. & Cheng, C.Y. 2011. Metallurgical processes for scandium recovery from various resources: A review. *Hydrometallurgy*, 108(1-2):100-108.

Wang, W., Pranolo, Y. & Cheng, C.Y. 2013. Recovery of scandium from synthetic red mud leach solutions by solvent extraction with D2EHPA. *Separation and Purification Technology,* 108: 96-102.

Wang, Y., Wang, C., Warshawsky, A. & Berkowitz, B. 2003. 8-Hydroxyquinoline-5-sulfonic acid (HQS) impregnated on Lewatit MP 600 for cadmium complexation:implication of solvent impregnated resins for water remediation. *Separation Science and Technology*, 38(1): 149-163.

Wang, Y., Yue, S., Li, D.Q., Jin, M.J. & Li, C.Z. 2002. Solvent extraction of scandium (III), yttrium (III), lanthanides (III), anddivalent metal ions with sec-nonylphenoxy acetic acid. *Solvent Extraction and Ion Exchange*, 20(6): 701-716.

Warshawsky, A. 1981. Extraction with solvent-impregnated resins. *Ion Exchange and Solvent Extraction*, 8: 229.

Warshawsky, A., Strikovsky, A., Jerabek, K. & Cortina, J.L. 1997. Solvent-impregnated resins via acid-base interaction of poly (4-vinylpyridine) resin and di (2-ethylhexyl) dithiophosphoric acid. *Solvent Extraction and Ion Exchange*, 15(2): 259-283.

Wu, D., Niu, C., Li, D. & Bai, Y. 2004. Solvent extraction of scandium (III), yttrium (III), lanthanum (III) and gadolinium (III) using Cyanex 302 in heptane from hydrochloric acid solutions. *Journal of Alloys and Compounds,* 374(1-2): 442-446.

Xie, F., Zhang, T.A., Dreisinger, D. & Doyle, F. 2014. A critical review on solvent extraction of rare earths from aqueous solutions. *Minerals Engineering*, 56: 10-28.

Yadav, K.K., Singh, D.K, Anitha, M. & Varshney, L. 2013. Studies on separation of rare earths from aqueous media by polyethersulfone beads containing D2EHPA as extractant. *Separation and Purification Technology*, 118 :350-358.

Yagmurlu, B., Zhang, W., Avdibegovic, D. & Regadio, M. 2018. Advances in scandium recovery beyond state of the art. *Proceedings of the ALTA 2018 Uranium-REE-Lithium Conference*, Perth (Australia), 19-26 May 2018., ALTA Metallurgical Services (ALTA); Perth. Australia.

Yoshizuka, K., Sakomoto, Y., Baba, Y. & Inoue, K. 1990. Distribution equilibria in the adsorption of cobalt (II) and nickel (II) on Levextrel resin containing Cyanex 272. *Hydrometallurgy*, 23(2-3): 309-318.

Yue, G., Xingyan, W. & Haifeng, H. et al. 1991. Kinetic studies of solvent impregnated resins for sorption of spiramycin. Department of Biochemical Engineering, East China University of Chemical Technology, Shanghai. *Journal of Chemical Industry and Engineering (China*), 42(5): 603-610.

Zagorodni, A.A. 2006. Ion exchange materials:properties and applications. Amsterdam: Elsevier.

Zhang, B., Liu, C., Li, C. & Jiang, M. 2014. A novel approach for recovery of rare earths and niobium from Bayan Obo tailings. *Minerals Engineering*, 65: 17-23.

Zhang, N., Li, H-X. & Liu, X-M. 2016. Recovery of scandium from bauxite residue—red mud: A review. *Rare Metals*, 35(12): 887-900.

Zhang, W., Yu, S., Zhang, S., Zhou, J., Ning, S., Wang, X. Wei, Y. 2019. Separation of scandium from the other rare earth elements with a novel macro-porous silica-polymer based adsorbent HDEHP/SiO2-P. *Hydrometallurgy*, 185: 117-124.

Zhou, G., Li, Q., Sun, P. & Guan, W. 2018. Removal of impurities from scandium chloride solution using 732-type resin. *Journal of Rare Earths*, 36(3): 311-316.

Zhu, Q., Moggridge, G.D. & D'Agostino, C. 2016. Adsorption of pyridine from aqueous solutions by polymeric adsorbents MN 200 and MN 500. Part 2:Kinetics and diffusion analysis. *Chemical Engineering Journal*, 306: 1223-1233.

Zhu, X., Li, W. & Guan, X. 2015. An active dealkalization of red mud with roasting and water leaching. *Journal of Hazardous Materials*, 286: 85-91.

Zhu, X., Li, W., Tang, S., Zeng, M., Bai, P. & Chen, L. 2017. Selective recovery of vanadium and scandium by ion exchange with D201 and solvent extraction using P507 from hydrochloric acid leaching solution of red mud. *Chemosphere*, 175: 365-372.

Zhu, Y., Zheng, Y. & Wang, A. 2015. A simple approach to fabricate granular adsorbent for adsorption of rare elements. *International Journal of Biological Macromolecules*, 72: 410-420.

APPENDICES

APPENDIX A: EFFECT OF SORBENT DOSAGE OF UNMODIFIED AMBERLITE XAD-4 RESIN ON SC^{3+} SORPTION

	1st Run	2nd Run	3rd run	Mean	% Sorption
Sorbent Mass	**Conc (mg/L)**	**Conc (mg/L)**	**Conc (mg/L)**		
0.10	5.00	4.11	5.20	4.77	52
0.25	4.47	4.39	5.20	4.69	53
0.50	4.76	4.47	4.67	4.63	54
1.00	3.92	3.65	4.63	4.07	59
1.50	3.95	3.26	4.30	3.84	62
2.00	2.88	3.17	3.54	3.20	68
2.50	3.27	2.83	3.77	3.29	67
3.00	3.14	2.31	3.20	2.88	71

APPENDIX B: EFFECT OF SORBENT DOSAGE ON SC3+ SORPTION

Mass of sorbent	**% Sc Sorption**
(g / 25mL)	
0.1	56
0.25	99
0.5	99
1	100
1.5	100
2	100
2.5	100
3	100

APPENDIX C: EFFECT OF SORBENT DOSAGE ON SC^{3+} AND CA^{2+} SORPTION

Mass of sorbent (g)	% Ca Sorption
0.10	91
0.25	97
0.50	99
1.00	100
1.50	99
2.00	100
2.50	99
3.00	99

APPENDIX D: ELUTION CURVE DATA FOR 3 ML COLUMN AT A FLOW RATE OF 5 ML/MIN

Fractions	Sc Concentration (mg/L)	Ca Concentration (mg/L)
1	0.00	11.32
2	0.00	32.8
3	0.15	49.6
4	0.33	50
5	0.5	47.2
6	0.61	37.6
7	0.65	8.37
8	0.6	7.14
9	0.54	2.44
10	0.48	0.65
11	0.43	0.32
12	0.38	0.21
13	0.33	0.053
14	0.29	0.04
15	0.24	0.038
16	0.21	0.038
17	0.17	0.038
18	0.14	0.02
19	0.12	0.04
20	0.09	0.08
21	0.08	0.05
22	0.06	0.03
23	0.04	0.08
24	0.02	0.03
25	0.01	0.08
26	0.16	0.26
27	0.03	0.00
28	0.00	0.00

29	0.00	0.00
30	0.00	0.00
31	0.00	0.00
32	0.00	0.00
33	0.00	0.00
34	0.00	0.00
35	0.00	0.00
36	0.00	0.00
37	0.00	0.00
38	0.00	0.00
39	0.00	0.00
40	0.00	0.00
41	0.00	0.00
42	0.00	0.00

APPENDIX E: ELUTION CURVE DATA FOR 5 ML COLUMN AT A FLOW RATE OF 5 ML/MIN

Fractions	Ca Concentration (mg/L)	Sc Concentration (mg/L)
1	5.6	0.0
2	7.0	0.0
3	37.0	0.0
4	47.0	0.0
5	73.8	0.2
6	50.8	0.2
7	33.8	0.4
8	10.5	0.5
9	11.2	0.5
10	4.9	0.5
11	1.7	0.5
12	0.4	0.5
13	0.1	0.4
14	0	0.4
15	0	0.4
16	0	0.3
17	0	0.3
18	0	0.3
19	0	0.3
20	0	0.2
21	0	0.3
22	0	0.2
23	0	0.2
24	0	0.1
25	0	0.1
26	0	0.6
27	0	0.3
28	0	0.1

29	0	0.0
30	0	0.0
31	0	0.1
32	0	0
33	0	0
34	0	0
35	0	0
36	0	0
37	0	0
38	0	0
39	0	0
40	0	0
41	0	0
42	0	0

APPENDIX F: ELUTION CURVE DATA FOR 10 ML COLUMN AT A FLOW RATE OF 5 ML/MIN

Fractions	Sc Concentration (mg/L)	Ca Concentration (mg/L)
1		
2	0.00	0.82
3	0.00	5.36
4	0.00	9.80
5	0.00	24.40
6	0.00	38.00
7	0.00	46.00
8	0.00	40.00
9	0.00	31.40
10	0.00	14.44
11	0.00	8.60
12	0.00	6.20
13	0.00	2.53
14	0.00	0.81
15	0.00	0.18
16	0.01	0.00
17	0.03	0.00
18	0.08	0.00
19	0.06	0.00
20	0.07	0.00
21	0.10	0.00
22	0.09	0.00
23	0.10	0.00
24	0.10	0.00
25	0.11	0.00
26	0.57	0.00
27	0.73	0.00
28	0.51	0.00
29	0.36	0.00
30	0.27	0.00

31	0.19	0.00
32	0.14	0.00
33	0.09	0.00
34	0.06	0.00
35	0.04	0.00
36	0.005	0.00
37	0	0.00
38	0	0.00
39	0	0.00
40	0	0.00
41	0	0.00
42	0	0.00

APPENDIX G: BREAKTHROUGH CURVE DATA FOR D2EHPA-XAD-4 FOR SCANDIUM AND CALCIUM

Fractions	Sc Concentration (mg/L)	Ca Concentration (mg/L)	Sc (Ct-Co)	Ca (Ct-Co)
0	0	0	0	0
1	0.001	0.504	0.001	0.003
2	0.471	133.837	0.236	0.669
3	0.466	127.118	0.233	0.636
4	0.476	118.730	0.238	0.594
5	0.289	116.793	0.145	0.584
6	0.557	112.925	0.278	0.565
7	0.634	106.266	0.317	0.531
8	0.742	103.205	0.371	0.516
9	0.788	78.860	0.394	0.394
10	0.885	79.246	0.442	0.396
11	0.891	87.133	0.445	0.436
12	0.938	85.340	0.469	0.427
13	0.976	86.429	0.488	0.432
14	1.018	83.401	0.509	0.417
15	1.021	79.318	0.511	0.397
16	1.036	68.999	0.518	0.345
17	1.045	73.253	0.522	0.366
18	0.915	71.630	0.457	0.358
19	1.067	65.953	0.533	0.330
20	1.025	66.768	0.513	0.334
21	1.102	66.986	0.551	0.335
22	1.101	63.373	0.551	0.317
23	1.078	61.532	0.539	0.308
24	1.101	62.270	0.550	0.311
25	0.000	60.517	0.549	0.303

APPENDIX H: ETHICAL CLEARANCE CERTIFICATE

Cape Peninsula University of Technology

P.O. Box 1906 · Bellville 7535 South Africa ·Tel: +27 21 953 8677 (Bellville), +27 21 460 4213 (Cape Town)

Ethics Approval Letter **Reference no: 197095895/01/2020**

Office of the Chairperson **Research Ethics Committee**	**Faculty of Applied Sciences**

On 31 January 2020, the Ethics Committee of the Faculty of Applied Sciences granted ethics approval to ADONIS SHAHEEDA for research activities related to a project to be undertaken for a degree (PHD IN CHEMISTRY) at the Cape Peninsula University of Technology.

Title of project:	A technique for the separation of a Tb radioisotope from proton bombarded Gd targets

Comments (Add any further comments deemed necessary, e.g. permission required)

1. Part of the study involves radioactive materials; hence, must be carried out in access controlled laboratories within iThemba LABS Radionuclide Production facility. Support letter from iThemba was submitted to ethics committee.
2. Human subjects are not included in the proposed study.
3. This permission is granted for the duration of the study.
4. Research activities are restricted to those detailed in the research proposal.
5. The research team must comply with conditions outlined in AppSci/ASFREC/2015/1.1 v1, CODE OF ETHICS, ETHICAL VALUES AND GUIDELINES FOR RESEARCHERS.

Signed: Chairperson: Research Ethics Committee	**31/01/2020** **Date**

APPENDIX I: GRAMMARIAN LETTER

22 Krag Street
Napier
7270
Overberg
Western Cape

27 November 2022

LANGUAGE & TECHNICAL EDITING

Cheryl M. Thomson

A COMPARATIVE STUDY OF THE EFFICIENCY OF ION EXCHANGE AND EXTRACTION CHROMATOGRAPHY FOR THE SEPARATION OF MILLIGRAM AMOUNTS OF SCANDIUM FROM GRAM AMOUNTS OF CALCIUM

Supervisor: Dr T Oosthuysen

Supervisor (external): Prof T N Van der Walt

This is to confirm that I, Cheryl Thomson, executed the language and technical edit of the above-titled PhD thesis of **Shaheeda Adonis, student number 197095895**, at the CAPE PENINSULA UNIVERSITY OF TECHNOLOGY in preparation for submission of this thesis for assessment.

Yours faithfully

CHERYL M. THOMSON

Email: cherylthomson2@gmail.com

Cell: 0826859545